TECHNISCHE UNIVERSITÄT WIEN

DISSERTATION

Development of aluminum nitride material systems suitable for additive manufacturing

ausgeführt zum Zwecke der Erlangung des akademischen Grades eines Doktors der technischen Wissenschaften unter der Leitung von

Associate Prof. Dipl.-Ing. Dr.techn. Thomas Konegger

E164

Institut für Chemische Technologien und Analytik

eingereicht an der Technischen Universität Wien

Fakultät für Technische Chemie

von

Johannes RAUCHENECKER

Mat.Nr: 01326463

Wien, August 2022 _____

Acknowledgements

Working on a PhD thesis comes with a wide variety of challenges. This includes the lack of explanations for experiments with curious outcomes, fixing of broken equipment or the search for motivation when multiple problems come crashing down on one at once. My work on this thesis would not have been possible without the help of family, friends and my co-workers at TU Wien and I am very thankful to each and every one of them.

Thomas Konegger for acquiring the funding and laying the groundwork for this project, always being open to helpful discussions, and for going through my thesis, on the hunt for mistakes and inconsistencies.

My partners at Lithoz GmbH, Martin Schwentenwein, Julia Rabitsch, Dominik Brouczek and Anna-Katharina Hofer who did their best to produce AlN samples on the CeraFab system, even when the slurries did not always comply.

Christian Gierl-Mayer for helping with thermal analysis of my samples, and for coercing the nitrogen/oxygen analyzer into cooperation, when it had gone haywire.

Werner Artner from TU Wien X-Ray Center because without his expertise and guidance XRD analysis and interpretation would have taken considerably longer.

Sabine Schwarz (USTEM, TU Wien) for conducting TEM analysis and helping with the interpretation of the results.

Johannes Frank and Andreas Huber from the workshop at the institute for fixing furnaces and other devices I used to generate my results whenever they decided to stop working.

Anton Reiser (OSRAM GmbH) and Jaroslav Sedláček (Slovak Academy of Sciences) for their support with thermal conductivity measurements using the flash method.

A special thanks goes to…

…my family Andreas, Christian, Martha and Johann and my partner Helene who provided motivation, instrumental and emotional support and who were understanding, when other obligations were pushed into the background because of my work.

…all the co-workers at the institute and friends, especially Johannes Eßmeister, Christina Drechsel, Bernadette Kirchsteiger and Patrick Fritz who supported me informationally and mentally through the years, always had an open ear for me when things did not go according to plan and who were there to celebrate, when they did.

Abstract

Thermal management systems become ever more important in modern applications. Owing to its outstanding properties, such as high thermal conductivity, supported by good mechanical and chemical stability in its sintered form, aluminum nitride (AlN) is a prime candidate for thermal management applications. However, especially thermal conductivity relies on the purity of the AlN lattice, with oxygen defects being the most detrimental, requiring close monitoring of the oxygen intake in process chains. This in combination with additional challenges related to processing and sintering is the reason for industrially produced AlN being mostly offered in simple geometries.

The main goal of this project was to develop powder systems containing AlN and sintering additives to produce samples with high thermal and mechanical properties. Multiple AlN powders were characterized and their stability in various environments and during multiple processing steps was investigated by elemental analysis and X-ray diffraction. The powders were then hot-pressed either alone or with sintering additives. The properties of hot-pressed samples were to be used as benchmark values for fully densified samples.

The powder mixtures were also cold-isostatically pressed (CIP) and sintered without the application of external pressure to investigate the influence of varying parameters like sintering additives and additive content, sintering time, and sintering environments. Phenomena during the sintering in reductive environments were observed and intensely studied to gain a better understanding of the material system.

The most promising powder mixture was used in additive manufacturing (AM) via lithography-based ceramic manufacturing (LCM), an AM method, in which three-dimensional structures are built by selective and layerwise photopolymerization of ceramic slurries containing an organic binder system and ceramic particles. Simple and complex shaped printed samples were generated, sintered, and characterized with respect to mechanical and thermal properties.

CIP samples with characteristic Weibull strength of up to 390 MPa with thermal conductivities exceeding 180 W m^{-1} K^{-1} were produced. AM samples exhibited comparable properties, which highlights the suitability of the developed powder systems in the LCM process. Several phenomena during sintering, such as migration behavior of a secondary phase, resulting in depletion of samples from sintering additives were observed and studied.

This work demonstrates that by careful design of a suitable materials system, the implementation of a novel shaping method, resulting in parts with comparable properties to parts from conventional shaping methods, can be achieved.

Kurzfassung

Aluminiumnitrid (AlN) kombiniert Eigenschaften wie hohe Wärmeleitfähigkeit bei geringer Wärmeausdehnung und guter mechanischer, sowie chemischer Stabilität in einem keramischen Material, weshalb es eine gute Wahl für „thermal management"-Systeme darstellt. Besonders die Wärmeleitfähigkeit des Materials ist aber von der Reinheit abhängig, wobei Sauerstoffdefekte im Kristallgitter die größte Rolle spielen, was die Kontrolle des Sauerstoffgehalts während der Prozesskette notwendig macht. Dieser und andere Umstände sorgen dafür, dass AlN industiell vor allem in simplen Geometrien angeboten wird.

Das Hauptziel dieses Projektes war es ein AlN-System zu finden, mit welchem gesinterte Materialien mit hoher Dichte, Wärmeleitfähigkeit und mechanischen Eigenschaften erzielt werden können, sowie die Verwendung dieses Systems in einem additiven Fertigungsprozess.

Drei AlN-Pulver wurden von zwei Herstellern bezogen, charakterisiert und ihre Stabilität in diversen, für den Prozess relevanten Umgebungen mittels Elementaranalyse und Röntgendiffraktion überprüft. Da die Stabilität der Pulver in allen Prozessierungsschritten gegeben war, mussten keine Schritte zum Schutz der Pulver getroffen werden. Die Pulver wurden dann heißgepresst und charakterisiert, um Benchmarkwerte für die Eigenschaften voll verdichteter AlN-Proben zu erhalten.

Pulvermischungen von AlN in Kombination mit diversen Sinterhilfsmitteln wurden schließlich konventionell über kaltisostatisches Pressen (CIP) und Sintern hergestellt und der Einfluss mehrerer Prozessparameter auf die Eigenschaften der Proben wie Wärmeleitfähigkeit und mechanische Festigkeit überprüft, wobei besonderes Augenmerk auf die Sinterung unter reduzierenden Bedingungen gelegt wurde. Die vielversprechendsten Pulversysteme wurden mittels „Lithography-based Ceramic Manufacturing" (LCM), einem Prozess zur additiven Fertigung (AM) von Keramiken durch schichtweise Photopolymerisation nicht-wässriger keramischer Schlicker, verarbeitet.

Es konnten CIP Proben mit einer charakteristischen Weibullfestigkeit von 390 MPa und einer Wärmeleitfähigkeit von 180 W m^{-1} K^{-1} hergestellt werden. Additiv gefertigte Proben erreichten vergleichbare Werte, wodurch die Eignung von AlN in diesem Fertigungsprozess bestätigt werden konnte. Während der Sinterung wurde eine Wanderung einer bei hohen Temperaturen gebildeten Sekundärphase und die daraus resultierende Entfernung von Sinterhilfsmitteln aus den Proben beobachtet und studiert.

In dieser Arbeit konnte gezeigt werden, dass durch die Entwicklung eines geeigneten Materialsystems die Implementierung einer neuen Formgebungsmethode, die die Herstellung von Proben hoher Qualität und Komplexität erlaubt, ermöglicht werden könnte.

Table of Contents

1 Introduction, motivation, and objectives

A combination of multiple intriguing properties makes AlN a candidate for high-performance thermal management materials to be used in a multitude of different applications. High thermal conductivity, a coefficient of thermal expansion close to silicon and good electrically insulating properties allow for the use as substrate material in high power electronics. Mechanical strength in the range of alumina ceramics [1] also allow for the utilization of AlN in structural applications, especially when thermal cycling has to be considered.

The shaping and sintering of AlN provides a number of challenges, which hold back the widespread use of the material in many industrial settings. AlN powders are prone to react with water, in a hydrolysis reaction, introducing oxygen into the powder [2]. Thermal conductivity relies heavily on the purity of the material, especially when it comes to oxygen defects in the lattice of the AlN grains [3]. This makes shaping the material more complicated than other ceramic materials, since no aqueous processing methods, such as slip casting or gel casting can be used with AlN and industrially available geometries are often very simple. Aqueous processing is only enabled by coating techniques to prevent surface reactions of AlN particles [4]. Non-aqueous processing enables the shaping of AlN ceramics without risk of hydrolysis and without the need for protective coatings. With the increasing interest in additive manufacturing and the development of non-aqueous processing methods new possibilities to shape AlN ceramics are emerging.

Sintering of AlN proves to be another challenge. Typical for a nitride ceramic material, diffusion coefficients are low and as such high sintering temperatures and sintering additives have to be utilized to enable densification [1]. Most often oxides are used as sintering additives, which form a eutectic melt with the Al_2O_3 present on AlN grains during sintering. This leads to liquid phase sintering and increased densification, but also a purification of the AlN lattice from oxygen defects, increasing thermal conductivity of the materials [5]. Reducing conditions during sintering also affect the distribution of secondary phase, influencing properties of the ceramic material [6]. To sinter AlN ceramics multiple factors from sintering times, temperatures, environments, and additives must be considered and coordinated.

This collaborative work with Lithoz GmbH was conducted in the framework of a project called ADDHANCE funded by the Austrian Research Promotion Agency (FFG, Grant number 864842) and should explore a novel shaping approach for complex-shaped aluminum nitride parts utilizing the lithography-based ceramic manufacturing (LCM) technology provided by

Lithoz GmbH. The goal of the project was to produce additively manufactured AlN ceramic parts with high thermal conductivity (180 W m^{-1} K^{-1}). For this, the stability of AlN powders during processing had to be monitored to limit oxygen intake. Next, an appropriate powder system with sintering additives for sintering at temperatures at or below 1700 °C, which was compatible with the LCM process, had to be found. This powder system would then be used by Lithoz GmbH in an additive manufacturing process.

The exploration of different AlN powders with a multitude of sintering additive combinations, shaped and sintered in various ways should provide an understanding of handling AlN and achievable material properties. In addition to an investigation towards the stability of the AlN powders in various environments, an overview of process parameters - powder composition and sintering - and correlating changes in material properties such as density, microstructural evolution, flexural strength, and thermal conductivity was achieved.

The most promising AlN system would be chosen and used in the LCM process, a form of additive manufacturing (AM) using photopolymerization of non-aqueous ceramic slurries. The realization of complex shaped AM parts from AlN with properties comparable to conventionally processed AlN parts would prove the viability of the material and process combination.

To achieve the above multiple objectives were defined for this work:

AlN powder evaluation: Three different AlN powders were investigated by elemental analysis and scanning electron microscopy (SEM) and their stability in various environments critical for the following processing steps was investigated by elemental analysis and X-ray diffraction analysis (XRD).

Hot pressing of AlN samples: Samples of the AlN powders with varying amounts of sintering additives were hot-pressed and characterized (density, mechanical properties and thermal conductivity) to generate benchmark values for fully densified samples that can be compared to conventionally sintered parts.

Sintering of AlN: By far the most ambitious part of this project was to investigate the sintering behavior of AlN without prior experience with this material system. Three different AlN powder grades and multiple sintering additive (CaO, SrO, Y$_2$O$_3$) and their influence on the properties of the materials were to be investigated in cold-isostatically pressed (CIP) samples. Additionally, an extensive investigation of the effect of different sintering environments (non-

reducing, reducing and high gas pressure conditions) on the sintering behavior and resultant properties of the materials was conducted due to several phenomena observed during initial experiments. The goal was to achieve dense ceramic materials with high thermal conductivity ($\geq$ 180 W m^{-1} K^{-1}) at a maximum sintering temperature of 1700 °C with high repeatability.

Additive manufacturing of AlN: The optimized powder system developed in the last step was to be used in the LCM process by Lithoz GmbH. Many processing parameters influencing the shaping (printing parameters: e.g., energy dosage, layer height, slurry viscosity) and sintering (altered sintering additive system due to incompatibility with slurry components) were identified and customized to yield AlN samples with properties comparable to CIP samples generated in the past step. Lastly, complex shaped parts were to be generated by LCM to demonstrate the applicability of the shaping technology.

Two research papers were published on the results of this project. One research paper [7] discusses the influence of different sintering environments on the microstructural development and properties of AlN, while the second research paper [8] describes the additive manufacturing of AlN samples by the LCM process. The data and results published will be discussed in sections 4.3.4.2 and 4.4, respectively.

2   Theoretical background

This section aims to give the reader an understanding of AlN as a ceramic material by providing information on its properties, synthesis, reactivity and processing. Additionally a short description of thermal conductivity in solids and an overview on additive manufacturing of ceramic materials will be given.

2.1   Aluminum nitride

High thermal conductivity, low thermal expansion and good electrically insulating capabilities are the most intriguing properties of aluminum nitride. One of the earliest academic studies from 1959 by Long and Foster [9] investigated the applicability of the material for refractory purposes, especially as crucible material for molten aluminum, due to its stability and inertness, which, at the time, was something not many other materials could be used for. While the material Long and Foster used was far from pure or fully densified and only showed thermal conductivity below 10 W m^{-1} K^{-1}, it set a foundation for further research. In 1973 Slack [3] published his work on nonmetallic crystals with high thermal conductivity, highlighting the importance of crystal structure on thermal conductivity in solids. He investigated "adamantine" or diamond-like compounds and proposed four properties, a nonmetallic solid should exhibit to be a potential high thermal conductivity solid, that can be found in AlN. This will be discussed further in chapter 0. From then on extensive research into sintering behavior, stability in various environments and properties of aluminum nitride was conducted by researchers across the globe due to the material's potential uses especially as electronic packaging material.

2.1.1   Properties and applications of aluminum nitride

Typical for nitride ceramic materials, AlN exhibits mostly covalent bonding character with a low diffusion coefficient. At room temperature and ambient pressures AlN crystallizes in a wurtzite crystal structure (Fig. 1), in which every Al-atom and O-atom is tetrahedrally coordinated. This is the same crystal structure that BeO, another material with high thermal conductivity, crystallizes in [1].

AlN is mostly seen as electrical insulator and used as such in electronic substrates and electronic packaging due to its thermal properties. However, due to the band gap of 6.2 eV studies have been conducted on using AlN in UV-LEDs as a semiconductor [10].
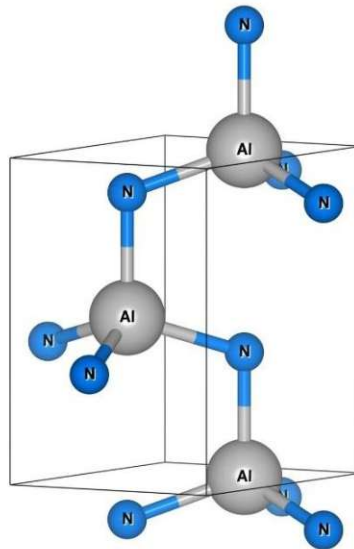
Fig. 1: Unit cell of AlN, showing tetrahedral coordination of Al-atoms.

Representative properties of AlN, reported in academic literature and data from two industrially available materials are shown in Table 1. The data should only give the reader a general idea about the expected properties of the material and by no means should comparisons be made between the different materials, since material preparation and measurement conditions have to be taken into account, as well as different sintering additives that may lead to vastly different properties, potentially even introducing inherently new properties to the material, which will be discussed later.

Table 1: Properties of AlN, as reported in the academic literature and by AlN producers.

	Academic research papers	Toshiba TAN-250 [11]	CeramTec Alunit 170 C [12]
Density (g/cm³)	3.26 [13]	3.3	3.26
Thermal conductivity (W m^{-1} K^{-1})	272 (polycrystalline material, measured) [14] 319 (theoretical limit for a single crystal) [15]	250	170
Coefficient of thermal expansion (10^{-6}/K)	4.4 [1]	4.6 (RT to 500 °C)	3.7 - 5.7 (100 - 200 °C)
Flexural strength (MPa)	280 - 350 [13] 340 - 490 [1]		320
Dielectric strength (kV/mm)	8.25 (10.9 GHz) [16]	14 - 15 (50 Hz)	15
Dielectric loss (tan δ)	0.0020 (10.9 GHz) [16]	0.0005 (1 MHz)	0.01 (1 GHz)
Electrical resistivity (Ω cm)	4.0 x 10^{11} [13]	> 10^{14}	10^{14} (20 °C)
Band gap (eV)	6.2 [10]		

Owing to its high thermal conductivity and coefficient of thermal expansion (CTE) close to Si the proposed and actual applications of AlN are to be found mostly in the electronics industry as packaging and substrate material [17]. In 1985 Kurokawa et al. [18] realized several semiconductor devices (Transistor, Light-emitting diode, Laser diode) with AlN as substrate by metallization of AlN heat sinks via sputtering of Ti, Pt or Au and confirmed its applicability for the purpose, exhibiting similar or even better behavior than conventional materials. Another intriguing application of AlN is as electrostatic chucks in semiconductor fabrication [19]. For such applications basic geometric shapes suffice, however, there is also potential for heat exchangers or microchannel substrates for active cooling of electronics, requiring shaping methods to allow for the generation of complex structures.

Given the right purity, composition (sintering additives) and thermal treatment AlN can be sintered to transparency, allowing it to be used in optical applications [16, 18, 20, 21].

To give a better overview how AlN performs in relation to other substrate materials, Miyashiro et al. [22] published a graph comparing important properties of AlN, Al_2O_3, BeO and SiC, which has been redrawn in Fig. 2. Since the paper was published in 1990 some arguments they make for and against certain materials might be outdated (esp. cost and availability of pure raw materials), but the values given for the properties for each material still hold true.
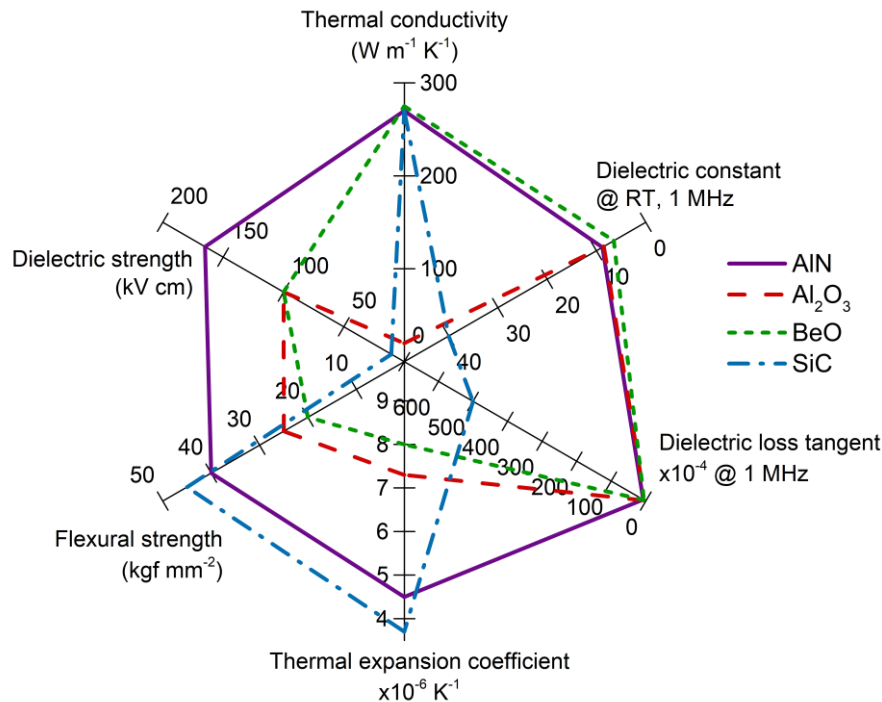

Fig. 2: Properties of AlN in comparison to other substrate materials. Redrawn from [22].

Baik [1] gives more insights into this comparison by arguing that while the manufacturing of Al_2O_3 substrates is cheaper, its thermal conductivity is very low compared to AlN, and its thermal expansion is almost twice that of Si, resulting in a mismatch with Si circuitry. BeO has a theoretical thermal conductivity of 370 W m^{-1} K^{-1} and practical conductivity of 260 W m^{-1} K^{-1}, however, the coefficient of thermal expansion is even higher than that of Al_2O_3 and the material is inherently toxic.

Even though its properties are suited for a wide variety of applications, the utilization of AlN is not as widespread as one might presume, owing to challenges in its synthesis, processing and sintering. The properties of AlN are very dependent on its chemical purity, especially when it comes to oxygen lattice defects, which limit its thermal conductivity. This must be considered during all processing steps from synthesis to shaping and sintering.

2.1.2 Synthesis of AlN

Over the years a number of successful synthesis routes for AlN have been established, with nitridation of Al and carbothermal nitridation of Al_2O_3 being the most important in industrial settings. Other more exotic routes include the gas phase synthesis of AlN to produce thin films or powders, the use of alternative precursors for nitridation or even solvothermal approaches [23]. Haussonne [24] published an extensive review on the synthesis methods of AlN. The following paragraphs will give an overview over a few select synthesis methods.

2.1.2.1 Direct nitridation of Al

One of the earliest methods of direct nitridation of Al that yielded a product of more than 90 % purity was developed by Long and Foster [9], in which AlN forms as a lump in a DC-arc between two Al-electrodes in N_2 atmosphere. More generally it is described as reaction (1), which occurs above 1200 °C according to Sheppard [25], although other authors also reported complete transformation at lower temperatures, often due to the use of additives.

$$2\,Al_{(l)} + N_{2\,(g)} \rightarrow 2\,AlN_{(s)} \qquad\qquad (1)$$

This method comes with a number of problems. The molten aluminum may agglomerate, leading to coarse powders, which must be milled in order to obtain sinterable powder. Additionally, not all Al might react, due to an AlN layer forming, preventing further reaction of Al to AlN, leaving Al impurities in the powder, which have to be leached from the product [1].

In order to obtain purer AlN with less residual Al content and less oxygen contamination form direct nitridation of molten Al, Scholz and Greil [26] proposed using an Al-alloy containing 2.3 wt.% Li instead of pure Al. They observed complete conversion after 100 minutes at 1000 °C. The Li acts as an oxygen getter during the reaction, purifying the Al and AlN. Unreacted Li and compounds formed with oxygen volatilize during the reaction, leading to a purified AlN reaction product.

By adding certain compounds, the particle structure of the AlN formed can be affected, as shown by Mashhadi et al. [27], who were able to synthesize whiskers by adding ammonium chloride to the Al powder prior to nitridation. They suggested a chlorination-nitridation as the reaction pathway for the whiskers.

While Al in direct nitridation is usually in a liquid state, gaseous Al also reacts with nitrogen-containing gases, if temperatures are high enough. Baba et al. [28] utilized rf-plasma to vaporize Al powder. The Al vapor reacts with ammonia to form ultrafine (30 m² g^{-1} specific surface area, 60 nm particle size) AlN.

In an attempt to find alternative ways to produce AlN, Zeng et al. [29] used microwave heating to produce pure AlN powder at 1050 °C in 30 minutes in N_2 with NH_4F and Zn additives. Fast heating rates and tailored nitridation-assisting additive compounds proved to be critical in the synthesis process.

2.1.2.2 Carbothermal reduction nitridation of Al$_2$O$_3$

For this approach Al_2O_3 powder is mixed with a carbon source and heated to a temperature range between 1400 to 1700 °C in N_2 atmosphere, as shown in reaction (2). After the reaction excess carbon is removed by heating the reaction mixture to 600 to 900 °C [1].

$$Al_2O_{3\,(s)} + 3\,C_{(s)} + N_{2\,(g)} \rightarrow 2\,AlN_{(s)} + 3\,CO_{(g)} \qquad\qquad (2)$$

Tsuge et al. [30] conducted an extensive investigation of different aluminum sources and found that carbothermal nitridation is affected by the type of aluminum oxides or hydroxides used. Investigated phases included η-Al$_2$O$_3$, θ-Al$_2$O$_3$, α-Al$_2$O$_3$, γ-Al$_2$O$_3$ and Al(OH)$_3$. The study showed that γ-Al$_2$O$_3$ reacted at 1500 °C (5 h), with less than 1.6 wt.% oxygen content remaining after the reaction, whereas the products from hydroxides had higher oxygen contents at that temperature and the products from other oxides showed oxygen contents exceeding 20 wt.%. At 1550 °C (5 h) products from all investigated precursors exhibited oxygen contents of 2 wt.% or less, with the only exception being η-Al$_2$O$_3$, products of which exhibited an oxygen content of 37.6 wt.%. When hot-pressed the samples showed thermal conductivity increase with decreasing oxygen content of the AlN powders.

Although carbon black is one of the most used carbon sources, other carbon sources, such as sucrose have been investigated for their suitability in the process. Baik et al. [31] propose that sucrose is a superior carbon source compared to carbon black, due to improved mixing with the Al source, and complete reaction could be reached following stoichiometric ratios of C to Al$_2$O$_3$ equaling 3 to 1, whereas an excess of C was necessary to achieve compete conversion with other carbon sources.

In patent US5674465A [32], filed by Ravenel et al., a continuous reactor for the carbothermal reduction nitridation of alumina is described. This process utilizes a feed, consisting of a granulated mixture of alumina, carbon black and a binder resin. The granules are fed into the reactor from the top. First the binder in the granules is pyrolyzed before the alumina is reduced and nitrided at a temperature of 1450 to 1500 °C in a N_2 flow. The exhaust gases transfer heat to the granule feed, while the reacted granules transfer heat to the N_2 flow below the reaction zone. After thermal removal of excess carbon at 700 °C in an oxygen containing atmosphere, the resultant AlN powder has a particle size between 0.5 and 5 µm, residual Al_2O_3 content of less than 0.5 wt.% and BET specific surface area between 2 and 5 m^2 g^{-1}.

2.1.2.3   Alternative methods

Several alternative methods for the synthesis of AlN have been proposed in the past. Below is a list of select methods.

Chemical vapor deposition:
AlN powders or thin films on substrates can be produced by the reaction of gaseous precursor compounds with ammonia. In general aluminum halide precursors are used for chemical vapor deposition (CVD) but other compounds, such as trialkylaluminum compounds may be used as well [33].

Sputtering:
Chen et al. [34] successfully used sputtering to deposit AlN thin films with thicknesses of 1 µm on a Si substrate. They used an aluminum target and sputtered in an Ar and N_2 atmosphere in an RF sputtering system.

Self-propagating synthesis:
Shin et al. [35] produced AlN powders in a self-propagating synthesis, using Al powder and AlN as diluent of the reaction mixture, which was then put inside a graphite crucible inside a reaction chamber pressurized with N_2 gas. After ignition Al rapidly reacted to AlN. By varying process parameters, such as N_2 pressure, diluent content and Al grain size, they were able to control the morphology of the resultant AlN powder. While this method is a form of direct nitridation, it is mentioned as its own bullet point due to the heat being supplied by the reaction itself rather than a furnace.

Solvothermal method:

A method to synthesize nano-sized AlN powders by a solvothermal approach is proposed by Sardar et al. [36] They describe the reaction of aluminum cupferronate ($[Al(C_6H_5N_2H_2)_3]$) or $AlCl_3$ with 1,1,1,3,3,3-hexadimethysilazane ((CH_3)$_3$-SiNHSi(CH_3)$_3$) to produce AlN nano-powders with average grain sizes of 10 to 20 nm respectively.

Pyrolysis of preceramic polymers:

In the 1960s a novel production method for non-oxide ceramics by an organic-to-inorganic conversion utilizing the pyrolysis of preceramic polymers was proposed. Since then, many different polymers have been investigated for their applicability in the pyrolytic conversion to ceramics. Depending on the composition and structure of the polymers different ceramic materials can be obtained through pyrolysis. The manufacturing method has several advantages, such as the usability of polymer shaping methods, and in general lower processing temperatures [37]. Aluminum nitride has been prepared by this approach mostly using polyiminoalanes [38-41]

2.1.3 Reactivity and stability of AlN

AlN readily reacts with water in a hydrolysis reaction, resulting in aluminum hydroxides and ammonia. Especially in powders this reaction can lead to increased oxygen content and impurities, which get incorporated into the AlN lattice at elevated temperatures, limiting the attainable properties. Especially aqueous processing of the powders is not possible without taking precautions and preventing hydrolysis. The sintered material is usually considered chemically stable, even at high temperatures and in various environments.

2.1.3.1   Hydrolysis

Bowen et al. [2] investigated the reaction and kinetics of the hydrolysis of AlN. They found that AlN powder in water reacts following reaction (3), resulting in a porous layer of amorphous aluminum hydrate surrounding the particle.

$$AlN + 2\,H_2O \; \rightarrow \; AlOOH_{amorph} + NH_3 \qquad\qquad (\, 3 \,)$$
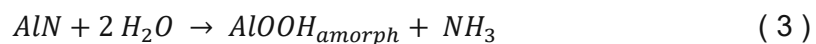
In the alkaline environment, resulting from the hydrolysis, the amorphous and porous hydrolysis product layer ages and reacts to crystalline bayerite after about 16 hours of exposure to water (reaction (4)).

$$AlOOH_{amorph} + H_2O \; \xrightarrow{OH^-} \; Al(OH)_3 \qquad\qquad (\, 4 \,)$$
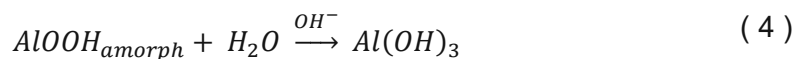
They found that after 24 hours about 80 % of AlN is consumed by the reactions described above and, as such, they recommend processing of AlN in organic media, rather than water.

Fukumoto et al. [42] further elaborated on the hydrolysis of AlN by immersing AlN powder at various temperatures from 10 to 100 °C in either deionized water or aqueous solutions of HCl, NaOH and H_3PO_4. They confirmed the formation of Bayerite ($Al(OH)_3$) after the immersion in water at room temperature, however when the temperature was increased to 78 °C they also found signals of crystalline Boehmite (AlOOH) in the XRD. At 100 °C the XRD signals changed to almost exclusively crystalline Boehmite as reaction product. HCl and NaOH solutions accelerated the hydrolysis reaction, whereas H_3PO_4 prevented hydrolysis to a certain degree. Their hypothesis for the latter was that a phosphate layer might have formed on AlN and prevented hydrolysis.

Although the hydrolysis of AlN is very negative for the processing and properties of AlN as thermal management material, Kocjan [43] reviewed the utilization of AlN hydrolysis in the production of mesoporous alumina structures, lamellar nanocrystalline alumina coatings and the hydrolysis-assisted solidifaction of ceramic slurries. For the latter, AlN powder is added to aqueous slurries of alumina, zirconia, or silicon nitride. The hydrolysis reaction consumes water, and the hydroxides connect the particles of the suspension, leading to green parts with high strength.

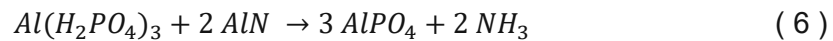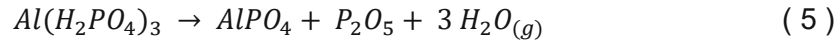### 2.1.3.2   Protection of AlN from hydrolysis

The hydrolysis of AlN prevents the utilization of many shaping methods established for other ceramic materials. Slip casting, tape casting and other methods often require processing in aqueous media, which is not possible for AlN, hindering the production of complex shaped parts. As such, efforts have been made to protect AlN from hydrolysis.

Hotza et al. [44] utilized a hydrophobing approach for AlN particles, using carboxylic acids and were able to show that AlN powder coated with stearic acid in cyclohexane showed no traces of bayerite in XRD measurements after 96 hours in water. However, infrared analysis suggested the formation of an amorphous hydrolysis product.

Krnel and Kosmač [45] showed that hydrolysis resistant AlN powder may be produced by soaking the powder in a solution of aluminum dihydrogen phosphate ($Al(H_2PO_4)_3$) at 70 °C, filtering and washing it. Upon redispersion in deionized water the pH-value of the suspension did not increase over the period of ten days, indicating that no hydrolysis reaction took place, which was confirmed by XRD, as no signals of hydrolysis products were detected. They do, however, state, that the oxygen content of the powder increased from 2.4 wt.% (starting powder was at 2.2 wt.%) to 5.2 wt.%, without further discussion. The same powder treatment with phosphoric or silicic acid was not as successful, as it only decreased the hydrolysis rate, but did not prevent hydrolysis.

Oliveira et al. [46] used a combination of phosphoric acid and an undisclosed carboxylic anionic surfactant to produce stable – in regards to hydrolysis and suspension stability – AlN slurries, which could be used for slip casting cylindrical samples. Olhero et al. [47] further investigated the behavior of phosphate protected AlN slurries, including organic additives by thermogravimetric analysis of green bodies pressed from AlN powder, which was freeze-granulated from the slurries and theoretical calculations using Factsage. They concluded that

the phosphate species might react by splitting off water vapor and ammonia in a temperature range between 100 and 150 °C, which was observed in TG measurements, as indicated by reactions (5) and (6).

$$Al(H_2PO_4)_3 \rightarrow AlPO_4 + P_2O_5 + 3\,H_2O_{(g)} \qquad\qquad (\,5\,)$$
$$Al(H_2PO_4)_3 + 2\,AlN \rightarrow 3\,AlPO_4 + 2\,NH_3 \qquad\qquad (\,6\,)$$

At elevated temperatures, encountered during the ramping phase to reach sintering temperatures, the phosphorus compounds might react with AlN to form volatile PN. While this could not be confirmed by TG, the absence of phosphate species in sintered materials and thermodynamic calculations suggested the following reaction (7).

$$5\,AlN + AlPO_4 + P_2O_5 \rightarrow 3\,Al_2O_3 + PN_{(g)} + N_{2\,(g)} \qquad\qquad (\,7\,)$$
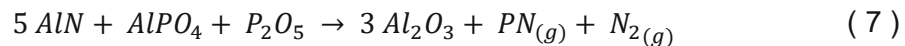
2.1.3.3   Degradation of sintered AlN at high temperatures

According to Werdecker and Aldinger [13] the oxidation of dense AlN in air starts at 1000 °C and proceeds with low reaction rates until 1450 °C, resulting in an oxide layer, hindering the oxidation. At higher temperatures the layer cracks, leading to higher oxidation rates. Table 2 shows the temperatures up to which AlN is stable in various atmospheres.

Table 2: Temperatures up to which AlN is stable in various atmospheres, according to [13]

Atmosphere	Stable up to (°C)
Oxidative	
Air	1000
Cl_2	500
Reductive	
H_2	1400
CO	1800
Vacuum	1500

Sato et al. [48] investigated the degradation of hot-pressed AlN samples in air and N_2 at different H_2O vapor pressures or air after being dried with P_2O_5. They discovered that at 1250 °C and 10 kPa water vapor (for wet conditions) in air the reaction follows parabolic

kinetics, regardless if wet or dry air was used. In wet N_2 the reaction follows linear kinetics, at a tenfold increase in weight gain, compared to wet air.

They also investigated the behavior of AlN in wet N_2 (20 kPa water vapor) at different temperatures. At 1100 °C no weight change was observed. Between 1150 and 1250 °C the weight gain was linear, which changed at 1350 °C, when the kinetics became parabolic (although the weight gain was still higher than at lower temperatures). SEM analysis of the oxide layers led them to believe, that below 1350 °C the layer would be too porous, to block the water vapor from reaching the AlN surface, whereas the layer at 1350 °C was dense and diffusion of H_2O became the limiting factor.

Kim et al. [49] further studied the oxidation behavior of sintered AlN samples in air with controlled humidity (from 10^{-6} to 10^{-3} MPa partial pressure of H_2O) at temperatures from 1100 to 1400 °C by measuring the weight gain of samples. They found a strong correlation between weight gain and temperature. The rate of weight gain was linear up to 1300 °C, when it became parabolic, presumably due to a dense oxide layer on the surface, similar to the results mentioned above. Equation (8) shows the presumed oxidation reaction for AlN.

$$2\,AlN + \frac{3}{2}\,O_2 \ \rightarrow \ Al_2O_3 + \ N_2 \qquad\qquad (8)$$
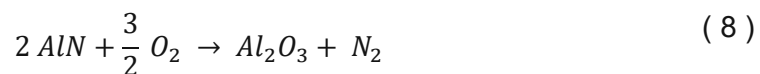
However, they also measured a strong correlation between weight gain rate and humidity. When they changed the partial pressure of the water vapor from 4×10^{-6} MPa to 10^{-3} MPa, they observed a tenfold increase of the weight gain rate at a temperature of 1200 °C. As such, they propose that reaction (9) also plays a major role in the oxidation behavior of the material.

$$2\,AlN + 3\,H_2O \ \rightarrow \ Al_2O_3 + \ N_2 + 3\,H_2 \qquad\qquad (9)$$
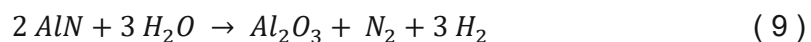
The flexural strength of samples exposed to wet air (10^{-3} MPa) at 1200 °C decreased significantly, which they presumed was due to cracks from the oxide layer (created by a mismatch between thermal expansion of the layer and the substrate) propagating into the AlN. They were not able to observe any effect on the material's strength after 100 h of exposure to dry (4×10^{-6} MPa) air at 1200 °C.

2.1.3.4   Stability of sintered AlN in acids, alkaline solutions and molten metals

Werdecker and Aldinger [13] also commented on the stability of dense AlN in various acids, alkaline solutions and water. A sample immersed in water for fifteen days at room temperature was not affected, while they continue to state that oxidation at 60 °C was also slow. In cold 26 % NaOH the weight loss after 20 hours of immersion was measured as 3.0 mg cm^{-2}. Fig. 3 shows their results of various immersion tests in acids, proving the stability of the material at room temperature. At higher temperatures hot mineral acids may dissolve AlN.
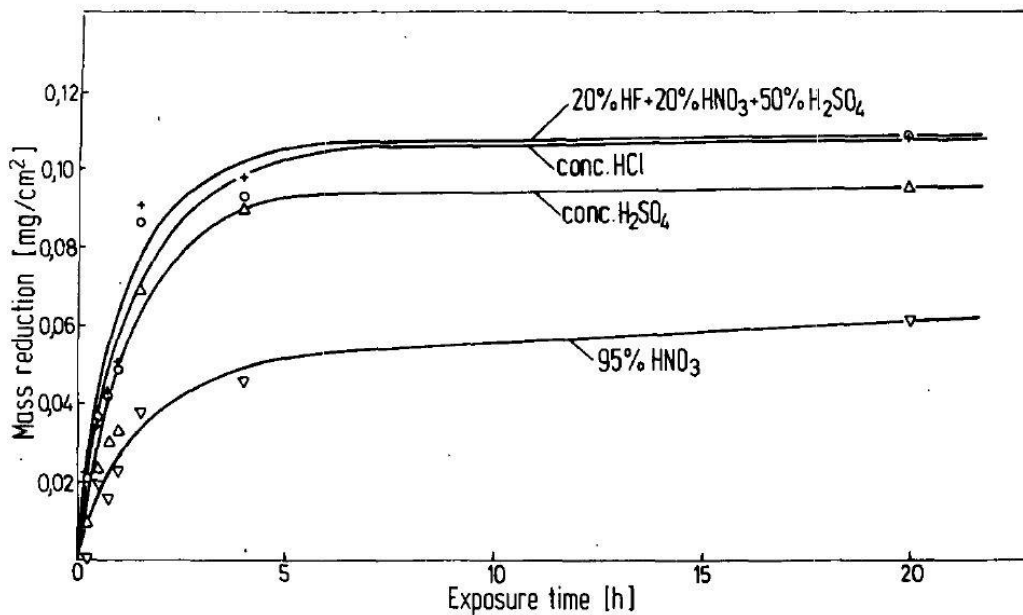

Fig. 3: Weight change of AlN in various acidic solutions at room temperature vs. exposure time. The image was taken from [13]. © 1984 IEEE

In addition, they also highlight the stability of AlN in molten metals (Al, Ga, Ge, Si, Ti (and Ti-alloys), III-V semiconductors), molten salts and molten boron oxide.

2.1.4 Liquid phase sintering and its application in AlN consolidation

Liquid phase sintering (LPS) describes the sintering of materials in which a liquid phase is developed during sintering, enabling rapid densification by multiple processes, which differentiate it from solid state sintering. According to Kingery [50] the driving force for liquid phase sintering is the change in free enthalpy due to the decrease of pore surface area in the liquid. He goes on to further describe three stages encountered during LPS, namely, the rearrangement of solid particles, solution-reprecipitation at contact points of particles and coalescence of solid particles, which marks the finalization of liquid phase processes.

Kingery [50] describes the three phases as follows:

Rearrangement: For the first stage solid particles slide over each other, driven by capillary pressure of the liquid, to increase packing density. By dissolution of connections between solid particles this process can increase density even further. Only in materials with high amounts of liquid phase this process alone can lead to high density materials.

Solution-Reprecipitation: In the second stage material at contact points of solid particles separated only by a thin film of liquid phase, are dissolved, and transported away from the contact points in a way, that the distance between the centers of the particles is reduced. The solubility at the contact points is higher due to higher compressive stresses, which increases the chemical potential at the contact points, facilitating material transport and in turn densification.

Coalescence: The third stage described by Kingery is the coalescence phase, in which particles, which were oriented in a way that prevents wetting by the liquid phase, are transformed. As no liquid phase is present between those particles, material transport will continue akin to solid state sintering through the solid phase.

As diffusion coefficients in aluminum nitride are rather low due to the covalent bonding character, impeding densification by solid-state sintering at temperatures below the dissociation temperature in a N_2 atmosphere, usually sintering additives are used to densify the materials. The basic working principle is that sintering additives form low melting secondary phases, which enhance densification and lead to additional processes during liquid phase sintering of AlN, which influence the properties of the material [1].
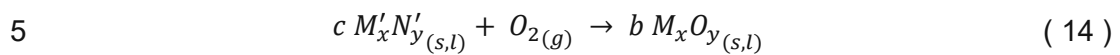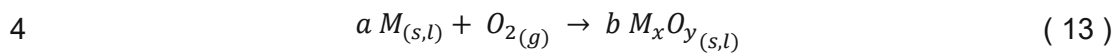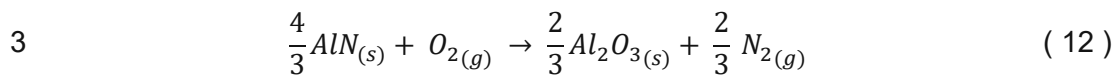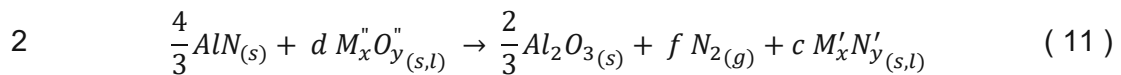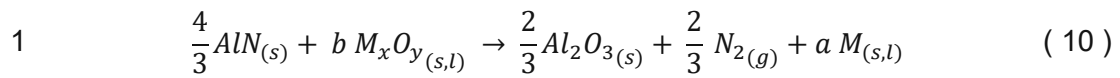
Many sintering additives have been investigated for their enhancement of the densification and properties of AlN over the past decades with the aim to obtain high thermal conductivity materials at low sintering temperatures. In addition to density playing a major role for thermal conductivity, oxygen impurities have been identified as being most detrimental to thermal conductivity which is why the correlation between oxygen concentration in the AlN crystal lattice and thermal conductivity, as well as methods to reduce oxygen content in the lattice, for example through sintering additives or by controlling the sintering environment, have been studied [51].

However, AlN may also be densified without adding sintering additives, as shown by Hirano et al. [21], who were able to sinter a translucent AlN sample to more than 99 % relative density, with a thermal conductivity of 114 W m^{-1} K^{-1} after 8 hours at 1900 °C in 1 MPa of N$_2$ gas atmosphere. Through the addition of 4 wt.% Y$_2$O$_3$ thermal conductivity of the material was improved to 218 W m^{-1} K^{-1} and they were also able to consolidate an AlN material with 4 wt.% Y$_2$O$_3$ by sintering at 1770 °C for 2 hours with a thermal conductivity of 194 W m^{-1} K^{-1}. When sintered samples with 1.5 wt.% Y$_2$O$_3$ addition were reheated to 1900 °C in a graphite furnace for 50 hours thermal conductivity could be increased from 150 to 258 W m^{-1} K^{-1}, while its density decreased from 3.28 to 3.26 g cm^{-3}. This was presumed to happen due to reduction and elimination of secondary phase, as well as increased grain growth. This research shows multiple major influences, that sintering additives and sintering environments have on AlN materials, which will be further explored below.

2.1.4.1   Additives for sintering of AlN

The most used sintering additives in the production of AlN ceramics are rare earth and alkali metal oxides, which fulfill two major roles. Firstly, they react with Al$_2$O$_3$ on the surface of AlN particles to form phases with low melting temperatures, which enables liquid phase sintering, leading to enhanced densification by particle rearrangement and solution-precipitation mechanisms. Secondly, the secondary phases have higher affinity for oxygen, effectively removing oxygen from the AlN lattice. Virkar et al. [5] describe the effectivity of a sintering additive in purifying the AlN lattice with the Gibbs' free energy of the formation of aluminates between the oxygen in the AlN lattice (dissolved Al$_2$O$_3$) and for example yttrium oxide, which is a very common sintering additive. The lower ΔG^0 of the formation reaction, the higher is the expected thermal conductivity of the material.

Watari [52] describes this approach in more detail in a 2001 paper on high-thermal conductivity non-oxide ceramics by showing a thermodynamic plot with ΔG^0 of reactions ((12), (13), (14)) relevant to sintering AlN. Reactions (10) and (11) represent the oxidation of AlN by sintering additives, which must not take place during sintering. They result from the subtraction of (13) and (14) from (12). The numbers left of the reactions indicate which ΔG^0-values in Fig. 4 the reactions correspond to. As long as ΔG^0_3 is higher than ΔG^0_4 and ΔG^0_5, the oxidation of AlN by the additives is suppressed, which is true for the shaded area in the plot. The vertical axis in the plot presents the Gibbs' free energy of formation for various secondary phases with Al_2O_3. As long as the sintering additives form stable secondary phases, oxygen does not diffuse into the AlN lattice and lower ΔG^0_f-values lead to the purification of the AlN lattice and high thermal conductivity AlN materials, as indicated above.

$$1 \qquad \frac{4}{3} AlN_{(s)} + b\, M_xO_{y\,(s,l)} \rightarrow \frac{2}{3} Al_2O_{3\,(s)} + \frac{2}{3} N_{2\,(g)} + a\, M_{(s,l)} \qquad (\,10\,)$$

$$2 \qquad \frac{4}{3} AlN_{(s)} + d\, M''_xO''_{y\,(s,l)} \rightarrow \frac{2}{3} Al_2O_{3\,(s)} + f\, N_{2\,(g)} + c\, M'_xN'_{y\,(s,l)} \qquad (\,11\,)$$

$$3 \qquad \frac{4}{3} AlN_{(s)} + O_{2\,(g)} \rightarrow \frac{2}{3} Al_2O_{3\,(s)} + \frac{2}{3} N_{2\,(g)} \qquad (\,12\,)$$

$$4 \qquad a\, M_{(s,l)} + O_{2\,(g)} \rightarrow b\, M_xO_{y\,(s,l)} \qquad (\,13\,)$$

$$5 \qquad c\, M'_xN'_{y\,(s,l)} + O_{2\,(g)} \rightarrow b\, M_xO_{y\,(s,l)} \qquad (\,14\,)$$
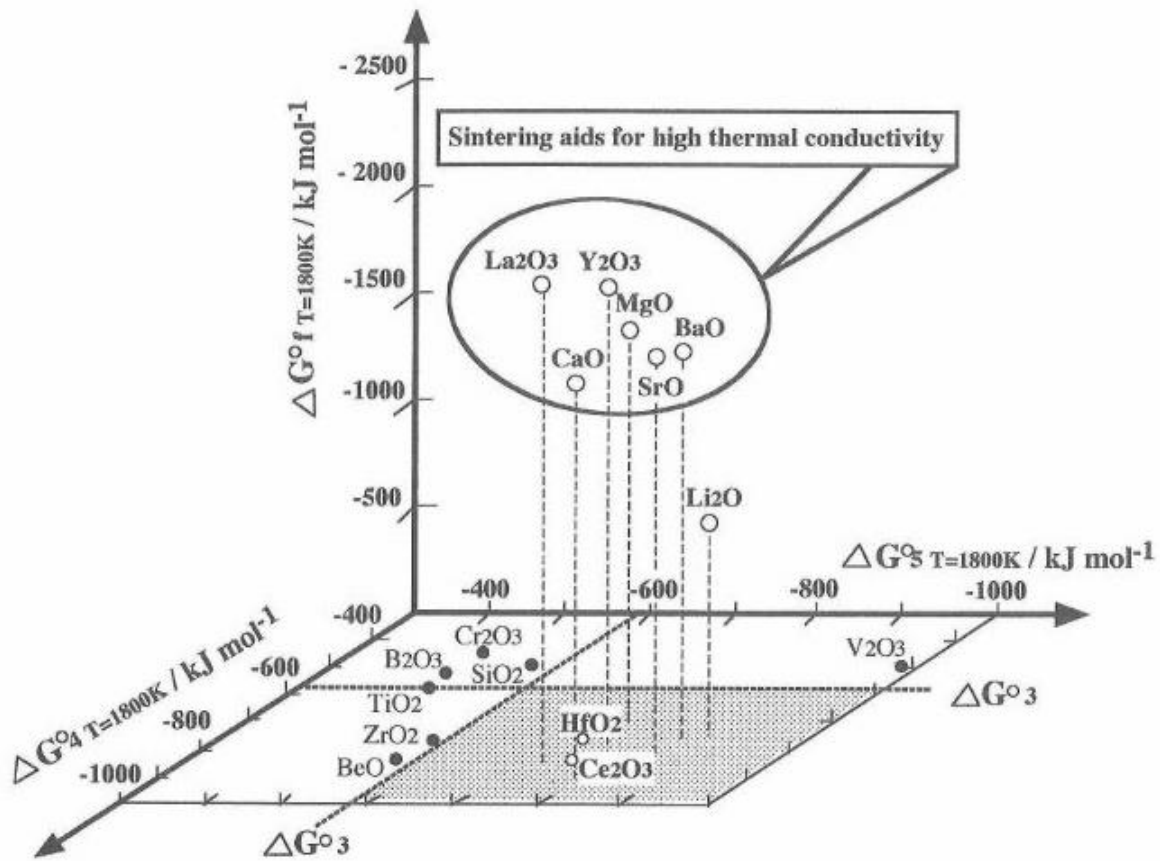
Fig. 4: Thermodynamic considerations for the formation of secondary phases in AlN, leading to high thermal conductuvities, according to [52]. The indices of the ΔG_0 values correspond to the reactions shown above this figure. Reprinted with permission from the Ceramic Society of Japan.

Secondary phases formed during sintering have lower thermal conductivity than AlN grains in general. The secondary phase may be removed by long sintering times at high temperatures, which will be discussed in chapter 2.1.4.3, but it might not even be necessary according to Jackson et al. [53], as the secondary phases are often found along grain boundaries and in triple grain junctions, due to a bad wetting behavior. They measured dihedral angles between the secondary phases and AlN exceeding 72.5°, which means that those phases are not stable in the material, and they tend to leave the sample. Even if the processing time is too short for the secondary phase to be completely removed, this leads to clean grain surfaces (because of the large dihedral angle) and direct AlN-AlN contact between grains. If this was not the case thermal conductivity would presumably be more limited due to secondary phases with lower thermal conductivity blocking conductive pathways.

To the knowledge of the author, the highest thermal conductivity in polycrystalline AlN reported in academic literature has been achieved using Y_2O_3 as sole sintering additive. Nakano et al. [14] were able to produce a polycrystalline AlN ceramic with Y_2O_3 as sintering additive with a

thermal conductivity of 148 W m^{-1} K^{-1} after one hour of sintering at 1800 °C in a tungsten resistance furnace. They managed to increase thermal conductivity up to 272 W m^{-1} K^{-1} by annealing at 1900 °C in a graphite crucible for 100 h, purifying the AlN lattice and removing secondary phase from the material. This leads to a second very important factor when sintering AlN, which must be considered, namely atmosphere control, which will be discussed in chapter 2.1.4.2. Horiguchi et al. describe a sample (1 wt.% Y_2O_3) with an even higher thermal conductivity of 275 W m^{-1} K^{-1} in patent US4847221A [54] at a sintering temperature of 1800 °C after 16 days of sintering on an AlN plate (covered in BN) in a carbon crucible. In general, samples with Y_2O_3 sintering additive reach high thermal conductivities at high sintering temperatures. Other sintering additives or combinations of additives can still deliver rather high thermal conductivities at lower sintering temperatures, which has been investigated by multiple research groups.
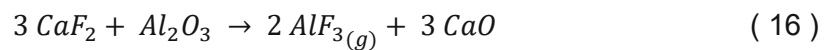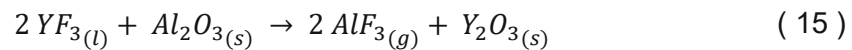
By varying the sintering additives and additive contents, sintering temperatures and final properties of the materials can be altered. Additives leading to secondary phases with lower melting temperatures such as CaO or Li_2O are used for low-temperature sintering of AlN. The system AlN-Al_2O_3-CaO forms a eutectic melt at 1265 °C [55], which is well below typical sintering temperatures. However, Molisani et al. [56] found that the viscosity of the melt is relatively high, preventing effective densification of the material without significant overheating and at high CaO contents large pores, preventing full densification, may form due to vaporization of the liquid phase, because of high vapor pressures at the sintering temperatures. Qiao et al. [57] also showed that while Ca-containing sintering additives might lower sintering temperatures, the properties of materials sintered exclusively with such additives are inferior to properties of samples using a combination of CaF_2 and Y_2O_3 as additives, even at a sintering temperature as low as 1650 °C. A sample with 2 wt.% CaF_2 reached 120 W m^{-1} K^{-1} after 8 h of sintering at 1650 °C, whereas a sample with 2 wt.% CaF_2 and 2 wt.% Y_2O_3 reached 148 W m^{-1} K^{-1} after the same heat treatment. In a different work [58] they added 2 wt.% Li_2CO_3 in addition to 2 wt.% CaF_2 and 2 wt.% Y_2O_3 and were able to increase thermal conductivity after the same heat treatment to 167 W m^{-1} K^{-1}. They attribute this improvement to the lower temperature at which a liquid phase forms and better wetting of the Li_2O containing liquid phase, leading to lattice purification of AlN even at low temperatures. Another advantage of Li_2O is its nature as fugitive sintering additive, leaving no impurities in the material, which confirms the findings of Watari et al. [55] who used Li-, Ca- and Y-containing sintering additive combinations in a work two years prior. It was found, that Li_2O lowers the liquidus temperature of the Y_2O_3-CaO-Al_2O_3-AlN system, enabling densification at low temperatures and volatilizes at temperatures exceeding 1300 °C. By using these additives, an inclusion of sintering

additives into the AlN lattice, which would limit heat transport, may be prevented, which is a potential problem when using additives such as SiO_2. Samples prepared with $LiYO_2$ and CaO additives exhibited a thermal conductivity of 172 W m^{-1} K^{-1} and a bending strength of 450 MPa after being sintered at 1600 °C.

Another approach for low-temperature densification with a combined sintering additive was investigated by Troczynski et al. [59] who achieved the highest densification at 1600 °C with a combined sintering additive, consisting of Y_2O_3, CaO, La_2O_3, CeO_2, SiO_2. This resulted in a material with high amounts of grain boundary phase and a thermal conductivity of 92 W m^{-1} K^{-1}. In an attempt to find another low-temperature sintering additive Lee et al. [60] used MCAS glass oxide powder (MgO-CaO-Al_2O_3-SiO_2) to sinter AlN. Full densification was achieved after sintering for 4 h at 1600 °C. Interestingly, the highest thermal conductivity of 46 W m^{-1} K^{-1} was measured in a sample sintered for 4 h at 1400 °C, while increasing the sintering temperature decreased thermal conductivity. By inclusion of nano-MCAS powder, thermal conductivity could be increased to 82.6 W m^{-1} K^{-1} at a sintering temperature of 1600 °C [60]. However, while SiO_2 might be an effective sintering additive for lowering sintering temperatures, Baranda et al. [61] pointed out that it leads to the incorporation of SiO_2 into the AlN lattice, which leads to increased scattering of phonons. By increasing SiO_2 contents the formation of SiAlONs was confirmed. In their study, AlN materials containing SiO_2 and Y_2O_3 sintering additives without traces of continuous grain boundary phase and a relative density exceeding 99 % were produced which had a low thermal conductivity of 25.8 W m^{-1} K^{-1}.

Yoshioka [62] describes the production of AlN materials with thermal conductivity of 200 W m^{-1} K^{-1} at sintering temperature lower than 1800 °C. Ytterbium oxide was used as sintering additive and sintering was conducted at 1700 °C using millimeter wave heating, in a hydrogen-containing nitrogen atmosphere.

Instead of oxide sintering additives, fluorides offer an intriguing alternative, which melt at lower temperatures and add another option of removing oxygen from AlN. Olhero et al. [47] used thermodynamic calculations and XRD data to get a better understanding of the behavior of CaF_2 and YF_3 during sintering. After the heat treatment, no fluoride compounds could be detected in the material and, as such, they propose the following reactions (15) and (16).

$$2\,YF_{3\,(l)} \,+\, Al_2O_{3\,(s)} \;\rightarrow\; 2\,AlF_{3\,(g)} \,+\, Y_2O_{3\,(s)} \tag{15}$$

$$3\,CaF_2 \,+\, Al_2O_3 \;\rightarrow\; 2\,AlF_{3\,(g)} \,+\, 3\,CaO \tag{16}$$

Large grain size can increase thermal conductivity of AlN, however, this usually comes with a negative impact on the material's strength. By using $CaZrO_3$ and Y_2O_3, Lee and Kim [63] were able to increase the flexural strength of an AlN material to 630 MPa after sintering at 1550 °C, due to a small grain size. Another sample composition exhibited 144 W m^{-1} K^{-1} after sintering at 1600 °C for 3 h, with a flexural strength of 568 MPa. In an attempt to increase thermal conductivity a two-step sintering process (3 h at 1600 °C and 2 h at 1400 °C) was employed, resulting in larger grain size (12.6 % increase), increased thermal conductivity of 155 W m^{-1} K^{-1}, while the flexural strength was mostly unaffected at 560 MPa. The secondary phase in one-step sintered samples was located along grain boundaries. Two-step sintering led to the secondary phase accumulating in triple-grain junctions.

Using different sintering additives can also lead to the development of properties inherently new to the material, as shown by Yoshikawa et al. [64], who used an optimized amount of Sm_2O_3 as sintering additive to establish conductive pathways of Sm-β-alumina at the grain boundaries of AlN to decrease the electrical resistivity by more than two orders of magnitude from 10^{-14} to a range of 10^{-10} - 10^{-12} Ω cm. However, such a network-like microstructure can have significant influence on thermal conductivity of the material, as shown by Kim et al. [65], who varied the microstructure of the secondary phases in AlN materials, using $CaCO_3$, Sm_2O_3 and Y_2O_3 as sintering additives. Materials with channel-like structures showed higher flexural strength and less electrical resistivity, whereas thermal conductivity was higher in materials with secondary phase in isolated pockets. Differences in oxygen content as the cause for the differences were not considered and maximum flexural strengths of less than 300 MPa seem rather low compared to other research.

2.1.4.2 Effect of the sintering environment and reducing conditions on AlN

By comparing results and discussions of multiple papers on the sintering of AlN it becomes quite clear that a reducing atmosphere leads to higher thermal conductivity in general, while it may lower mechanical properties. In section 2.1.4.1 the gettering function of the secondary phase, basically pulling oxygen atoms from the AlN lattice, was discussed. Reducing conditions also lower the oxygen content of the AlN lattice, as described in detail by Watari et al. [51].

Ishizaki and Watari [66] observed a decrease in oxygen content in sintered AlN parts, fired in a reducing atmosphere with Y_2O_3 as sintering additive. By increasing the sintering temperature, they were able to lower the oxygen content and increase the thermal conductivity from 30 W m^{-1} K^{-1} at 1500 °C to 140 W m^{-1} K^{-1} at 1800 °C. They proposed reaction (17) to reduce oxygen-containing compounds in typical AlN indcluding alumina or AlON:

$$\frac{2}{3} Al_2O_3 + \frac{2}{3} N_2 + 2\,C \ \rightarrow \ \frac{4}{3} AlN + 2\,CO \qquad\qquad (17)$$
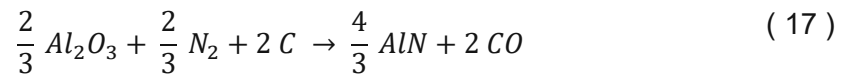
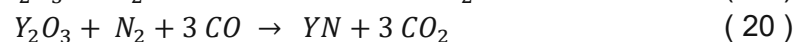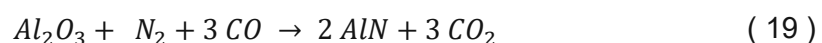Reaction (18), in which the yttrium oxide is reduced, was also proposed, even though no yttrium nitride (YN) was detected in XRD measurements.

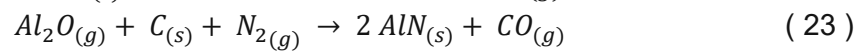$$\frac{2}{3} Y_2O_3 + \frac{2}{3} N_2 + 2\,C \ \rightarrow \ \frac{4}{3} YN + 2\,CO \qquad\qquad (18)$$
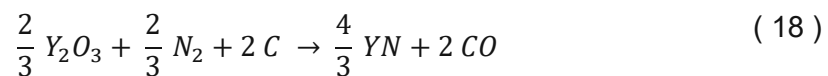
However, they also observed that at increased pressure (hot-isostatic pressing (HIP) at 60 MPa) the oxygen content in the sintered materials at all investigated sintering temperatures is conserved. Utilizing the Ellingham diagram, it could be shown that the increased gas pressure stabilized the oxides, preventing reduction by C.

In a later study, Watari et al. [51] proposed alternative reactions due to observations made by fracturing samples, which were wrapped in carbon foils during sintering, and analyzing the released gases by mass spectrometry. In addition to CO CO_2 was released, indicating that reactions (19), (20) and (21) are more likely to take pace.

$$Al_2O_3 + \ N_2 + 3\,CO \ \rightarrow \ 2\,AlN + 3\,CO_2 \qquad\qquad (19)$$
$$Y_2O_3 + \ N_2 + 3\,CO \ \rightarrow \ YN + 3\,CO_2 \qquad\qquad (20)$$
$$CO_2 + C \ \rightarrow 2\,CO \qquad\qquad (21)$$

Hundere and Einarsrud [67] were able to confirm the reduction of oxides through gaseous species by comparing the composition of samples sintered in differently packed powder beds, showing that in the powder bed with finer powder, the secondary phase was richer in Al_2O_3 than in a powder bed with coarse powder, indicating that the reaction is dependent on the diffusion of gases. Reactions (22) and (23) are proposed to take place. However, it is also suggested that at high CO partial pressures, the reaction of oxides with CO becomes dominant compared to the reduction through the formation of Al_2O (due to its lower diffusion through the powder bed).

$$Al_2O_{3(s)} + 4\,AlN_{(s)} \rightarrow 3\,Al_2O_{(g)} + 2\,N_{2(g)} \qquad (\,22\,)$$

$$Al_2O_{(g)} + C_{(s)} + N_{2(g)} \rightarrow 2\,AlN_{(s)} + CO_{(g)} \qquad (\,23\,)$$
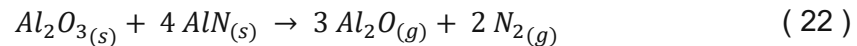
By removal of Al_2O_3 from the secondary phase, its composition changes from YAG ($Y_3Al_5O_{12}$, cubic (garnet)) to YAP ($YAlO_3$, orthorhombic (perovskite)) to YAM ($Y_4Al_2O_9$, monoclinic) to Y_2O_3. After all Al_2O_3 is consumed, yttria is reduced to YN.

In an attempt to further exploit the carbothermal reduction reactions described earlier, Nakamatsu et al. [68] coated AlN powder with carbon via thermal decomposition of methane gas at 800 °C. Using Y_2O_3 as sintering additive, the thermal conductivity of the material, which was sintered for 1 hour at 1800 °C in a tungsten furnace in N_2 atmosphere, increased from 184 W m^{-1} K^{-1} (without C) to 224 W m^{-1} K^{-1} (with C). It was also shown that an excess of C significantly reduces sintered density as well as thermal conductivity due to the formation of YN and gaseous reaction products (mainly CO_2). While the results of the approach to coat AlN powder with carbon speak for themselves, the carbon content has to be adapted to the powder to be sintered (i.e., starting oxygen content, sintering additives).

Kurokawa et al. [69] investigated a different approach for creating a reducing environment inside the samples by using CaC_2 as reductive sintering additive. When hot-pressed at 1800 °C for 1 h at 9.8 MPa, samples with 180 W m^{-1} K^{-1} with 2 wt.% CaC_2 were realized, whereas samples with the same amount of CaO exhibited 130 W m^{-1} K^{-1}. Oxygen defects at grain boundaries, which might act as thermal barriers, were presumed to cause this behavior. Such barriers were not present in samples produced with CaC_2.

In a study by Lee [6], all effects mentioned above are investigated simultaneously by sintering multiple AlN powders admixed with Y_2O_3 as sintering additive at 1820 °C in different environments (BN crucible, C crucible, AlN or no packing powder) for various times. It was shown that the amount of secondary phase has practically no influence on thermal conductivity, whereas all approaches that reduce Al vacancies in the material increase thermal conductivity. These approaches included the use of AlN powder with less oxygen content, longer sintering times and the addition of small amounts of carbon to the powder mixture as reducing agent. However, the reducing environment was found to be detrimental to densification due to a depletion of secondary phase, which is why a powder bed or BN crucible was used. This shows that while reducing conditions are important to increase thermal conductivity, they have to be balanced with densification.

2.1.4.3　Migration of the secondary phase and microstructural development

Multiple studies have found that secondary phases tend to move within the ceramic material during liquid phase sintering, thereby either agglomerating in triple junctions or segregating at sample surfaces.

One of the earliest works mentioning the migrative behavior of the secondary phase was conducted by Ueno and Horiguchi [70], in which AlN samples with Y_2O_3 sintering additive were sintered for up to 100 hours at 1800 °C in a furnace with a graphite heater in either an AlN or a C sagger. After 24 hours of sintering in the carbon sagger, a transparent sample, which achieved 258 W m^{-1} K^{-1} thermal conductivity, was obtained. Even though a decrease in density was observed with longer sintering times, thermal conductivity increased proportionally to the sintering time, which was more pronounced in the carbon sagger. Additionally, with longer sintering times in a carbon sagger, the secondary phase changed from $Al_2Y_4O_9$ to Y_2O_3 until signals from Y-compounds were not detectable anymore after 24 h. Samples sintered in the carbon sagger had a black YN film covering the surface of the samples. After removing the film and weighing the samples it was concluded that most Y was eliminated from the sample. This behavior is explained by a surface reaction of the grain boundary phase, which leads to an oxide concentration gradient, that in turn leads to grain boundary diffusion of the oxide. Fig. 5 illustrates this behavior, by first removing the secondary phase (purple) from the triple grain junctions, carbothermal nitridation of the secondary phase with the evolution of a YN layer on the surface of the samples and subsequently the removal of the YN layer by hydrolysis. Sintering in a tungsten resistance furnace on the other hand, led to negligible weight loss.
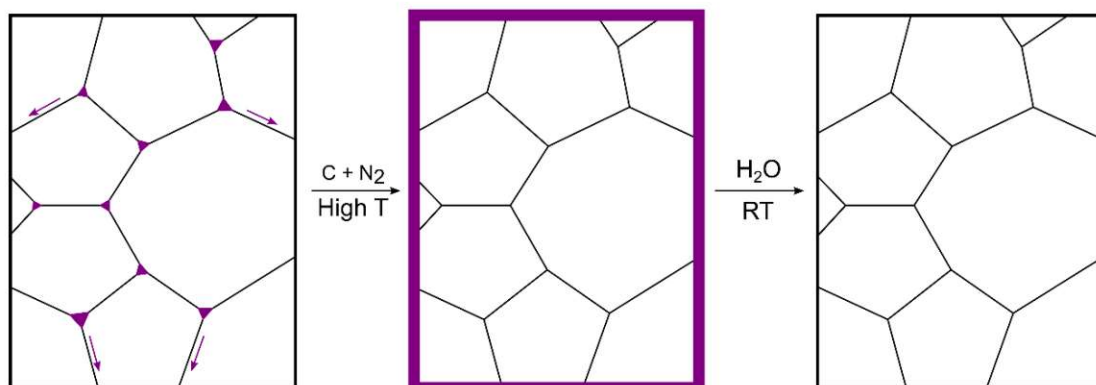

Fig. 5: Schematic of migrative behavior and elimination of the secondary phase in AlN materials. Redrawn from [70].

An investigation by Fu et al. [71] confirmed the migration of secondary phase from the bulk to the surface of samples produced with CaF_2 and YF_3 sintering additives and sintered in a BN crucible. However, despite describing the surface of samples as blueish-black, Y_2O_3 was detected on sample surfaces in XRD analyses instead of YN and below the surface of samples only mixed oxide phases were detected, which confirms the theory that mixed oxide phases migrate toward the surface, where they are reduced in a way that Al_2O_3 is reduced before Y_2O_3. The findings suggest an increased migrative behavior due to a change in chemical potential and capillary forces caused by the depletion of liquid phase.

Buhr and Müller [72] compared samples sintered in a graphite or a graphite-free Mo-furnace and found differences in the evolution of secondary phases along grain boundaries and grain edges. In the carbon-free environment, the secondary phase mostly accumulated as separate grains in the AlN matrix, whereas in the reductive environment, the secondary phase tended to form at grain edges. The investigations showed that the decrease in oxygen content due to the reducing atmosphere had a higher impact in increasing thermal conductivity than the microstructure and distribution of the secondary phase, which is suggested to have more influence in a material with low oxygen content in the AlN lattice but high secondary phase content.

Xu et al. [73] investigated the influence of packing powder on the sintering and properties of AlN ceramics with Sm_2O_3 sintering additive and found that sintering at 1830 °C in a graphite crucible without packing powder led to AlN materials with low amounts of secondary phase and a thermal conductivity of 166 W m^{-1} K^{-1}, whereas placing the green bodies inside AlN/BN packing powder led to materials with high amounts of secondary phase and lower thermal conductivity of 58 W m^{-1} K^{-1}. Another indication that carbothermal reduction reactions may have a major impact not only on thermal conductivity due to reducing oxygen impurities, but also on the migrative behavior of the secondary phase.

2.1.4.4   Sintering of AlN: Summary

The successful sintering of high thermal conductivity AlN utilizes a combination of multiple effect, which have been discussed extensively in the past sections of this work. For high thermal conductivity, samples have to be fully or close to fully densified, the AlN grains must be purified from defects (esp. oxygen defects) and contiguity between grains must be ensured. Most important for densification is the liquid phase formed by Al_2O_3 present on the surface and dissolved in the lattice of AlN grains and sintering additives as it not only leads to densification

but also purification of the AlN lattice because of the affinity of the secondary phases for oxygen. Multiple sintering additives with cations from alkaline earth metals group or lanthanide group have been confirmed to allow sintering of AlN, although the performance of the sintered samples can vary greatly, depending upon the additives used. CaO (added as carbonate or fluoride) and Y_2O_3 (added as oxide or fluoride) have been proven to be most useful. The sintering environment is another important factor for improving the properties of AlN, as reducing conditions may further purify the AlN lattice and lead to even higher thermal conductivity. Due to bad wetting behavior, the secondary phase tends to migrate toward the surface of samples. There, reducing conditions can further increase thermal conductivity by reducing the secondary phase, leading to even more secondary phase being pumped out. This clears the ceramic material from secondary phase at grain boundaries, which can contribute to higher thermal conductivity.

2.2 Thermal conductivity in solids

Materials with high and low thermal conductivity are sought after in today's industry. Insulators for various purposes need to block heat flow, requiring a low thermal conductivity, whereas thermal management systems, for example in high-performance electronics, require materials with high thermal conductivity to transfer the generated heat away from functional components to ensure stable operations.

Thermal conductivity λ describes the capability of matter to transfer heat from a source of higher temperature T_1 to a sink of lower temperature T_2, separated by distance d. Heat flux $\dot{Q}$ through the cross-sectional are A is described by Fourier's law (Eq. 1).

$$\dot{Q} = \lambda \cdot A \cdot \frac{T_1 - T_2}{d}$$

Eq. 1

Heat is transported by carriers. In metals most of this transfer is done by electrons, while in non-metallic solids phonons (often referred to as lattice waves) carry most of the energy. Derived from simple kinetic theory, Yang [74] describes thermal conductivity in solids as the sum of the products of total heat capacity C, particle velocity v and the mean free path of a particle l of various excitations α (electrons, phonons, photons, etc.), which is the distance the particles travel before a scattering event occurs (Eq. 2).

$$\lambda = \frac{1}{3} \cdot \sum_{\alpha} C_{\alpha} \cdot v_{\alpha} \cdot l_{\alpha}$$

Eq. 2

2.2.1 Thermal conductivity in AlN

In nonmetallic solids electrons cannot move freely and, as such, heat has to be transported by other means. As mentioned above, lattice vibrations, or phonons, are the major contributors to heat transport in nonmetallic solids. Slack [3] summarizes four criteria that have to be met in order to find nonmetallic solids with high thermal conductivity:

- Low atomic mass
- Strong interatomic bonding
- Simple crystal structure
- Low anharmonicity

AlN, as a ceramic material, relies on heat transport by phonons. By meeting those four criteria, AlN qualifies as potential high thermal conductivity material. A number of studies researched the correlation between oxygen content and thermal conductivity of AlN materials, however in research literature contradictory understandings of the thermal conductivity behavior can be found. Watari et al. [75] state grain boundaries and grain size of AlN grains are not as important as oxygen impurities and relate this to the fact that the calculated phonon mean free path is well below 100 nm and, as such, much smaller than the average grain size of polycrystalline AlN materials. Evidence of their theory in the form of AlN samples with similar oxygen content but vastly different grain sizes is shown. A normally sintered sample with 4 µm grain size exhibited 160 W m^{-1} K^{-1}, whereas a HIP sintered samples with 40 µm grain size had a thermal conductivity of 155 W $^{-1}$ K^{-1}, indicating no major influence of the grain size on thermal conductivity. Chen et al. [76], on the other hand, propose that the microstructure and porosity of the AlN material has a major influence on its thermal conductivity, observing that samples with secondary phase accumulated in triple-grain junctions exhibit higher thermal conductivity than samples in which the secondary phase was present at grain boundaries.

Harris et al. [77] intensively studied oxygen-related defects, their influence on thermal conductivity, and how the defects change with increasing oxygen contents by luminescence spectroscopy and X-ray diffraction. It could be shown that, at first, Al vacancies are caused by the incorporation of O in the AlN lattice. With increasing oxygen concentrations (> 0.75 %), the Al vacancies are removed in favor of octahedrally coordinated Al atoms, leading to increased phonon scattering. At even higher oxygen levels, the octahedrally coordinated defect Al-sites may form larger defects and stacking faults. Two regions for thermal resistance (inverse thermal conductivity) evolution depending on the nature of the oxygen defects are defined, which results in linear dependence of thermal resistance vs. oxygen content with different slopes, depending on the region. Potter et al. [78], on the other hand, did not find a clear indication for two distinct regions with different slopes for the thermal resistance vs. oxygen content in their study on oxygen defects in AlN, investigated by secondary ion mass spectrometry (SIMS).

As indicated by the previous paragraphs, thermal conductivity and the effect of certain parameters have not been fully understood yet. To the knowledge of the author no "agreed-upon" theoretical understanding has been developed. This is highlighted as well in the introduction of a work from 2019 by Xu et al. [79], who used a modern analytical approach as well as first-principles calculations to get a better understanding of the thermal conductivity of

AlN. It is estimated that phonons with mean free paths of 0.3 μm and 7 μm contribute to 50 % and 10 % of thermal conductivity in bulk materials, respectively.

2.3　Additive manufacturing of ceramic materials

With many additive shaping technologies emerging over the past years EN ISO/ASTM 52900 [80] was created to define categories and nomenclature.

Additive manufacturing (AM) has been a highly discussed topic in academic, industrial, and even hobbyist environments. Most three-dimensional parts, especially from metallic and ceramic materials, are produced by subtractive methods such as milling, or formative methods such as forging and casting. Especially for subtractive methods, tools are required and often the material removed from the workpiece is wasted. Formative methods use expensive molds and are not economical for processes in which only a few pieces will be produced in a series. AM replaces the need to remove material from the workpiece with building the desired geometry directly from a feedstock and without a mold, thus tool and material costs can be saved. This promotes prototyping of parts, because no major investment in tooling and molds must be made. Such processes, in which parts are manufactured directly into the desired shape by stepwise addition of material without the need for material removal (although some geometries might require support material to be removed) can be summarized as additive manufacturing methods. Many different approaches to additive manufacturing for a variety of materials have been developed, with the most diversity to be found in polymers. However, additive manufacturing of high-performance inorganic materials like metals, hardmetals and ceramics is a research focus of the material science community.

According to the EN ISO/ASTM 52900 [80] additive manufacturing can be divided into single-step and multi-step processes, depending on whether the geometry and the functional properties of a material can be realized in one processing step or in multiple distinctive steps (e.g., the shape is acquired in a first AM step, whereas properties of the material are acquired during a sintering step). It is important to distinguish between the fundamental properties of materials and the desired properties of the manufactured object. A single-step process may lead to the acquisition of shape and basic properties (e.g., metallic properties) of a material. However, to acquire the desired properties of the object heat treatments, hardening or other processing steps may be necessary. To better illustrate the difference between single- and multi-step processes, two examples, both supplying feedstock in a powder bed, are described. In both processes a slice of a three-dimensional structure is consolidated in the powder bed before new loose powder is supplied over the consolidated slice.

An example for a single-step process using a powder bed is selective laser sintering, for which a metal powder is selectively melted by irradiation and as such consolidated layer by layer. Using this process, an object with three-dimensional shape and metallic properties can be realized in one step; however, to achieve properties which may be required for a specific part, additional heat treatment steps may prove necessary. An example for a multi-step process would be binder jetting, in which a polymeric binder is deposited onto a powder bed consisting of ceramic or metallic particles and a three-dimensional green part is realized layer by layer. The green part, while it already has a shape close to the desired shape, does not possess the same properties as the inherent properties of the particles in its polymer matrix. Only after debinding and heat treatment steps, the properties of the object correspond to the ceramic or metallic material properties.

Additive manufacturing requires different strategies to tackle certain tasks and requirements for manufactured parts compared to conventional methods but it also opens a host of new possibilities in shapes accessible or in the combination of multiple materials in one part. [81, 82].

2.3.1   Methods for ceramic AM

Zocca et al. [83] have reviewed multiple methods for the additive manufacturing of ceramic materials. They make a distinction between indirect and direct methods, the difference being that, for indirect methods, the shape is inscribed into a large amount of feedstock (e.g. laser sintering in a powder bed), whereas in the case of direct methods, material is only deposited to give the modelled shape and no additional material (except for support structures) is needed. Table 3 shows a comparison of the AM methods described in the review. All described methods, except for laser sintering, would be considered multi-step processes as described in EN ISO/ASTM 52900 [80]. Below the table a short overview describing the technologies (using information from [83]) is given, with a focus on sterelithography, as it is the focus of this work.

Table 3: Comparison of additive manufacturing methods according to [83]. Reprinted with permission of John Wiley and Sons.

Technology[†]	Feedstock (liquid or solid)	Dense struts (dense ceramic, but limited volume)	Monolithic	Part dimension[‡] (size that can be produced economically)	Surface (quality of parts, not of single struts)	Precision	Cost of feedstock preparation	Cost of process	Direct versus indirect
P-3DP	Solid	No	No	M-XL	Medium	100 μm	Low	Medium	Indirect
P-SLS	Solid	No	No	M-L	Medium	100 μm	Low	High	Indirect
P-SLM	Solid	No	No	M-L	Medium	100 μm	Low	High	Indirect
S-3DP	Liquid	Yes	Yes	M-XL	High	100 μm	Low	Medium	Indirect
S-SLS	Liquid	Yes	Yes	M-L	High	100 μm	Low	High	Indirect
SL	Liquid	Yes	No	XS-M	High	<1 μm	Medium-High	Medium	Indirect
LOM	Solid	Yes	Yes	M-L	Medium	100 μm	Medium	Medium	Indirect
DIW/ Robocasting	Liquid	Yes	No	S-XL	Low	10 μm	Low-Medium	Low	Direct
FDM	Liquid	Yes	No	S-M	Low	100 μm	Medium	Low	Direct
DIP	Liquid	Yes	Yes	S-M	Medium	10 μm	High	Medium	Direct
Direct Dep	Liquid				Low				Direct

[†]The definition of the acronyms for each technology is given later in the text.
[‡]XS = 100 μm; S = 1 mm; M = 10 mm; L = 0.1 m; XL = 1 m.

Powder based 3 D Printing (P-3DP, "binder jetting")

For this method a powder bed is spread layer by layer and sliced cross sections of the object are solidified by deposition of a binder material. After the AM process, excess powder can be removed from the part, which can then be debinded and sintered. By using powders of preceramic polymer, which can be locally dissolved with the use of organic solvents instead of a binder, particles can be fused, bypassing the need for additional binder, which has to be burnt out.

Powder based selective laser sintering/melting (P-SLS / P-SLM)

Similar to the aforementioned process, in SLS a powder bed is used however, solidification is of the cross-sections is induced by a laser causing either a polymeric binder, admixed to the ceramic powder, to melt or directly sintering the ceramic powder, without a polymeric binder. SLM (selective laser melting) is an alternative to SLS in which preheated ceramic powders are melted, to form a solid object. SLS (without binder) and SLM are the only two techniques, which allow single-step AM processing of ceramic materials.

Slurry based 3 D Printing (S-3DP / S-SLS)

Akin to the two methods described above, cross-sections of the object to be printed are fixed with binder or laser-sintered in each layer. However, for depositing a layer, a slurry, consisting

of liquid medium and ceramic particles, is spread over the working area, using a doctor blade. The liquid medium is pulled into the porous, dry substrate, leading to a compaction of the particles left behind, which is higher than typical powder packing densities. The formed layer of particles then acts as the substrate for the next layer.

Stereolithography (SL)

In Stereolithography a part is realized by the photopolymerization of thin layers of photoactive polymer resin, including ceramic particles. High spatial resolution can be attained by either directing a laser to certain points to be polymerized in a layer or by illuminating the build area, blocking out areas (e.g., by LCD Screens), which are not to be polymerized. After removal of the part and cleaning of excess slurry, thermal processing (debinding and sintering) yields ceramic parts.

The first device for the additive manufacture of polymers by a stereolithography process, similar to methods used today, was patented by Hull in 1984 (US4575330A [84]). Devices before the one just mentioned used the interference of multiple beams of light in a liquid resin to polymerize three-dimensional objects. Griffith and Halloran [85] were the first to report the usage of stereolithography (SL) using photopolymerizable ceramic suspensions including alumina and silica in 1996. Even though the geometries produced in that study were rather simple and sintered parts appeared warped, compared to the CAD designs the feasibility of introducing ceramic particle into the SLA process was proven. Since then, research has been on-going to increase the spectrum of ceramic systems to be used in SL including alumina [86, 87], zirconia-toughened alumina [82, 88], zirconia-based materials [89], silicon nitride [90] and many more.

The precision and flexibility of SLA processes have opened many areas of application such as bone implants made from hydroxylapatite [91] or β-tricalcium phosphate [92], bioceramic materials, which can be printed as scaffolds for bone repair purposes. Another medical application is the use of additively manufactured zirconia (or yttria-stabilized tetragonal zirconia polycrystal) crowns and bridges in dental reconstruction [89].

Laminated object manufacturing (LOM)

Layers, formed by extrusion or tape casting are transferred over a building platform, where the cross-section of the part is cut out of the tape. The part can be moved down to allow for the next layer to be deposited.

Direct Inkjet printing (DIP)

As the name suggests, this technique functions similarly to an inkjet printer, as droplets of a slurry with low solids loading are deposited from a printhead. By moving the printhead and the part relative to each other, three-dimensional objects can be manufactured. Rheological properties of the ink are critical to ensure dimensional accuracy of the parts.

Fused deposition modeling (FDM)

Also called robocasting, a slurry with higher solids loading than in DIP, is deposited thorough a nozzle, building up a three-dimensional part, by relative movement of the nozzle and building platform.

2.3.2 Application of AM for AlN materials

A number of research papers on the additive manufacturing of AlN have been published recently. Due to vastly different processing parameters, ranging from different AM methods to sintering temperatures, sintering additives and properties characterized, a comparison of the literature is not possible. A short description of select papers on the topic is given below.

Jankowski et al. [93] published the first (to the knowledge of the author) report of AlN materials used in additive manufacturing. They realized AlN parts by stereolithography with a thermal conductivity of 165 W m^{-1} K^{-1}. They successfully produced substrates for microchannel cooling of thermal stacks.

Diaz-Moreno et al. [94] claim to have used binder-jetting to produce cylindric AlN ceramics without sintering additives. After fabrication of green parts and HIP treatment at 1900 °C and 206 MPa for 8 hours, the sintered parts reached relative densities of 60 % and thermal conductivities below 5 W m^{-1} K^{-1}.

Duan et al. [95] utilized digital light processing with a high-viscosity AlN paste with yttria sintering additive to produce complex shapes. Samples sintered at 1845 °C exhibited thermal conductivity of 155 W m^{-1} K^{-1} and a bending strength of 265 MPa (average of five samples).

Lin et al. [96] also used DLP to manufacture AlN ceramics with yttria sintering additive, however, their work focused mostly on the printing process and they only published bending strength of their sintered parts with more than 99 % relative density, which was 398 MPa.

Ozog et al. [97] used a printer from Lithoz GmbH to fabricate AlN parts and sintered them at 1800 °C. They used Al_2O_3 and Y_2O_3 sintering additives and achieved a relative density of 84 % and thermal conductivity of 4 W m^{-1} K^{-1} in printed parts. Pressed reference parts using the same starting powders and heat treatment yielded more than 96 % relative density and a thermal conductivity of 76 W m^{-1} K^{-1}.

Belmonte et al. [98] used robocasting as a direct method for additive manufacturing of AlN. They produced cellular structures with anisotropic thermal conductivity (relative to the building direction). Residual porosity in the resulting material amounted to of 14 %.

3   Experimental procedure

In this section the experiments conducted during this project will be discussed. They will be separated into investigations on the AlN powder properties and stability in various environments, the hot-pressing of AlN samples with varying amounts of sintering additives, conventional production of AlN samples by cold-isostatic pressing and sintering, the description of the additive manufacturing process used to produce AlN samples, and the characterization methods utilized.

3.1   Raw materials used in powder systems

Three AlN powders from two manufacturers were used in this study. Additionally, multiple sintering additives were used to enhance sinterability and final properties of AlN samples.

Aluminum nitride powder grades

Three aluminum nitride powder grades from two suppliers were utilized in this work, which are listed in Table 4 below. Grade BT and Grade C AlN powders are produced by H.C. Starck (Germany). Grade JM AlN powder is produced by Toyo Aluminium K.K. (Japan). Grade C powder was used for most investigations to ensure comparability. If other powders were used it will be clearly stated. Ceramic powder manufacturing of H.C. Starck has been sold to Höganäs (Sweden) during the course of this work, but due to consistency H.C. Starck will be used in the nomenclature.

Table 4: AlN powders used in this work. For simplicity, the powder grade names from the producers will also be used in this document.

Powder grade	Producer	According to supplier*		
		O-content (%)	N-content (%)	D50 (µm)
Grade C	H.C. Starck/Höganäs	1.1	33.9	1.7
Grade BT	H.C. Starck/Höganäs	0.8	34.4	2
Grade JM	Toyo Aluminium K.K.	0.6 - 0.8		2.0 - 3.1

*For Grade C and Grade BT, data from an analysis certificate of the first batch received in the project was used; and for Grade JM data from a "typical data sheet" was used.

Sintering additives (SA) and sintering additive precursors

Calcium oxide (CaO) and yttrium oxide (Y_2O_3, Grade C, H.C. Starck; average particle size 0.8 µm) were the two sintering additives with the highest impact in this study. As CaO is not stable in the regular laboratory atmosphere, precursors had to be used. If not otherwise stated, CaO was added as dried (2 h at 300 °C in air) calcium carbonate ($CaCO_3$, Alfa Aesar, 99.5 % metals basis, average particle size 5 µm), which would decompose during sintering or a preceding thermal treatment, to the exact amount of CaO. Calcium oxalate (CaC_2O_4, 99 %, Alfa Aesar) was used for AM samples, due to the instability of $CaCO_3$ in the AM slurry.

Alternative sintering additives investigated were strontium oxide (SrO), added as strontium carbonate ($SrCO_3$) as well as calcium nitrate ($Ca(NO_3)_2$), strontium nitrate ($Sr(NO_3)_2$), and yttrium nitrate ($YNO_3)_3$) as soluble additives which can be dissolved in the liquid medium during the wet mixing process.

3.2   Stability of AlN in various environments

AlN is prone to hydrolysis in certain conditions, which is why powders are often modified prior to processing. Ssurface modification of AlN powders as means of protection against hydrolysis during powder processing or additive manufacturing is not necessary if AlN powders are stable in the environments relevant to processing. As such, the hydrolysis behavior of the powders in various liquid media (water, isopropyl alcohol and a model binding agent for LCM), as well as laboratory atmosphere (30 to 40 % relative humidity) was characterized.

To evaluate the stability of AlN in various environments critical for processing, AlN powders were subjected to said environments for varying amounts of time and the resulting oxygen content was measured by inert-gas fusion technique using a TC400 Nitrogen/Oxygen Analyzer (LECO Corporation). Phase composition after the hydrolysis reactions was also measured by X-ray diffraction for a select few samples.

3.2.1   Sample preparation for stability investigations of AlN powders in various environments

Stability of Grade C, Grade BT and Grade JM AlN powders in the atmosphere in the laboratory (23 °C, 30 to 40 % relative humidity) was measured by exposing the AlN powders to the atmosphere in PP containers, covered with punctured Al foil, for up to 6 weeks. After this, the oxygen content of the powders was directly determined.

Samples for testing the stability of AlN in liquid media such as deionized water and isopropyl alcohol (technical grade) were produced by adding 10 wt.% AlN powder to the medium in a PE container, resulting in a typical sample size of 100 g. To minimize the effects of atmospheric water vapor and oxygen, the containers were flushed with N_2 and sealed using thermoplastic sealing film. The containers were then placed on a roller table to ensure continuous agitation. After set amounts of time samples were taken. The suspension samples were centrifuged (3000 rpm, 3 minutes), the liquid was decanted, and the solids were dried at 20 mbar at room temperature. In later experiments it was found that drying the samples overnight at 80 °C in a vacuum drying oven reduces the deviation of the measurements using a LECO elemental analyzer.

The stability of AlN powders in a model binding agent on acrylate basis provided by Lithoz GmbH, which was considered to be chemically similar to what would be used later in the project

for AM of AlN samples, was also investigated. The procedure up to the sampling was consistent with the experiments in other liquid media, with the exception that the powder-to-binding-agent-ratio was set to 1:1 by volume, which is closer to actual processing conditions during AM, for which slurries with 40 to 50 vol.% solid content are often used. Typically, 17 mL of slurry was prepared from each powder. After set amounts of time, a slurry sample (approx. 5 mL) was transferred to a centrifuge tube, mixed with acetone, followed by centrifugation and decantation. The solids were then washed once with isopropyl alcohol and twice with acetone. The washing steps were also always followed by centrifugation and decantation steps. The centrifuge tubes were then placed in a vacuum desiccator at a pressure of 20 mbar to remove most of the liquids. The powders were removed, placed inside 12 mL PP containers, and dried in a vacuum oven at 80 °C overnight.

Table 5 shows the samples that were prepared during the evaluation, arranged by powder type. The time denotes the maximum time after which a sample was taken. The oxygen content of samples was then determined by inert gas fusion technique, explained in section 3.7.2.

Table 5: Overview of hydrolysis stability experiments conducted with AlN powders. Experiments marked with an asterisk were conducted by Felix Frank during an elective lab course.

Powder Type	Reference	Water	Isopropyl alcohol	Model binding agent	Lab atmosphere
Grade C	-	24 h	72 h	18 weeks	6 weeks
Grade BT*	-	24 h	72 h	18 weeks	6 weeks
Grade JM*	-	24 h	120 h	18 weeks	6 weeks

3.3   Preparation of powder mixtures including AlN and sintering additives

Sintering additives (SA) were added to AlN in order to achieve adequate densification and thermal properties. Powder mixtures were prepared by a combination of wet and dry mixing/milling techniques. Milling was not the intention while preparing the powder mixtures, but due to the nature of the mixing techniques used, was not avoidable. To ensure consistency, the mixing process was not altered over the course of this work.

If sintering additives were added as precursor compounds, the number describing the powder mixture always refers to the amount of oxide sintering additive, after decomposition of the precursor compound. "1 Ca + 3 Y" translates to powder mixtures with 96 wt.% AlN, 1 wt.% CaO and 3 wt.% Y_2O_3 after the decomposition of the carbonate. CaO was added as $CaCO_3$ in all mixtures, if not explicitly stated otherwise.

3.3.1 Mixing

In a typical experiment, about 40 g of AlN was weighed into a zirconia (ZrO_2) container with four Y-TZP (yttrium stabilized zirconia) milling balls (diameter = 20 mm). The respective amounts of sintering additives (SA) were added and the container was filled with 40 mL of isopropyl alcohol (IPA, technical grade). The container was then closed, put into a planetary rotary mill (Fritsch Pulverisette 6), and milled for 5 minutes at 150 rpm. After milling the slurry was transferred to a beaker, using additional IPA. To prevent contamination of powder mixtures, the containers were cleaned between runs. If switching AlN powders, a cleaning run was performed by cleaning the containers, weighing in 10 g of the new AlN powder and 40 mL of IPA, milling for 10 minutes at 150 rpm, removing the contents and cleaning the containers again.

Subsequently, ultrasonic processing was conducted using a UP400S instrument (Hielscher) at 40 % amplitude with a cycle of 0.5 for 10 minutes, followed by removal of the IPA in a rotary evaporator at 137 mbar and 50 °C bath temperature. As soon as all solid contents were sticking to the side of the flask, the flask was removed, and the solids were scratched off using a polyamide spoon and crudely pulverized before the flask was fixed to the evaporator again. The rough powder was then dried at minimum pressure achievable by the pump for at least 20 minutes. After that time a pressure below 15 mbar was reached, which equals the pressure achievable with an empty flask installed. The dried powder was transferred to a 250 mL PE bottle with 40 Y-TZP milling balls (diameter = 10 mm). After 15 minutes on a tumbler mixer (Turbula T2F, WAB) the powder was sieved using a sieve with 1 mm mesh openings. The finished powder mixtures were transferred to PP containers, which were sealed under flowing N_2.

3.3.2 Optional thermal treatment of powder mixtures to decompose sintering additive precursor compounds

CaO turned out to be one of the most promising sintering additives, especially in combination with Y_2O_3. CaO reacts with the water in the atmosphere to $Ca(OH)_2$, which is why dried $CaCO_3$ (dried at 300 °C in air for 2 h) was used to produce stoichiometric mixtures. Upon heating to 900 °C, $CaCO_3$ decomposes to produce CaO and CO_2. In some samples the gas formed by this decomposition prevented densification of the powder compacts during sintering without external pressure applied. The decomposition temperatures of $CaCO_3$ and other precursor compounds were determined by thermal analysis, to estimate suitable temperatures for thermal treatments (see Table 17). Decomposition of all SA precursors was conducted at 950 °C, except for $SrCO_3$, which was decomposed at 1150 °C.

The powder mixtures were filled into alumina crucibles (approximately 20 g per crucible) and placed inside a tube furnace. The powders were heated to the respective temperatures with a heating and cooling rate of 3 K/min. Holding times were set between 2 and 4 hours. In early experiments it was found that 2 hours may not suffice for full decomposition of $CaCO_3$, which is why the holding time was increased to 4 hours. The calcinated powders were then again put on a tumbler mixer with Y-TZP milling balls (diameter = 10 mm) for 15 minutes, to enhance ease of processing.

To investigate oxygen uptake of AlN powders during powder processing and the heat treatment for the decomposition of sintering additive precursors, Grade C AlN powder without additives was treated as if a powder mixture was prepared (milling, rotary evaporation, mixing) and then heated to 950 °C and 1150 °C in N_2. Oxygen content was measured after the various preparation steps by the inert gas fusion technique (see section 3.7.2). It was found that the tube furnace used for the first experiments (SA-precursor decomposition furnace A) did not provide a sufficiently clean N_2 atmosphere, resulting in oxygen uptake. To counteract this, thermal treatment was also conducted in a different tube furnace setup (SA-precursor decomposition furnace B), which allowed for purging of the tube (three times vacuum followed by N_2) and purification of the N_2 by using a drying, as well as an oxygen absorber column. SA-precursor decomposition furnace B is thermally limited to temperatures below 1100 °C, so experiments at 1150 °C were not conducted in this furnace. Thermal treatment to form oxide sintering additives from additive precursors prior to shaping will be denoted with "TT A" and "TT B", which is short for "thermal treatment" in the respective tube furnaces.

3.4 Hot-pressing of powder mixtures

Hot-pressing of AlN powders and powder mixtures including sintering additives was carried out to generate fully densified samples which were then used to generate benchmark values for thermal and mechanical properties to be reached with conventionally sintered samples.

AlN powders without additives or powder mixtures were filled inside a round graphite die. Approximately 13 g of powder were used in a die with 30 mm diameter and 75 g in a die with 50 mm to obtain samples with heights of more than 5 mm or 10 mm, respectively, after hot-pressing. To prevent consolidated samples from sticking to the die surfaces after hot-pressing, the faces of the cylinder dies were covered with graphite foil. To increase the powder compaction, the powder was filled into the die under light tapping. The die was then transferred into the hot press (HP W 150, FCT, Germany) and pre-compacted with a force of 5 to 10 kN. The hot-press was then purged multiple times with vacuum and N_2 cylces.

Hot-pressing was conducted at a N_2 pressure of 1050 mbar. Due to the use of a pyrometer to measure the temperature of the die, the hot-press was first heated with a constant power draw of 4 kW, resulting in a heating rate of 10 K min^{-1} up to 600 °C, the temperature at which the pyrometer starts to give a signal. At 650 °C the uniaxial force was increased from 10 kN to 25 kN (for the 30 mm die) or 69 kN (for the 50 mm die) over the span of 5 minutes, resulting in a pressure of 35 MPa for both dies. After the correct pressure was reached, heating was continued at a rate of 10 K min^{-1} to 1800 °C. This temperature was held for 2 h before cooling at a rate of 10 K min^{-1}. At 600 °C the pressure was released.

The pressed samples had to be removed using a laboratory press, and the faces of all samples were cleaned and ground (120 µm diamond embedded wheel) to provide a clean and even surface. The initial surface after hot-pressing was rather uneven, owing to the fact that powder was filled into the die manually, possibly leading to uneven packing density. After grinding, the density of all samples was measured by liquid displacement or an infiltration (immersion method as described in EN 623-2 [99]) method using water.

Due to a critical failure of the hot-press, only few samples were produced in-house, with most samples being hot-pressed by RHP-Technology (Austria) using a HPW 315/400-2200-1000-PS/SP instrument (FCT, Germany). The only major difference in the hot-pressing process was that five samples were produced per run and that graphite foil was put between the powder and the die on the lateral surfaces, instead of only the faces.

Table 6 shows an overview of samples produced by hot-pressing. Highlighted samples were produced by RHP-Technology, also denoted by "RHP" instead of "HP" in their nomenclature.

Table 6: Hot-pressing experiments conducted during this study. CaO was added as $CaCO_3$. The sample highlighted with an asterisk was produced and characterized by Felix Frank during an elective lab course.

Name	AlN powder grade	Sintering additives	Sample Diameter (mm)
HP_C_30_1	Grade C		30
HP_C_30_2	Grade C		30
HP_C_3Y_30_1	Grade C	3 wt.% Y_2O_3	30
HP_C_50_1	Grade C		50
HP_JM_50_1*	Grade JM		50
RHP_C_50	Grade C		50
RHP_BT_50	Grade BT		50
RHP_JM_50	Grade JM		50
RHP_C_1Y_50	Grade C	1 wt.% Y_2O_3	50
RHP_C_2Y_50	Grade C	2 wt.% Y_2O_3	50
RHP_BT_1Y_50	Grade BT	1 wt.% Y_2O_3	50
RHP_C_05C05Y_50	Grade C	0.5 wt.% CaO + 0.5 wt.% Y_2O_3	50
RHP_C_1C_50	Grade C	1 wt.% CaO + 1 wt.% Y_2O_3	50
HP_C_50_2	Grade C		50

3.5   Sintering of AlN without application of external pressure

In contrast to hot-pressing, the powder mixtures were shaped prior to heat treatment for "conventional" sintering experiments. Cold-isostatic pressing was chosen as shaping technique. Green bodies were sintered with variations in sintering times and environments. To realize the latter, sintering was conducted in three different furnaces, which were all equipped to enable evacuation and purging cycles with N_2.

To ensure comparability between sample series with varying sintering parameters, only one AlN powder was extensively studied. If not stated otherwise, Grade C AlN powder was used in CIP samples.

Properties typically investigated in CIP samples included density, thermal conductivity, mechanical strength, Vicker's hardness and microstructure (SEM).

3.5.1   Shaping of samples by cold-isostatic pressing (CIP)

For cold-isostatic pressing, powder mixtures were filled into silicone molds under light tapping to fill the molds with sufficient amounts of powder. The molds were then sealed and submerged in the pressure liquid. The samples were compacted at 300 MPa for one minute in a laboratory press (PW KIP, P/O/WEBER), before the pressure was released over the course of two minutes. Special care was taken to prevent samples from getting into contact with the pressure liquid. Three cylindrical molds and one cuboid mold were used. Typical green body dimensions are given in Table 7. The cuboid shaped specimens were often warped or thinner at one end. If severe deviations from the expected geometry were observed, specimen geometry was adjusted using SiC paper (600 grit). Green bodies were weighed and measured before sintering.

Table 7: Typical sample shapes produced by CIP. The dimensions and weight refer to the samples in the green state.

	Dimensions (mm)		Weight (g)
	Diameter	Height	
Cylinder, small	10.0	4.5	0.7
Cylinder, large	13.5	2 - 4	up to 1.2
Cylinder, long	10	30	4.5
Cuboid	7 x 7 x 40		3.6 to 3.8

3.5.2 Sintering of samples

Two different types of crucibles were used for sintering. In reducing environments cylindrical graphite crucibles were used, whereas in non-reducing atmosphere a cuboidal alumina crucible was used. The samples were placed onto coarse alumina grains to prevent the samples from either sintering onto the alumina crucible or to create distance between the samples and the graphite crucible, if no other powder bed surrounding the samples was used.

The following furnaces were used for sintering:

Graphite furnace (HP W 150, FCT, Germany): The hot press used in this study can also be used without the application of external pressure and reaches temperatures up to 2200 °C in vacuum, N_2 or Ar atmospheres. As stated in section 3.4, a pyrometer aimed at the crucible was utilized for temperature measurement and control. The insulation and heating elements inside the furnace are made from graphite, leading to a reducing environment during sintering. Graphite crucibles were used in this furnace.

Hot-isostatic press (FP W 1, FCT, Germany): The hot-isostatic press (HIP) used in this study allows for sintering at gas pressures of up to 120 bar with Ar or N_2. Graphite parts inside the furnace lead to a reducing environment during heat treatments. In this furnace a crucible made of graphite was used.

Corundum tube furnace (CTF-1800, Carbolite Gero, UK/Germany): The tube of this furnace can be evacuated or filled with a variety of gases. A thermocouple is used for temperature measurement. However, the thermocouple is outside of the tube, which might

entail less accurate and less responsive readings. Unlike the other two furnaces described, this furnace utilizes $MoSi_2$ heating elements, located outside of the furnace which allow for a maximum temperature of up to 1800 °C. Thus, no graphite parts are located inside the tube, and the sintering atmosphere is not reducing when N_2 is used during sintering. Alumina crucibles were used for sintering in this furnace.

Major parameters like heating rate, purging cycles and N_2 grade (99.999 %) were consistent between the sintering cylces in the different furnaces. For consolidation without application of external pressure three purging cycles (vacuum followed by N_2) were conducted. In the graphite furnace an absolute pressure between 10^{-3} to 10^{-2} mbar was reached after 5 minutes of evacuation. The pressure inside the HIP reached approximately 10^{-1} mbar during evacuation. The corundum tube furnace was not equipped to measure absolute pressures, and instead the evacuation was stopped after 5 minutes, which was proposed to be adequate, given the lower volume of the tube, compared to the hot-press.

3.5.2.1   Preliminary sintering experiments without utilization of powder beds

Preliminary experiments (Table 8) without using a powder bed inside the crucibles were conducted in the graphite furnace, as well as in the corundum tube sintering furnace. "TT A" or "TT B" indicates thermal treatment of the powder mixtures to decompose precursor sintering additive compounds (e.g., carbonates and nitrates) in the respective SA-precursor decomposition furnace. Table 8 gives an overview over the preliminary experiments conducted.

Table 8: Preliminary consolidation experiments conducted with samples shaped by CIP. Grade C AlN powder was used in all experiments. All samples were sintered at a maximum temperature of 1700 °C and 2 h of holding time. If not stated otherwise, SrO and CaO were derived from the respective carbonate compounds. Michael Göschl and Eva Szoldatits conducted the experiments listed in this table in elective lab courses.

Sintering conditions	Sintering additives	Thermal treatment
Corundum tube furnace	None	No
	1/2/3 wt.% Y_2O_3	No
	1/2/3 wt.% CaO	No
	0.5 wt.% CaO + 0.5 wt.% Y_2O_3	No
	1 wt.% CaO + 1 wt.% Y_2O_3	No
	1.5 wt.% CaO + 1.5 wt.% Y_2O_3	No
Graphite furnace	3/5 wt.% CaO	TT A
		TT B
	1/3 wt.% SrO	No
		TT A
	1 wt.% CaO + 1 wt.% Y_2O_3	No
		TT A
		TT B
	1.5 wt.% CaO + 1.5 wt.% Y_2O_3	No
		TT A
		TT B
	1 wt.% SrO + 1 wt.% Y_2O_3	No
		TT A
	1.5 wt.% SrO + 1.5 wt.% Y_2O_3	No
		TT A
	1 wt.% CaO + 1 wt.% Y_2O_3 (from Nitrates)	TT A
	1.5 wt.% CaO + 1.5 wt.% Y_2O_3 (from Nitrates)	TT A
	1 wt.% SrO + 1 wt.% Y_2O_3 (from Nitrates)	TT A
	1.5 wt.% SrO + 1.5 wt.% Y_2O_3 (from Nitrates)	TT A

3.5.2.2 Sintering experiments utilizing powder beds

The preliminary experiments showed inconsistencies during the consolidation (see section 4.3). To alleviate this, powder beds were employed to enhance the densification behavior when sintering in the different furnaces. The embedding powders were mixed on a shaker mixer (Turbula T2F, WAB) for 15 minutes without milling media. Table 9 gives an overview of powder mixtures used as powder beds.

Table 9: Powder beds used for sintering experiments.

Powder mixture	AlN (Grade C, H.C. Starck) (wt.%)	BN (HeboFill BL-SP 035, Henze) (wt.%)	Graphite (Timrex KS 4, Timcal) (wt.%)
A	100		
AB	50	50	
ABC	47.5	47.5	5

For sintering, green bodies were placed on top of the respective embedding powder inside the crucible and covered with more embedding powder before the crucible was transferred into the furnace.

Different sets of experiments investigating the behavior of samples sintered in a powder bed were conducted. The order of variations listed below reflects the order in which the results of said experiments will be presented:

Variation of sintering additive content and sintering time in the graphite furnace: powder mixtures with 1 wt.% CaO (as $CaCO_3$ or decomposed prior to sintering) and varying amounts of Y_2O_3 were prepared and sintered at 1700 °C in a graphite furnace with either powder bed AB or ABC for 2, 4 or 6 h.

Variation of sintering environments: CIP samples from a powder mixture with 1 wt.% CaO and 3 wt.% Y_2O_3 were sintered in three different furnaces and powder beds, while sintering temperature (1700 °C) and time (6 h) were not varied. The focus of these experiments was on investigating the migration and removal of secondary phase.

Approach A: Graphite furnace + powder bed AB

Approach B: Graphite furnace + powder bed ABC

Approach C: Corundum tube furnace + powder bed A

Approach D: Hot isostatic press + powder bed ABC

Variation of sintering temperature: One sintering run was conducted at 1600 °C for 6 hours in the graphite furnace, with samples containing 1 wt.% CaO and up to 5 wt.% Y_2O_3, in a powder bed AB.

Variation of starting powders: Powder mixtures with 1 wt.% CaO and 3 wt.% Y_2O_3 with three AlN powders (Grade C, Grade BT and Grade JM) from two manufacturers were prepared by CIP. The samples were sintered in the graphite furnace in an ABC powder mixture for 6 hours at 1700 °C.

Table 10 shows the parameter variations for the systematic investigation of AlN samples, produced by CIP and sintered while being submerged in a powder bed.

Table 10: Overview of systematic sintering experiments conducted with samples submerged in a powder bed. The variations of starting powders are not included in this table.

Sintering conditions	Sintering additives	Thermal treatment	Sintering Parameters
Graphite furnace	1 wt.% CaO + 1 wt.% Y_2O_3	None	1700 °C, 4/6 h 1600 °C, 6 h
		TT furnace B	1700 °C, 2/4/6 h
	1.5 wt.% CaO + 1.5 wt.% Y_2O_3	None	1700 °C, 4/6 h
		TT furnace B	1700 °C, 2/4/6 h
	1 wt.% CaO + 2 wt.% Y_2O_3	None	1700 °C, 2/4/6 h
		TT furnace B	1700 °C, 4/6 h
	1 wt.% CaO + 3 wt.% Y_2O_3	None	1700 °C, 2/4/6 h 1600 °C, 6 h
		TT furnace B	1700 °C, 4/6 h
	1 wt.% CaO + 5 wt.% Y_2O_3	None	1700 °C, 2/4/6 h 1600 °C, 6 h
	1 wt.% CaO + 3 wt.% Y_2O_3 (using Grade C, Grade BT and Grade JM AlN powders)	None	1700 °C, 6 h
Corundum tube furnace	1 wt.% CaO + 3 wt.% Y_2O_3	No	1700 °C, 6 h
Hot isostatic press	1 wt.% CaO + 3 wt.% Y_2O_3	No	1700 °C, 1 + 5 h

The hot-isostatic pressing cycle consisted of 1 h of pre-sintering at 1700 °C, after which the pressure was increased to 6 MPa and the temperature was held for five additional hours.

3.6   Additive manufacturing of AlN materials

Lithography-based ceramic manufacturing (LCM), a type of vat photopolymerization, was the AM method of choice for fabricating AlN parts, for which a polymeric ceramic slurry including a photo initiator is selectively polymerized layer by layer through selective exposure to light. The ceramic powder mixtures were dispersed in the organic liquid (photoreactive (meth)acrylate monomers, rheological and dispersing agents and a photo-initiator) using a laboratory mixer (Speedmixer DAV 400.1 FVZ, Hauschild). Additive manufacturing was conducted on a Cerafab 7500 (Lithoz GmbH) platform. For this, the slurry is filled into a vat with a clear bottom and a building platform is lowered into the slurry, leaving the distance of the thickness of one layer to the vat bottom. The photoreactive slurry is then irradiated by a light engine, including a mirror array, which can either irradiate select areas or block light from reaching the vat. This results in solidified pixels of binder and ceramic powder mixture, where the light hits the slurry. With this method the whole area of the building platform can be irradiated at once, in contrast to other methods, which irradiate a layer pixel by pixel. This process is repeated layer by layer, resulting in a three-dimensional green part, which can be removed from the building platform and cleaned from excess slurry. Fig. 6 shows an image of the device used, along with a schematic description of the printing device.
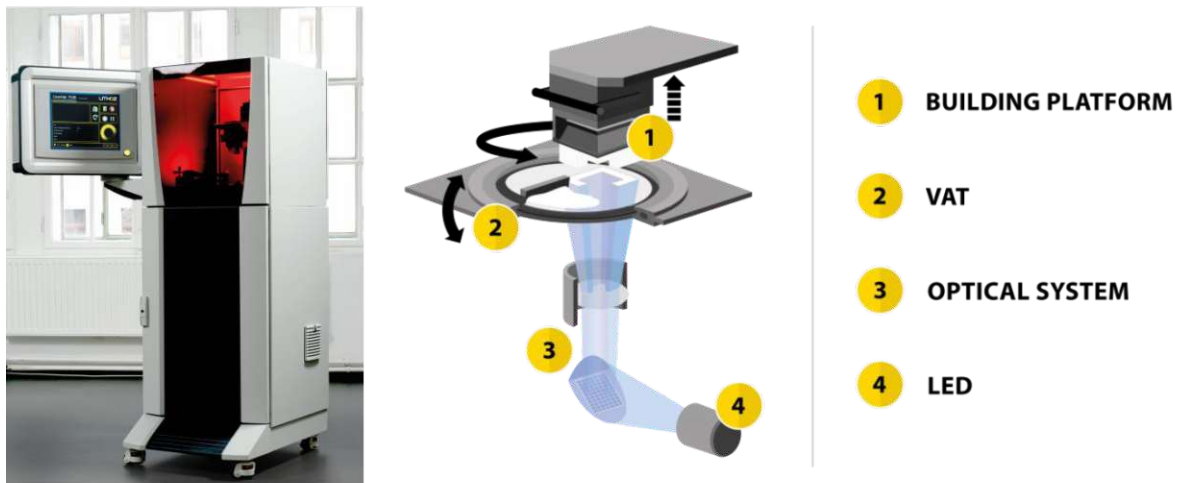

Fig. 6: Device used for additive manufacturing (Cerafab 7500), including a schematic representation of the printing process [8].

Parameters such as slurry composition, layer thickness and energy dosage were varied for the different AM batches. Since the variation of said parameters was not conducted by the author, those changes and their influence on the properties of finished parts will not be discussed in detail. Typical slurry compositions included between 40 and 50 vol.% solid content.

Early AM experiments suggested reactivity of the $CaCO_3$ sintering additive with components of the slurry, which is why it was substituted by dried (2 h at 300 °C) CaC_2O_4 for most AM samples. The decomposition of CaC_2O_4 during debinding was investigated by determination of the carbon content of samples after debinding and comparing it to the theoretical value of the powder mixture with 1 wt.% CaO added as $CaCO_3$, which was the expected composition after thermal debinding.

The only powder mixture composition used in systematic evaluations of the properties of AM samples included 1 wt.% CaO (via CaC_2O_4) + 3 wt.% Y_2O_3. Based on results from CIP experiments, two different AlN powders - grade C and grade JM - were investigated. Table 11 gives an overview of the printing parameters used.

Table 11: Parameters used for additive manufacturing of samples for the systematic investigation of the usability of grade C and grade JM AlN powders in the LCM process. The data in this table was also published in [8].

Parameter	Grade C-based powder system	Grade JM-based powder system	Influencing Parameters
Geometry			
Layer thickness (µm)	15	25	Curing behavior & energy dosage
Coat			
Rotation speed (steps/s)	200		Rheological behavior
Contact			
Settling time backlight layer (s)	120		Rheological behavior & cured area
Settling time general (s)	8		Rheological behavior & cured area
Tilt up speed general (steps/s)	10		Design & orientation
Expose			
Backlight layer exposure time (s)	2.0		Design & orientation
Energy dosage general (mJ/cm^2)	350	200	Curing behavior & layer thickness
Separate			
Tilt down speed general (steps/s)	7		Design & orientation

Thermal debinding was performed at 600 °C in air. The main limiting factor for AM parts was crack formation during debinding steps. The first debinding experiments were conducted at TU Wien, but debinding of later samples was carried out by Lithoz GmbH, following the same debinding program. The debinded parts were then transported to TU Wien, weighed and measured, before being transferred to the sintering crucibles for final consolidation. The debinding characteristics were investigated by thermogravimetric analysis and assessment of oxygen uptake of AlN powders using the inert gas fusion technique.

Sintering of the parts was conducted in the graphite furnace in N_2 atmosphere, utilizing a powder bed ABC (see section 3.5.2.2). A maximum temperature of 1700 °C was held for 6 hours.

Akin to conventionally prepared samples, properties typically investigated included density, mechanical strength, and microstructure (SEM). Thermal conductivity in AM samples - and CIP samples as references - was measured by Xe-flash technique.

3.7 Characterization

In this section characterization methods and sample preparation techniques needed to conduct them are described.

3.7.1 Polishing optimization

Many of the characterization methods used require polished sample surfaces. Typically, ceramic materials are polished with pastes or suspensions containing diamonds, starting from large diamond grain sizes, which are reduced after each step. However, after polishing AlN samples with 1 μm diamond paste, a common finishing step in surface preparations of ceramic materials, high amounts of porosity were still observed on sample surfaces. This was presumed to not stem from defects in the samples generated during their production, but rather from grain pluck-out during polishing. To alleviate this problem, a finishing step using colloidal silica suspension was performed. Fig. 7 shows light-microscopic images of a typical polished sample (hot-pressed Grade C AlN, without sintering additives) before and after the treatment with colloidal silica suspension. Long polishing times using silica suspension led to a relief surface structure, observable by SE-SEM, due to varying rates of material removal in different AlN grains.

50 μm
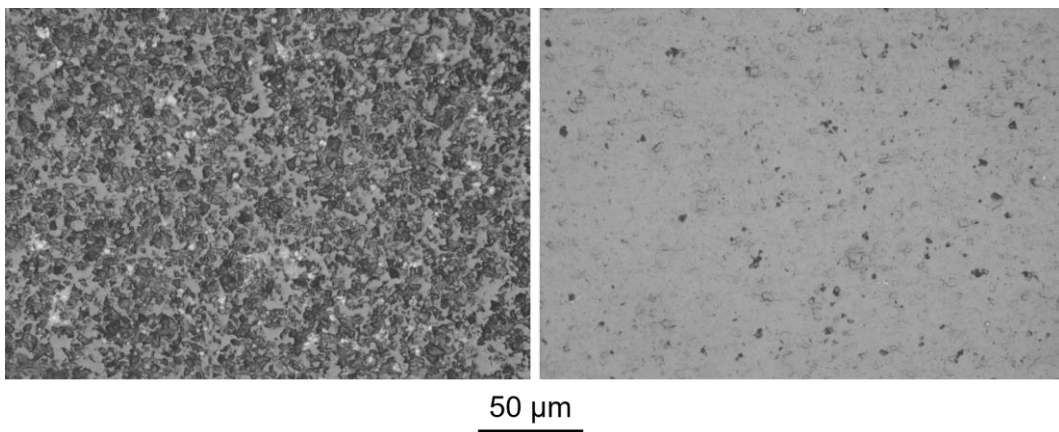
Fig. 7: Light-microscopic images of hot-pressed sample HP_C_30_1, polished with 1 μm diamond paste (left) and colloidal silica suspension (right)

Two polishing procedures were then defined. One procedure was used for manual polishing of samples, which was used for the preparation of bending bars (Table 12).

Table 12: Polishing procedure used for manual polishing of AlN samples.

Step	Abrasive	Disk	Rotational speed (min^{-1})	Duration (min)
1	120 µm resin embedded diamonds	Cameo Platinium 1	300	As needed
2	15 µm diamond paste (monocrystalline)	MD-Plan (Struers)	300	10
3	6 µm diamond paste (monocrystalline)	MD-Dac (Struers)	300	10
4	1 µm diamond paste (monocrystalline)	MD-Nap-T (Struers)	300	10
5	40 nm silica particle suspension	MD-Chem (Struers)	150	10

The second polishing procedure was used with a Tegramin-30 automatic polishing machine by Struers (Table 13), which was used for samples embedded in epoxy resin or samples glued onto sample holders that would allow for automatic processing.

Table 13: Automatic polishing procedure used on automatic polishing device by Struers. The values for the Dosage in step 4 represent initial values proposed by Struers and were reduced over time, because suspension consumption was excessive and the polishing results were satisfying even with lower dosage.

Step	Abrasive	Dosage (Struers specific)	Disk	Rotational speed (min^{-1})	Force (N)	Duration (min)
1	68 µm resin embedded diamonds	n.a.	MD-Piano 220	300	30	As needed
2	DiaPro 9 µm (Struers)	3/6	MD-Largo	150	30	7
3	DiaPro 3 µm (Struers)	3/6	MD-Largo	150	30	15
4	OP-S NonDry (0.25 µm) (Struers) - diluted with 50 vol.% water)	3/8	MD-Largo	150	20	30 to 60

3.7.2 Elemental analysis

Two different elemental analysis methods for oxygen and carbon content were used. Additional elemental analysis was carried out by energy-dispersive X-ray spectroscopy during scanning and transmission electron microscopy.

Oxygen assessment by inert gas fusion technique

Oxygen and nitrogen contents of the dried powders were determined with the inert gas fusion technique utilizing a LECO TC400 Oxygen/Nitrogen Analyzer. For analysis the sample is placed inside a tin capsule, which is then placed in a nickel basket (as flux). During the analysis the basket is dropped into a graphite crucible, which is then heated by induction under helium flow. Due to heating the sample decomposes or is reduced by the graphite to form CO, CO_2 and N_2. A carrier gas (He) transports the gaseous reaction products through a copper oxide catalyst column in which the CO is converted to CO_2, and a second column in which water vapor is removed from the gas stream. The gases are detected by infrared (CO_2) or thermal conductivity (N_2) detectors. The measurement equipment was calibrated using iron powder (JK47, Jernkontoret, 1.09 ± 0.02 wt.% O) as oxygen reference and silicon nitride powder (ERM ED101, European Reference Material, 38.1 ± 0.02 wt.% N) as nitrogen reference. At least three repetition measurements of each reference material were conducted and then used for one-point calibrations. For samples also at least three repetition measurements were conducted.

Carbon assessment by combustion technique

A LECO CS 230 carbon/sulfur analyzer was used for the determination of the carbon content in an AM sample after debinding. For this the weighed sample was placed in an alumina crucible with tungsten chips. Utilizing induction of current in the tungsten chips, the sample is heated in an oxygen atmosphere, which leads to the formation of carbon and sulfur containing compounds to CO_2 and SO_2. Those gases are then quantified by an infrared detector. Calibration was conducted with a cast iron reference material provided by LECO (carbon content = 3.29 ± 0.04 %) in three repetition measurements. Samples were also measured at least three times.

3.7.3 Density measurements

Geometric density measurements were typically conducted using to determine green density of CIP and AM samples. However, for some sintered samples used for the determination of thermal conductivity (cuboid shape), the geometric density was also determined.

Density of sintered samples was determined by the liquid displacement method. For samples sintered in a powder bed ABC or in a corundum tube furnace in powder bed AB the YN layer that formed on the surface of the samples (see section 4.3.4) was thermally removed at 500 °C in air for 4.5 hours to lower deviations of the measurements. The weight of the samples when dry and when submerged in water was determined. Using the archimedic principle, their density was calculated. For select samples with large amounts of pores (e.g. from incomplete densification) or with a complex shape that was not easily permeated by the water, an immersion method, according to EN 623-2 [99] was used to estimate the skeletal density of the samples. When doing this, the immersion liquid can still penetrate unwanted porosity of the sample if there is any, which might lead to less accurate measurements, overestimating the actual density of the sample. This immersion method was also used for hot pressed samples.

As theoretical density of the samples 3.26 g cm^{-3}, the theoretical density of pure AlN, was used. The value was chosen due to inhomogeneous distribution and elimination of secondary phases during sintering, leading to unknown amounts of secondary phase, and, as such, the theoretical density would have had to be estimated on a per-sample basis, often using inaccurate measurements, as secondary phase content was often at or below the detection threshold for XRD analysis.

3.7.4 Electron microscopy

Scanning electron microscopy (SEM)

Microstructural analyses using scanning electron microscopy (SEM) were conducted using a Quanta 200 (FEI). A tungsten cathode is used as electron emitter and the microscope is equipped with a detector for secondary electrons (SE), allowing for contrast in topological features and a detector for backscattered electrons (BSE), allowing for contrast between elements, as higher atomic numbers result in more backscattered electrons reaching the detector. BSE micrographs were especially useful in identifying secondary phases, since Y, as

constituent of the sintering additives, possesses a higher atomic mass than Al, N, O or C, resulting in bright areas. For most micrographs the BSE signals were used, if not listed otherwise.

For SEM imaging, samples were fractured and glued onto a sample holder with the fracture surface facing, towards the detectors. Micrographs of polished samples could be taken directly from the samples, which were embedded in epoxy resin for polishing. Imaging of powders was conducted by attaching the powders to self-adhesive graphite tape. To reduce charge build-up on powder particles, a conductive gold layer was applied utilizing an AGAR sputter coater.

Transmission electron microscopy (TEM)

Transmission electron microscopy was conducted by Sabine Schwarz at the University Service Centre for Transmission Electron Microscopy (TU Wien). A TECNAI F20 (FEI) was used for imaging and electron scattering purposes. Samples for transmission experiments were prepared from sintered samples using the focused ion beam (FIB) technique.

3.7.5 X-ray diffraction analysis (XRD)

Most X-ray diffraction analyses of powder samples and solid bodies were conducted using an XPERT II material research diffractometer (Malvern Panalytical). The sample carriers used allowed for samples of up to 5 mm thickness and enabled rotation during measurement. Measurements of larger samples and measurements under atmosphere exclusion were conducted with an Empyrean diffractometer (Malvern Panalytical). Cu Kα radiation was used for all analyses.

3.7.6 Thermal conductivity determination

A steady state, constant heat flow method, as well as the flash technique were used to determine thermal conductivity of sintered AlN samples. Only the steady state method was accessible at TU Wien. Flash measurements were done either at the Slovak Academy of Sciences or at OSRAM GmbH (Germany).

Steady state equal heat-flow method

Fourier's law describes heat flow in a solid as proportional to its thermal conductivity, the temperature difference between two measurement locations, the thermal conductivity of the material and the cross-sectional area of the sample, while it is inversely proportional to the distance between the measurement spots. Using two materials in a comparative method in which equal heat flow is ensured by insulating the set-up, is a simple way to eliminate the need to measure the exact heat flow through the sample. This leaves the thermal conductivities of the materials as the only unknowns in the equation. If one of the materials is a reference material with a known thermal conductivity value, the thermal conductivity of the sample is the only unknown.

An in-house built rig for measuring thermal conductivity by the steady-state equal heat-flow comparative method, as described by Edtmaier et al. [100], was used. A schematic representation of the testing rig is shown in Fig. 8. A thermostat, heated to 95 °C, supplies heat to a brass reference of known thermal conductivity λ_R (113 W m^{-1} K^{-1}), to which the sample is connected. The temperature in the second thermostat, to which the other end of the sample is connected, is set to 5 °C.

Cuboid shaped samples (approx. 5 x 5 x 30 mm) were prepared on a cutting machine (WOCO 50, Uniprec) using a cup wheel (75 µm diamonds) and a custom sample holder to ensure plane parallel faces. After parallelization the faces were manually finished on a 20 µm diamond wheel. The dried samples were then weighed, measured using calipers, and connected on one end to the brass reference and on the other end to a thermostat (5 °C). Thermal compound (Fischer WLPK) on connected surfaces and spring pressure fixation was utilized to ensure optimal heat flow. Four resistance temperature detectors (Pt1000 for the sample and Pt100 for the reference) were used to measure the temperature gradients in the sample and the reference. Insulating foams were placed around the reference and sample to prevent heat loss. Calibration of the system was not necessary, due to the internal reference; however, iron samples with known thermal conductivity were measured regularly to verify accurate operation of the system.
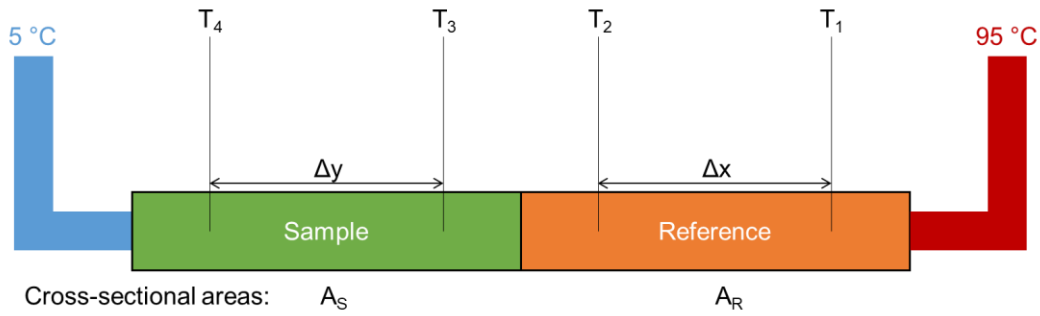
Fig. 8: Schematic representation of the comparative steady-state equal heat-flow rig. T_i denotes temperatures measured by resistance temperature detectors. Δx and Δy represent the distance between the thermocouples on the reference and the sample, respectively. A_R and A_S denote the cross-sectional areas of the reference and the sample, respectively.

The equation for evaluating the thermal conductivity of the sample λ_S is given in Eq. 3.

$$\lambda_S = \frac{\lambda_R \cdot A_R \cdot (T_1 - T_2) \cdot \Delta y}{A_S \cdot (T_3 - T_4) \cdot \Delta x}$$ Eq. 3

For many variations investigated in this study only one or two samples could be measured due to spatial constraints in the crucibles and time expenditure of preparing samples for the measurement. However, this steady state method is a bulk measurement, probing rather large sample volumes, as compared to other methods. Defects encountered in the material, such as pores and other irregularities, do not have a big influence on the overall result, which was also shown by measurements of multiple samples from multiple sintering runs from the most promising variation, which showed high repeatability once appropriate sintering conditions were found.

Thermal diffusivity by flash analysis

Flash analysis is an established method for measuring thermal diffusivity of samples. By multiplying thermal diffusivity α with the specific heat capacity C_p and density ρ of samples, thermal conductivity λ can be calculated (Eq. 4).

$$\lambda = \alpha \cdot C_p . \rho$$ Eq. 4

Molar heat capacity c_p, was calculated using a formula (Eq. 5) published by Koshchenko et al. [101], which was converted to specific heat capacity by multiplication with the molar mass of AlN.

$$c_p = 45.94 + 3.347 \cdot 10^{-3} \cdot T - 14.98 \cdot 10^5 \cdot T^{-2} \qquad \text{Eq. 5}$$

The calculated value for molar heat capacity of AlN at 25 °C equates to 30.09 J mol^{-1} K^{-1}. In comparison, the molar heat capacity at 25 °C of AlN is listed in the Handbook of Chemistry and Physics [102] as 30.1 J mol^{-1} K^{-1}. One of the earliest reports on the use of a flash as incident radiation to cause heat flow through a sample was published by Parker et al. in 1961 [103]. Optical heating of one face of the sample via a flash pulse caused heat flow through the sample. The temperature increase over time on the other side of the sample was captured by thermocouples. The collected data enabled the determination of thermal diffusivity α.

In modern setups a laser pulse or xenon flash is used as incident radiation and samples are often coated with graphite to increase absorption as well as emissivity. Oftentimes IR detectors are employed instead of thermocouples to measure the temperature rise. Multiple models to extract α from the data exist.

Due to the short, pulsed excitation and quick response time of the method, losses through radiation are small and losses through convection can be alleviated by measurement in vacuum.

For the measurements sintered cylindrical samples (diameter = 11 - 12 mm, height = 1.5 - 3 mm) were plane parallelized using the same method as for the cuboid bars used for steady state equal heat flow thermal conductivity measurement. Two different flash analysis devices were used. Measurements and data analysis were conducted by a third party and, as such, the theoretical models behind the analysis are not known, other than "best fit" was used in the analysis software, supplied by the manufacturer of the device.

Linseis LFA 1000 (Slovak Academy of Sciences): This model features optical heating by a laser pulse. 6 samples with 10 mm diameter can be measured simultaneously. A furnace enables measurements up to 1000 °C.

Linseis XFA 500 (OSRAM, Germany): XFA 500 utilises a xenon discharge to heat the samples. Akin to the LFA 1000, 6 samples may be measured at the same time at elevated temperatures up to 500 °C. For this device further information on accuracy and repeatability, provided by the manufacturer, was available. The repeatability of thermal diffusivity measurements amounts to ±3 %, while the accuracy amounts to ±5 %

3.7.7 Flexural strength testing

Flexural strength testing is common for ceramic materials due to tensile strength not being easily accessible. Two different methods were used in this study. Hot-pressed samples were of substantial size (50 mm diameter, 12 mm height) and as such it was viable to prepare bending bars (2.0 x 2.5 x 25 mm) for four-point bending tests from the samples, which were tested in accordance to EN 843-1 [104]. Such bending bars are not easily manufactured by CIP, as the ratio of length to the other dimensions leads to heavy warping and other defects while pressing. Therefore, a ball-on-three-balls (B3B) method, for which cylindrical samples may be used, was utilized. AM samples could be prepared to be used in either method, however, to ensure comparability with the strength values of CIP samples, cylindrical samples were printed - standing and lying on the building platform - to be tested parallel and perpendicular to the building direction using the B3B method.

Four-point bending strength

Specimens for four-point bending tests were cut from large, cylindrical, hot-pressed samples by first cutting slabs (cutting plane perpendicular to face plane of the sample). The slabs were then cut to bars. The length of the bars has no significant influence on the test, as long as the bars are longer than the distance of the support points, the bars were mostly kept at their original length. However, some of the bars were longer than twice the support distance, which could then be cut in half to increase the number of specimens (up to 60 per sample).

One side of the longitudinal bar samples was ground and polished manually using the procedure outlined in Table 12. For this, several bars were glued to a sample holder. After polishing the faces, chamfers at a 45° angle between the longitudinal faces of the samples were created. The chamfers of each sample were individually polished again. To prevent scratches going across the shorter side of the samples, the relative movement of the grinding disk/polishing cloth was always parallel to the longitudinal axis of the sample. Scratches going across could lower bending strength, as outlined in standard EN 843-1 [104].

Testing was conducted on a universal testing machine (1474, Zwick, Germany). The rig used for the bending tests features 4 movable and tiltable rolls, so errors by friction and deviations from plane-parallelism of the samples can be prevented. Force transmission is done by a steel ball (10 mm diameter) to a load cell allowing forces up to 100 kN. Before testing, the upper

part of the rig is lowered onto the sample and an initial load of 10 N is applied. Testing was conducted using a crosshead speed of 0.5 mm min^{-1}.

Using the maximum force applied during the test F, the width b and height h of the bending bars and the average distance of the inner and outer support roles d (5 mm for the testing rig used) the flexural stress σ_f can be calculated according to Eq. 6, taken from EN 843-1 [104].

$$\sigma_f = \frac{3Fd}{bh^2}$$ Eq. 6

Ball-on-three-balls method

This method was conducted following the description by Börger et al. from Montanuniversität Leoben [105].

For CIP samples, 30 mm long cylinders with approximately 9 mm diameter were cut into smaller cylinders (height = 0.6 to 1.0 mm) on an Accutom-10 (Struers, Denmark) precision cutting machine. AM samples were already separate cylinders, so they could be used directly after sintering. The samples were ground by hand on one face using a 20 µm diamond disk to ensure smooth surfaces. 6 to 7 samples were then glued onto a cylindrical sample holder (diameter = 30 mm) and plane parallelized using a diamond cup wheel mounted on a WOCO 50 (Uniprec, Germany) cutting machine. After parallelization, the samples were automatically ground and polished on a Tegramin-30 (Struers, Denmark) polishing machine with automatic dosage of polishing suspensions, following the procedure outlined in Table 13.

After polishing, the samples can be used directly for strength testing, without the need for chamfering. The testing rig in testing position is schematically shown in Fig. 9. A hardmetal ball is placed on a hardmetal disc on the base of the rig (grey). The mantle (yellow) is placed on the cylinder, which extrudes from the base and pressed onto a spacer (not shown), which ensures that the lower hardmetal ball does not exceed the height of the mantle while loading. The sample (cyan) is then placed on the inner rim of the mantle with the polished side facing upwards, and three additional hardmetal balls and a die (green) with a hardmetal face are placed on top of it. The rig is then transferred to the universal testing machine (1474, Zwick, Germany) and an initial load of 10 N is applied onto the rig via a steel ball (10 mm, blue in

schematic). The initial load keeps the sample in place, while the placeholder is removed, and the mantle is lowered onto the base (this position is shown in Fig. 9). The test can then be started with a crosshead speed of 0.5 mm min^{-1}. The rig allows for sample sizes from 7.7 to 12.6 mm in diameter and 0.3 mm thickness upwards. Diameter and thickness are not independent and should also be adapted to the load sensor used. In this study samples ranging from 0.3 to 1.0 mm thickness were tested. Due to lower expected forces than for the four-point bending tests a load cell with a 1 kN limit could be used, allowing for more accurate measurements at low loads.
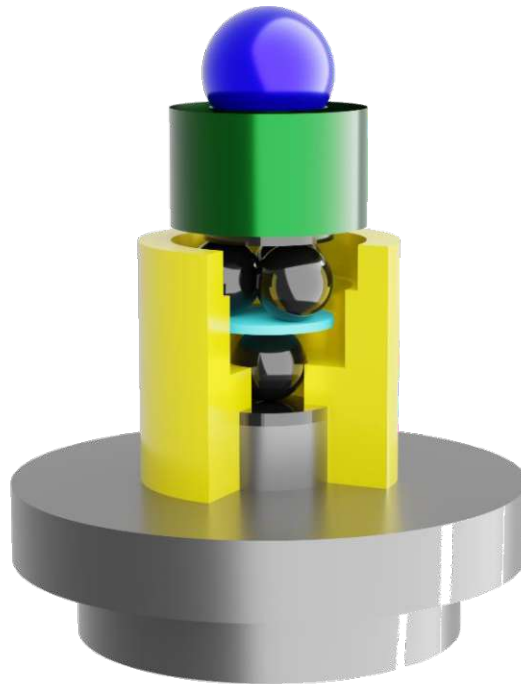
Fig. 9: Schematic drawing of the B3B setup used in this work.

Using the force at the occurrence of the fracture and the dimensions of the samples, the bending strength could be evaluated following an analytical model proposed by Börger et al. [105]. Usually, a finite element analysis model has to be utilized to approximate the actual bending strengths of the samples in this method. However, it was shown by Börger et al. [105] that the errors generated by using an analytical model for cylindrical samples are insignificant, which allows for quick calculations according to Eq. 7 of the maximum tensile stress σ_{max} using the applied Force F, the thickness of the sample t, and a pre-factor f, which accounts for sample and testing rig geometry (support radius R_a, sample radius R and sample thickness t), as well as the Poisson's ratio v of the material. The support radius is the radius of the circle which intersects the centers of the supporting balls with radius R_b and can be calculated using Eq. 8. With Eq. 9 the pre-factor can be calculated. The Poisson's ratio is considered in

constants c_i, which are given in the publication for ratios of 0.2, 0.25 and 0.3. Boch et al. [106] reported a Poisson's ratio of 0.245 for dense AlN (hot-pressed, no additives), which was considered close enough to utilize the constants given in [105] for $v = 0.25$.

$$\sigma_{max} = f \cdot \frac{F}{t^2} \qquad \text{Eq. 7}$$

$$R_a = \frac{2\sqrt{3}}{3} R_b \qquad \text{Eq. 8}$$

$$f\left(\frac{t}{R}, \frac{R_a}{R}, v\right) = c_0 + \frac{\left(c_1 + c_2 \frac{t}{R} + c_3 \left(\frac{t}{R}\right)^2 + c_4 \left(\frac{t}{R}\right)^3\right)}{1 + c_5 \frac{t}{R}}\left(1 + c_6 \frac{R_a}{R}\right) \qquad \text{Eq. 9}$$

Statistical evaluation of flexural tests

The failure of ceramic materials is considered to be dependent on defects in the material (such as pores or notches at the surface). Munz and Fett [107] describe the evaluation of the statistical distribution of strength values utilizing a Weibull distribution. The process to find the distribution, which is defined by the characteristic Weibull strength σ_0 and the Weibull modulus m is conducted by arranging measured strength values σ_c in ascending order. Each value is matched with a rank i and a probability of failure F_i, according to Eq. 10, with n as the total sum of strength values.

$$F_i = \frac{i - 0.5}{n} \qquad \text{Eq. 10}$$

Next, datapoints are plotted in a Weibull diagram ($ln \frac{1}{1-F}$ vs. $ln\, \sigma_c$). By fitting a linear straight line in this plot, the characteristic Weibull strength σ_0 can be found along it at $F = 0.632$ ($ln\, ln \frac{1}{1-F} = 0$), while the slope of the fit equals the Weibull modulus m. The fitting of the line (and with it the parameters for the Weibull distribution) can be estimated with a Maximum-Likelihood method.

Put simply, according to EN 843-5 [108], which also describes this method, σ_0 is the strength at which the probability of failure equals 63.2 %, whereas m represents the width of the distribution, and is thus an indicator for the reliability of the actual material.

3.7.8 Average grain size and Vicker's hardness testing

Fracture parts of samples were embedded in epoxy resin and automatically polished using the polishing procedure outlined in Table 13. The backsides of the embeddings were manually grinded to result in sufficiently plane parallel samples (less than 0.1 mm deviation on opposite sides of cylindrical samples with 3 cm diameter, which equals a skewness of less than 0.2°).

Average grain size of the materials was estimated by determining the average intersecting lines according to EN ISO 13383-1 [109] using SEM. Multiple regions close to the center of the samples were analyzed per sample. As all materials showed comparable microstructures, the average length of intersecting lines was used as a comparative measure for average grain size, without attempting to calculate the average grain size from this measure.

The method likely overestimates grain size, as the contrast in the micrographs often was not good enough to distinguish all individual grains in the micrographs.

After SEM investigations were completed, indentation tests were performed on the samples using a diamond indenter for Vicker's hardness testing according to EN 843-4 [110] in an M4U-025 hardness tester (Emcotest). The diagonals of hardness indents were measured on a GX51 optical microscope (Olympus). Most hardness indents were not compliant with the standard, due to grains missing on edges, making the measurement less accurate.

3.7.9 Thermal analysis

Thermogravimetric and differential thermal analyses were performed on various samples in this project using different devices, depending on the samples characterized.

Powder precursors: The decomposition temperatures of sintering additive precursor compounds were studied on two different devices by Netzsch (STA 449 C and STA 449 F3) in N_2 atmosphere.

Debinding of AM samples: The debinding process of printed samples was studied by thermogravimetric analysis of polymerized slurry samples. For this, slurry was spread onto glass substrates and photopolymerized. The hardened slurry was then scraped from the substrates and used in thermogravimetric analysis using a TGA Q500 (TA Instruments) device in air, to gain insight into the debinding process.

High-temperature dilatometry: To investigate the sintering process, cold-isostatically pressed samples were heated to 1500 °C in a dilatometer (DIL 402 C, Netzsch) in N_2 atmosphere with a heating rate of 10 K min^{-1}. Although this is lower than the actual sintering temperature, the onset of sintering can be observed.

4 Results

In this section the results of the experiments will be discussed in the order they were mentioned in section 3.

4.1 Characterization and hydrolysis of AlN powders in environments

This section will detail the characterization of the three AlN powder grades used in this project, their stability in various environments relevant for processing, and the oxygen intake of the powders during processing steps such as milling and thermal treatment.

4.1.1 Characterization of starting AlN powders

Starting powders were characterized by SEM investigation and their oxygen content was analyzed by inert gas fusion. Grain size and specific surface area were taken from data sheets provided by the manufacturers. Fig. 10 shows SEM micrographs of the AlN powder grades used in this work. Grade C and Grade BT powders were off-white in color, whereas Grade JM was white.
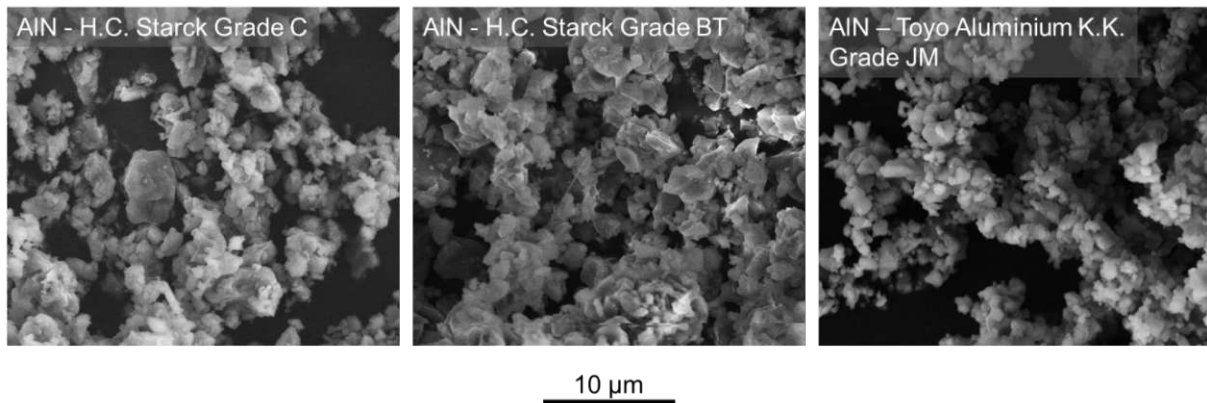
Fig. 10: SEM micrographs of AlN powders used in this work.

Table 14 shows observed properties of AlN powders in comparison to information supplied by the manufacturers.

Table 14: Properties of AlN powders used in this work. The values from the suppliers are the same as listed in Table 4.

	Observed		According to supplier*		
	O-content (%)	N-content (%)	O-content (%)	N-content (%)	D50 (µm)
Grade C	1.29 ± 0.02	32.73 ± 0.68	1.1	33.9	1.7
Grade BT	0.95 ± 0.06	33.13 ± 0.52	0.8	34.4	2
Grade JM	0.88 ± 0.02	33.45 ± 0.57	0.6 - 0.8		2.0 - 3.1

*For Grade C and Grade BT, data from an analysis certificate of the first batch received in the project was used; and for Grade JM, data from a "typical data sheet" was used.

4.1.2 Elemental analysis and hydrolysis stability

The hydrolysis behavior of the three different AlN powders was studied in various environments over the span of several hours to several weeks. For the stability tests only small amounts of powder were taken from the supplied AlN containers in N_2 atmosphere to prevent any reactions prior to the investigations. The data point at 0 hours reflects the oxygen content of powders directly taken from the supplied container in a protective N_2 atmosphere. Fig. 11 shows development of oxygen content of powders with increasing exposure times to the various environments, showing that the different AlN powders behave similarly in the different environments. The only environment in which the powders were highly unstable was water, which was also confirmed by a slight ammonia odor, noticeable during sampling after several hours of exposure. After 24 hours, the suspensions smelled strongly of ammonia, and pH values were about 11, according to tests on pH indicator paper.
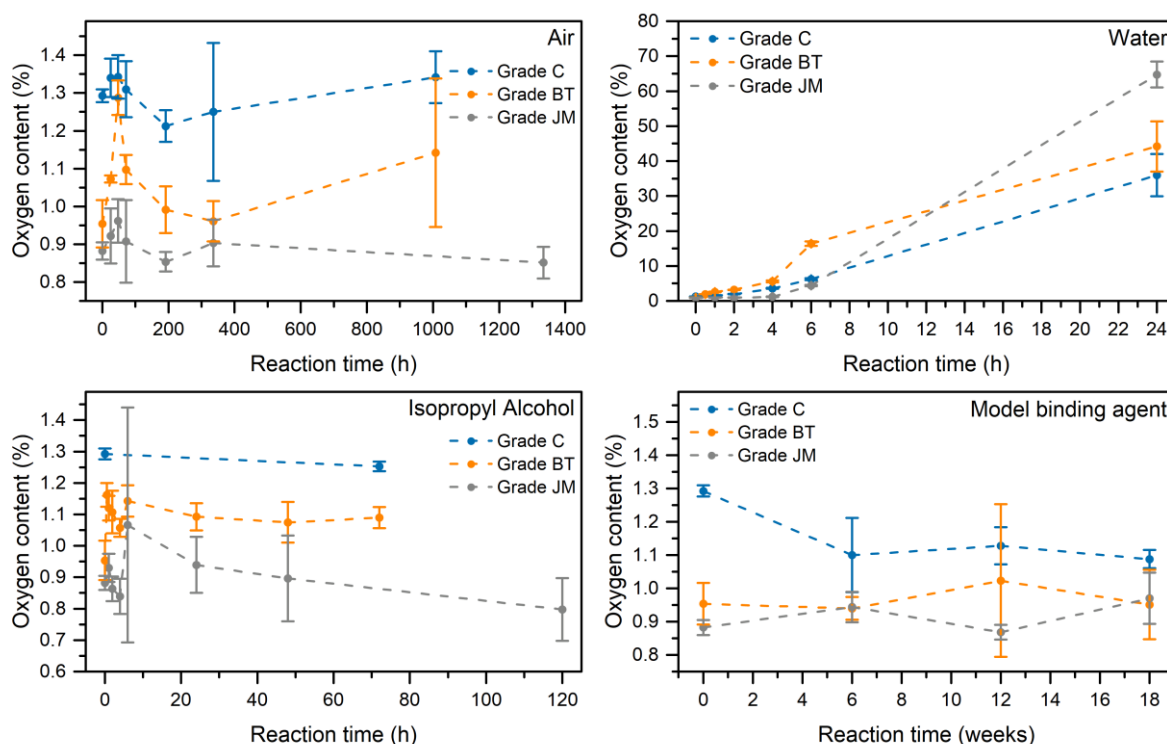
Fig. 11: Oxygen contents of AlN powders, exposed to different environments. Data for grade BT and grade JM powders was contributed by Felix Frank in an educational internship.

In addition to the elemental analysis, XRD analysis of the Grade C powder before and after hydrolysis in water for various amounts of time was conducted. Fig. 12 shows the combined results of the analysis. From the reference up to 6 hours of hydrolysis, only AlN signals were

detected. After 24 hours, signals from Bayerite (marked with a blue outline) were detected in addition to AlN signals.
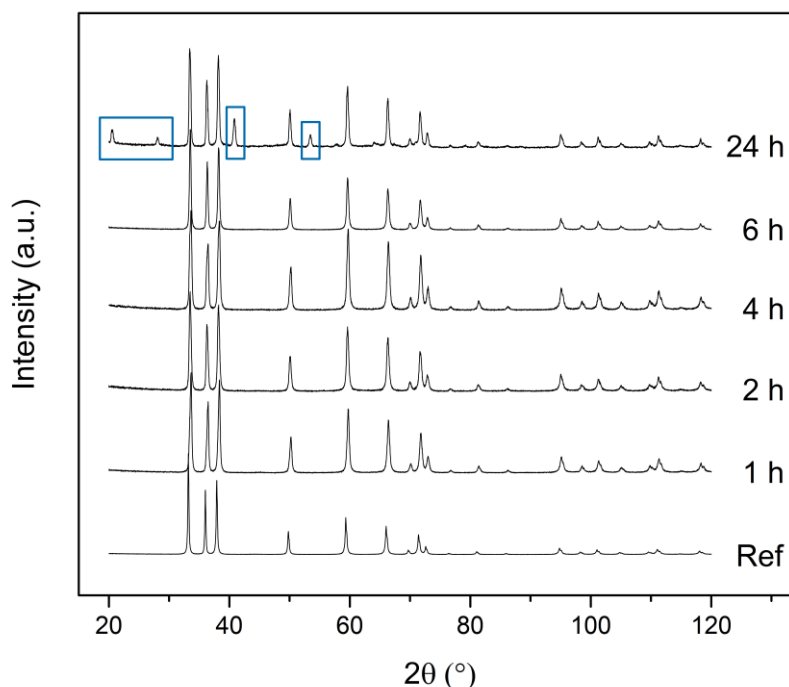
Fig. 12: XRD analyses of the hydrolysis products of Grade C AlN powder exposed to water for various amounts of time. Signals highlighted with blue outlines stem from bayerite, whereas the rest of the signals can be attributed to AlN.

4.1.3 Stability of AlN during preparation of powder mixtures

Isopropyl alcohol or air by themselves did not lead to significant hydrolysis in AlN powders. However, it was assumed that mechanical energy introduced by milling might lead to hydrolysis or oxidation reactions, presumably also by destroying the protective oxide layer on the powder particles. Additionally, the effect of thermal treatment for sintering additive precursor decomposition at 950 °C and 1150 °C of AlN powder in tube furnaces was investigated. SA-precursor decomposition furnace B was only used up to 950 °C due to thermal limitations. Fig. 13 shows the results. A repetition measurement of the powder after wet and dry milling is also shown, because of high oxygen content measured in the first experiment, which was then lower after dry milling. The oxygen content in the repetition measurement is lower than the value of the first measurement and in the range of the reference AlN powder.
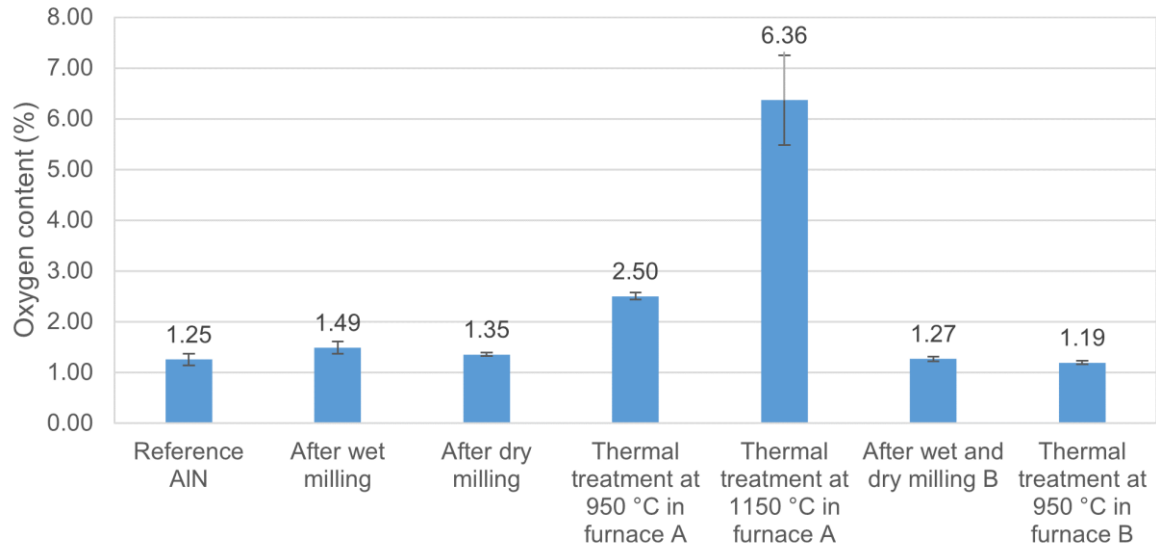
Fig. 13: Oxygen analysis of Grade C AlN powders subjected to the powder processing steps used to produce powder mixtures. The first bar represents Grade C AlN powder directly after removal from the storage container. Bar two to five represent the oxygen content of a first experiment investigating the process chain, which concluded in the powder being heated to either 950 °C or 1150 °C in N_2 atmosphere in SA-decomposition furnace A. The oxygen content of the powders represented by the last two bars were generated in a second experiment in which the powder was heated to 950 °C in N_2 in SA-decomposition furnace B.

4.2 Observations and properties of HP samples

Hot-pressing is a proven method of consolidation for ceramic materials that are challenging to sinter. To obtain reference materials with adequate properties from the starting powders sourced for this project, AlN with and without sintering additives was hot pressed and characterized.

4.2.1 General observations of HP samples

The following analyses and observations were collected from one representative sample (HP_C_30_1) from Grade C AlN powder without sintering additives, which was hot-pressed at 1800 °C for 2 hours in the HP W 150 instrument, located at TU Wien. The sample, once removed from the hot-press dies, was covered by an anthracite-colored layer, which could not be removed by wiping or scraping with tools (as would be the case for graphite residue) but only by grinding. When the sample was submerged in water, gas evolution from the surface layer was observed. Fig. 14 shows cross-sections of the sample. Aside from light-grey bulk material, a white layer and an anthracite-colored surface layer are present.
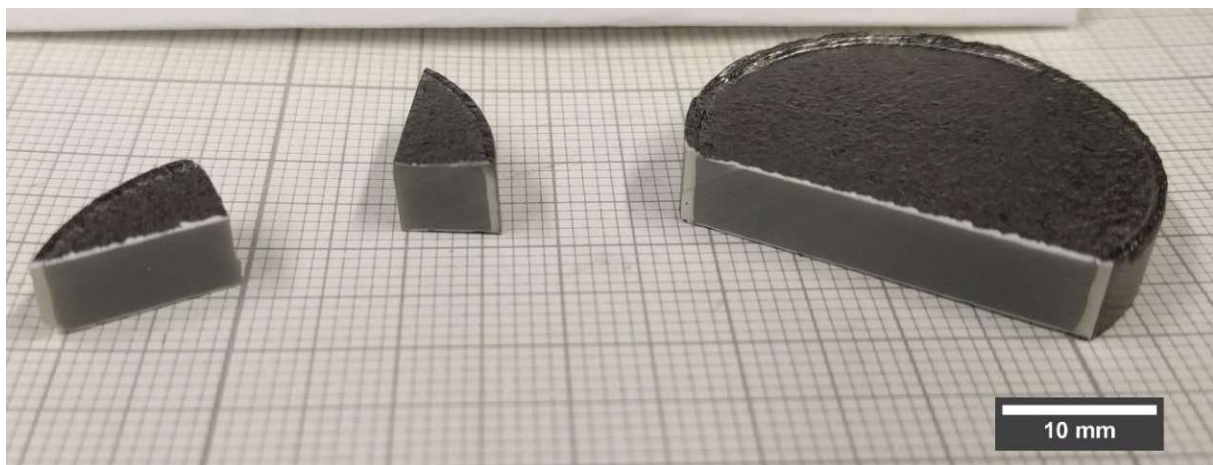
Fig. 14: Photograph of sample HP_C_30_1, showing the layers observed in the cross-sections of the sample.

Fig. 15 shows SEM images of a cross-section of HP_C_30_1, embedded in epoxy resin and polished manually with diamond paste (15 µm – 6 µm – 1 µm). All the micrographs in Fig. 15 were recorded using a secondary electron detector, except for the image with the "BSE" overlay, which was recorded utilizing a backscattered electron detector. In the first image a clear distinction between the white layer and the gray bulk is visible. In the "BSE" image, which shows a smaller section of the sample, no difference except for increased porosity in the

surface layer can be seen, which means that the compositions of both the dark surface and the white subsurface layer are similar. The lower left image shows a higher magnification of the area close to the surface of the sample, which shows the dark surface layer, as well as the white layer beneath it. The lower right image shows the transition from the white layer (left) to the gray bulk material (right), revealing that the white layer is more porous. Considering the porosity, it also has to be pointed out that grains are plucked out of the material during polishing, so some of the apparent porosity might be created during polishing. The anthracite-colored layer was 35 µm thick, whereas the white layer was 80 to 100 µm on the circular faces and approximately 800 µm on the curved faces. The sample part that was used for the measurement of the layer thickness was cut close to the center of the sample, however, inaccuracy during cutting may lead to higher thickness values on the sample sides.
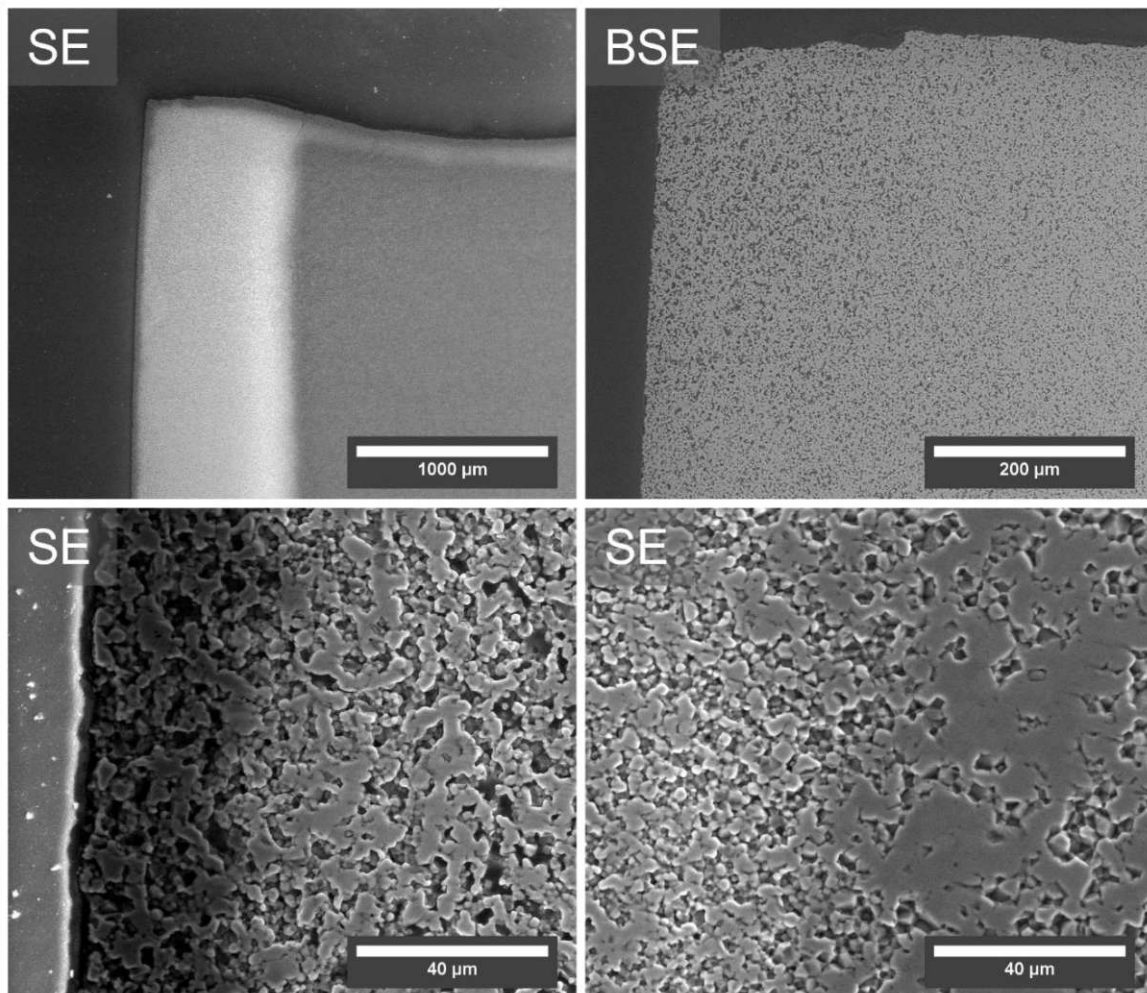
Fig. 15: SEM micrographs of a polished cross-section of sample HP_C_30_1, embedded in epoxy resin, showing details of the layers observed in the sample. The lower images represent the transitions from the black surface layer to the white subsurface layer (left) and the white layer to the gray bulk (right).

Fig. 16 shows SEM micrographs (SE) of the fracture surface of sample HP_C_30_1. The upper micrograph shows an overview of the sample with the edge of the fracture surface in the top part of the image. The white layer is about 100 µm wide in this area. The distinction between the white layer and the gray bulk is clearly visible, especially at higher magnifications. The lower left micrograph shows a higher magnification of the white layer, whereas the lower right image shows the gray bulk material. Aside from a more porous microstructure in the layer and small pores in the bulk, it is also apparent that different mechanisms of fracture are present in the materials. The white layer shows mostly intergranular fracture, while the bulk shows transgranular fracture behavior.
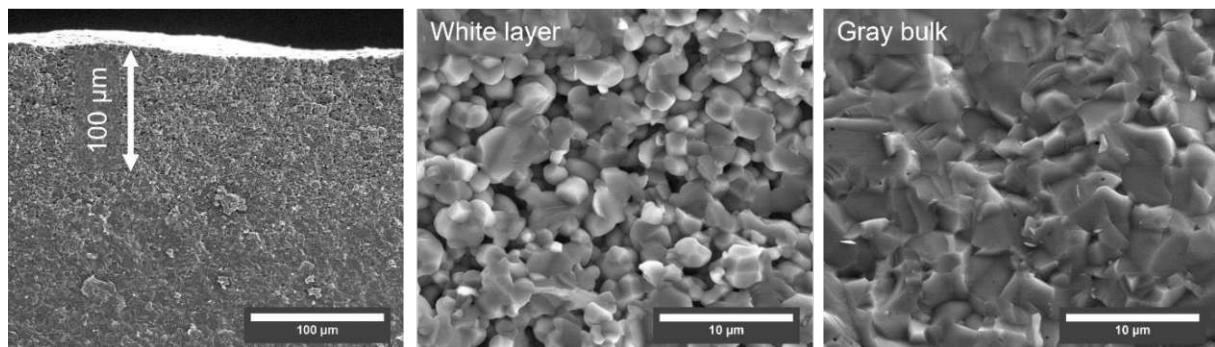
Fig. 16: SEM micrographs (SE) of fracture surfaces of sample HP_C_30_1, detailing the bulk and the white subsurface layer

XRD measurements (Fig. 17) of the white layer and the grey bulk material revealed no difference, with both showing signals resulting from AlN, except for one additional signal in each diffractogram, which is not present in the other (at 56° and 46°, respectively) but neither signal could be matched with an additional phase.
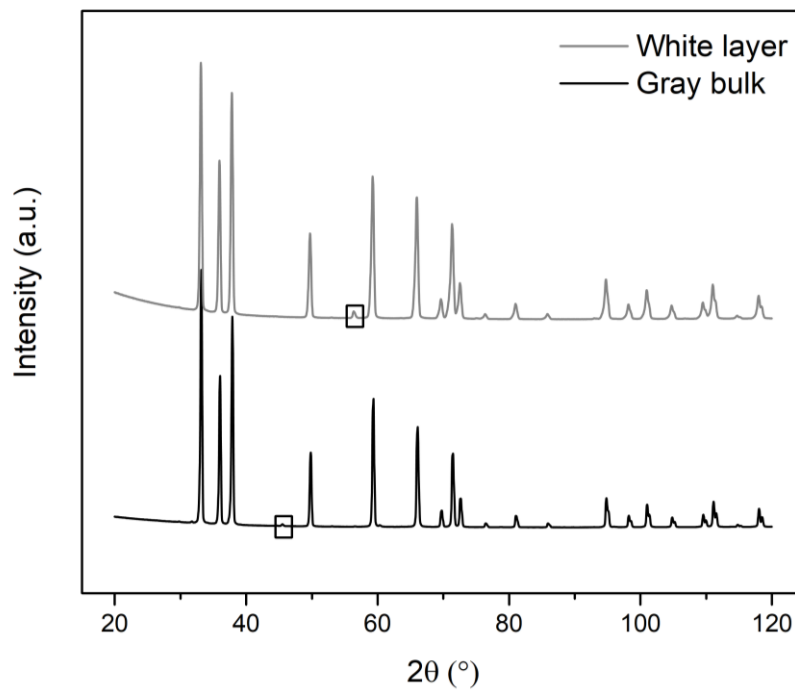
Fig. 17: X-ray diffractograms of the gray bulk and the white subsurface layers, observed in sample HP_C_30_1, showing only AlN signals except for one signal in each diffractogram not present in the other (marked with a black rectangle). The single signals could not be assigned to an additional phase.

The dark surface and white subsurface layers were not observed on samples produced externally on the HPW 315/400-2200-1000-PS/SP instrument but the color of the samples differed from composition to composition (lighter gray in samples with no sintering additive to darker gray in samples with Y_2O_3 and light gray with dark spots about 1 mm in size for samples with CaO). The black spots in samples with CaO were not visible in either light microscopic or SEM images. Fig. 18 shows photographs of all samples produced externally. The faces of the samples were ground on a 20 µm diamond embedded grinding wheel. All samples have a diameter of 50 mm.
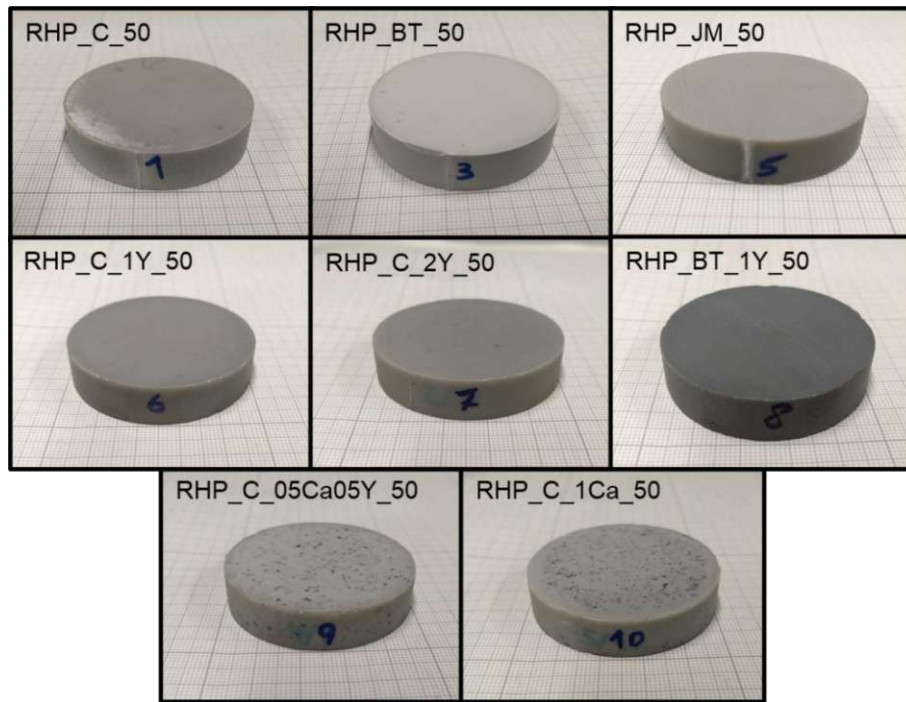
Fig. 18: Photographs of RHP samples, showing different colorations of the samples. All samples have a diameter of 50 mm.

4.2.2 Properties of HP samples

The density of hot-pressed samples was measured by liquid displacement method. Table 15 shows the results. For each value the density of one sample was determined at least 3 times, because most of the consolidation experiments yielded only large, singular samples (about 74 g), which were then cut to smaller specimens for thermal conductivity and bending strength determinations and further characterization.

Before the density determination, the faces of the cylinders were ground on a 20 µm diamond embedded grinding wheel to remove burrs and general unevenness, as well as the anthracite-colored layer covering the faces, which turned out to react with water, producing bubbles. While the RHP samples did not show the dark surface layer, the faces were still ground before measurement.

Table 15: Results of the density measurements of HP samples and number of flexural tests performed. The sample marked with an asterisk was characterized by Felix Frank.

Sample	Density (g/cm³)	Relative density (%)	Number of flexural tests performed
HP_C_30_1	3.24	99.3	
HP_C_30_2	3.25	99.6	
HP_C_3Y_30_1	3.28	100.7	
HP_C_50_1	3.26	99.9	11
HP_C_50_2	3.18	97.4	
HP_JM_50_1*	3.25	99.7	16
RHP_C_50	3.26	100.1	26
RHP_BT_50	3.15	96.5	32
RHP_JM_50	3.26	100.1	
RHP_C_1Y_50	3.28	100.5	47
RHP_C_2Y_50	3.29	101.0	35
RHP_BT_1Y_50	3.27	100.5	34
RHP_C_05Ca05Y_50	3.26	99.9	34
RHP_C_1Ca_50	3.25	99.7	36

Parts of the large samples were cut to bending bars, which were then polished and chamfered to reduce the influence of surface defects on the bending strength. The bars were then tested on an in-house built rig for four-point-bending tests, according to EN 843-1 [104], with two deviations from the standard; for one, the sample length was not cut to the exact dimensions mentioned in the standard, and the longer bars, which were long enough for a second test after fracturing, were sampled a second time. The number of flexural tests performed for each variation is given in Table 15. The results in Fig. 19 show that the introduction of Y_2O_3 as sintering additive entails a significant decrease in the bending strength of the samples, while the Weibull modulus actually increases. CaO and mixed CaO/Y_2O_3 additives do not lower bending strength significantly, but also increase the Weibull modulus.
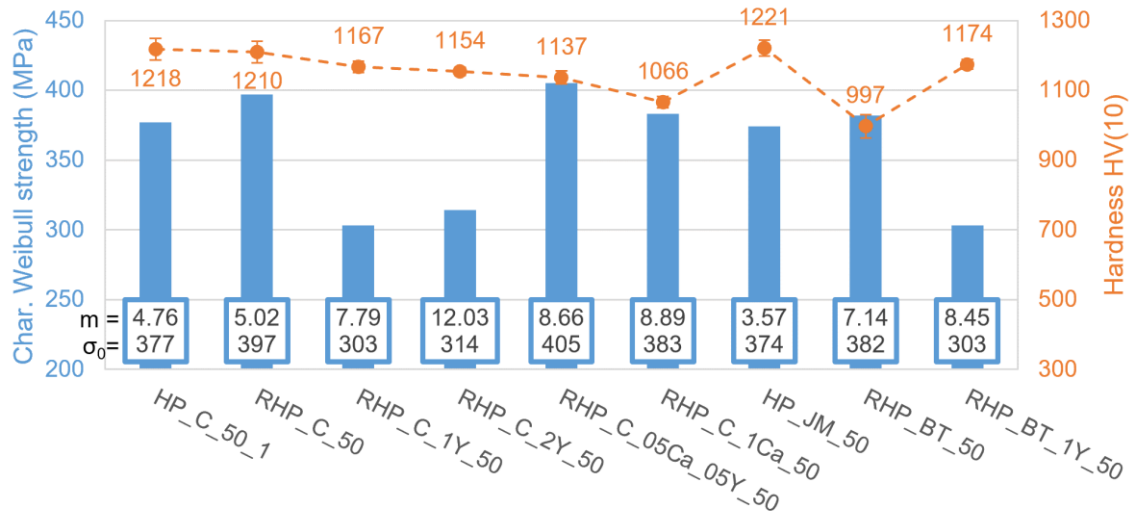
Fig. 19: Characteristic Weibull strength σ_0, and Weibull modulus m of hot-pressed samples, as determined by four-point bending tests. The number of tests performed is listed in Table 15 for each sample. The hardness of the samples was determined by Vicker's hardness testing.

Fig. 20 shows SEM images of the microstructures of the fracture surfaces of bending bars, which were prepared from hot-pressed samples. All the images were recorded using a BSE detector, except for the two from samples without sintering additives, which were recorded using a SE detector. The contrast in the BSE micrographs from samples with additives corresponds to the average atomic number of the microstructural features, with elements with a high atomic number appearing brighter than lighter elements. In this specific case the secondary phase contains yttrium (Z = 39), which has a higher atomic number than aluminum (Z = 13).

The microstructure of the fracture surfaces leads to the conclusion that for samples without sintering additives a transcrystalline fracture mode applies, whereas sintering additives tend to shift the fracture mode towards intercrystalline fracture. Secondary phase can be found primarily as thin lines along the grain boundaries in sample RHP_C_1Y_50. However, samples RHP_C_2Y_50 and RHP_BT_1Y_50 show pockets of secondary phase rather than lines. In sample RHP_C_1Ca_50, no secondary phase could be observed while in sample RHP_C_05Ca_05Y_50 with a combination of CaO and Y_2O_3 sintering additives, the distribution of secondary phase along grain boundaries was similar to the sample RHP_C_1Y_50. The grain size appears to be larger in samples RHP_C_2Y_50 and RHP_C_05Ca_05Y_50, but no grain size analysis was conducted.
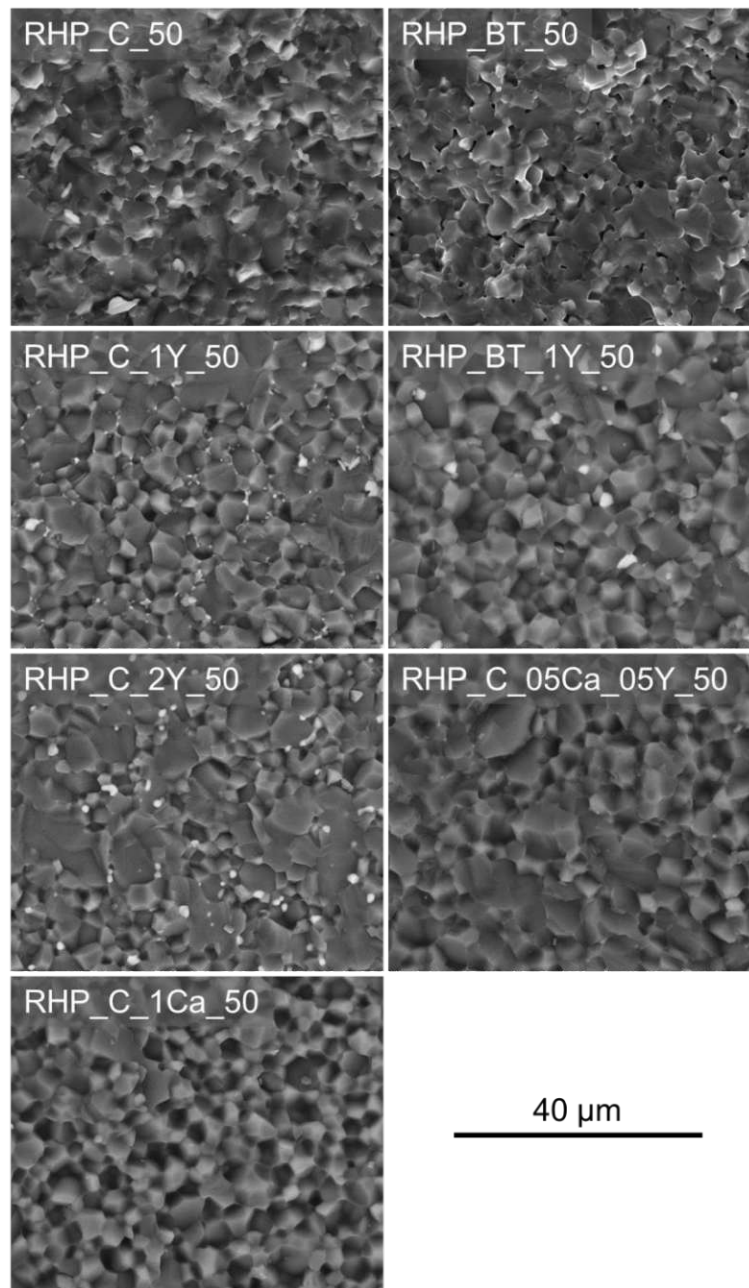
Fig. 20: SEM micrographs of fracture surfaces of bending bars machined from HP samples. The top two images are micrographs for which the SE signals were used, whereas all other micrographs show BSE micrographs, in which the brighter areas correspond to the secondary phase. The fracture behavior changes from a transcrystalline to an intercrystalline mode with the introduction of sintering additives.

The thermal diffusivity of six hot-pressed samples was measured by laser flash analysis at the Slovak Academy of Sciences. To calculate thermal conductivity, the density and specific heat capacity at the measuring temperature must be known. The method to calculate values for specific heat capacity of AlN at different temperatures are described in section 3.7.6. The thermal conductivity values of the samples are plotted in Fig. 21.
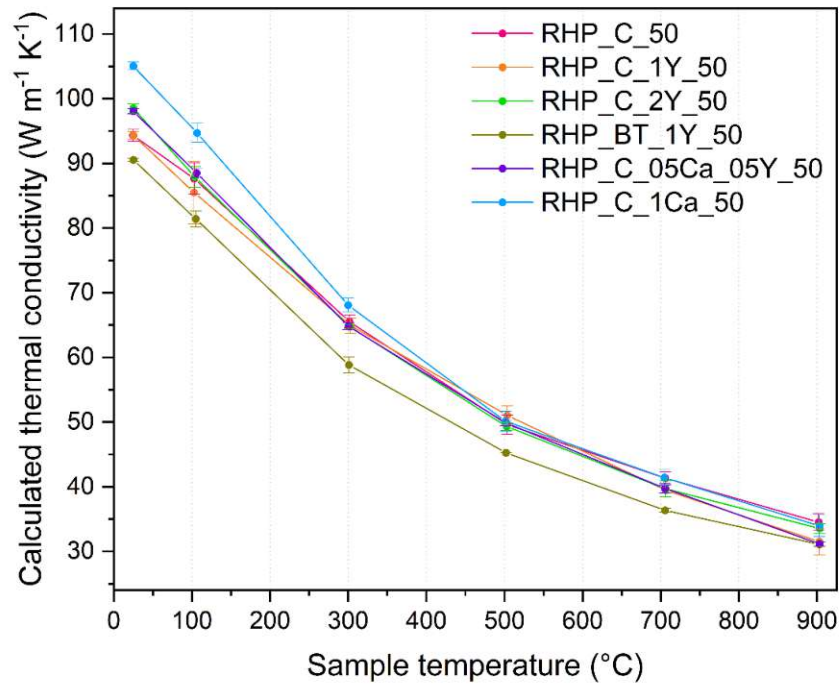
Fig. 21: Thermal conductivities of hot-pressed samples at different temperatures.

Thermal conductivity of two hot-pressed samples was also determined by the steady-state equal heat-flow method. The results are shown in Table 16.

Table 16: Thermal conductivities of HP samples as measured by flash and steady state analysis.

	Thermal conductivity (steady-state) (W m^{-1} K^{-1})
HP_C_50_2	85 ± 1
RHP_BT_50	85 ± 2

4.3 Influence of sintering parameters and additives on CIP samples

A dilatometry experiment using a CIP sample in a push-rod dilatometer was conducted to gain first insights into the sintering process of AlN. Additional preliminary experiments on the conventional processing of AlN powder mixtures by cold-isostatic pressing and sintering in two different furnaces were performed during two internships. The conclusions from those preliminary experiments led to the systematic investigation of combinatory sintering additives (CaO and Y_2O_3) in AlN powder mixtures and the influence of different sintering times in different sintering environments. For the most promising additive combination, the effect of the sintering parameters and sintering environments on the migration and removal of the secondary phase on the densification behavior, mechanical, microstructural, and thermal properties of AlN materials was investigated. Additional experiments at a lower sintering temperature or using alternative AlN powders were also conducted to investigate the influence of those parameters on the final properties of the materials.

4.3.1 Dilatometry of a CIP samples up to 1500 °C

A CIP AlN sample made from a Grade C AlN powder mixture containing 1 wt.% CaO (as $CaCO_3$) and 3 wt.% Y_2O_3 was heated to 1540 °C in a dilatometer in N_2 atmosphere. While 1540 °C is too low for actual sintering of this sample, the on-set of the sintering at approximately 1450 °C was observable in the data gathered from the experiment (Fig. 22).
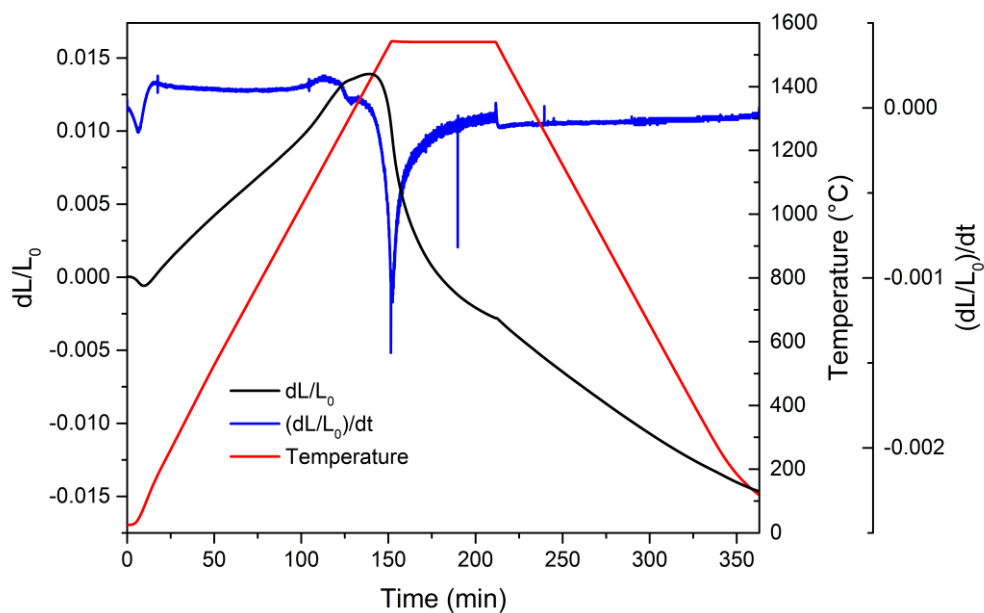

Fig. 22: Results of a dilatometry experiment with a sample made of Grade C AlN powder mixture with 1 wt.% CaO (as $CaCO_3$) and 3 wt.% Y_2O_3 up to 1540 °C in N_2 atmosphere, indicating an on-set of the shrinkage at approximately 1450 °C.

4.3.2 CIP samples sintered in a corundum tube furnace

Multiple samples were sintered in a corundum tube furnace at 1700 °C for 2 h in N_2 atmosphere without a powder bed. The results of the density evaluations shown in Fig. 23 indicate that the addition of Y_2O_3 does not lead to significant densification at this temperature. The presence of CaO leads to increased densification, but higher amounts of CaO may decrease density again. The combination of CaO and Y_2O_3 proved to be the most effective sintering additive system in these experiments, with all samples exceeding 95 % of the relative density. The results of Vicker's hardness testing show similar trends as the density measurements (Fig. 24).
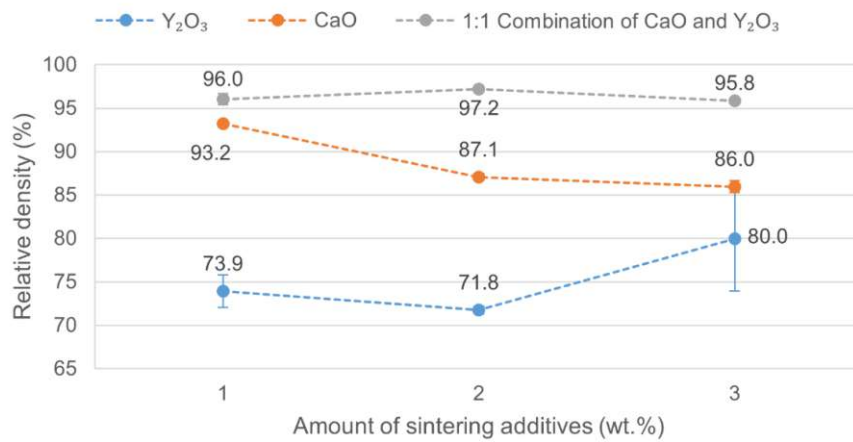
Fig. 23: Relative density of AlN samples with varying sintering additives, sintered in a corundum tube furnace without powder bed. The grey line represents samples from a powder mixture with equal parts of CaO and Y_2O_3 (e.g. a sample with 2 wt.% sintering additives added contains 1 wt.% CaO and 1 wt.% Y_2O_3).
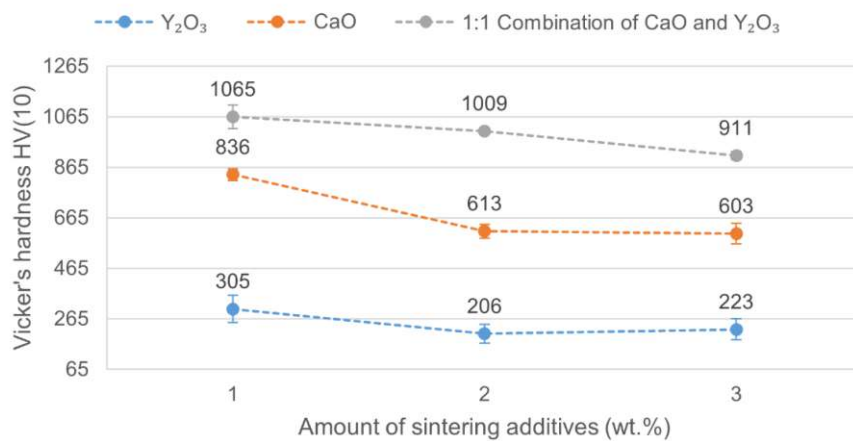
Fig. 24: Vicker's hardness of AlN samples with varying sintering additives, sintered in a corundum tube furnace without powder bed. The grey line represents samples from a powder mixture with equal parts of CaO and Y_2O_3. A sample with 2 wt.% sintering additives added contains 1 wt.% CaO and 1 wt.% Y_2O_3.

Comparative micrographs in Fig. 25 confirm the results of the density measurements, revealing sintered microstructures for samples with CaO addition, whereas samples with solely Y_2O_3 addition only show signs of initial sintering stages, and the Y-rich phase (bright in the micrograph) does not show clear signs of melting. The micrographs of samples with CaO as sintering additive do not show a secondary phase. In the samples with combined sintering additives, an accumulation of secondary phase along grain boundaries can be observed.
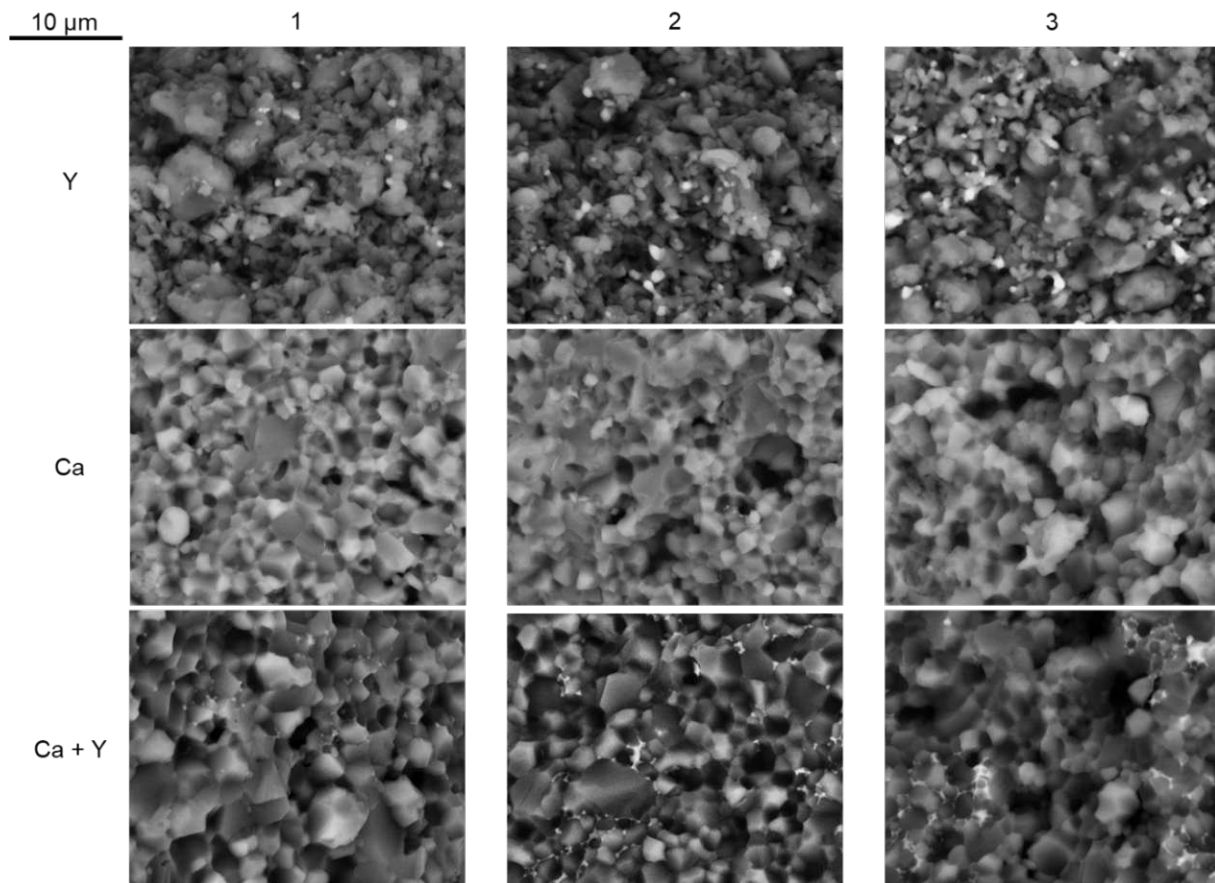
Fig. 25: BSE-SEM micrographs of fracture surfaces of samples sintered in a corundum tube furnace without powder bed. The columns represent the sum of sintering additives added. For samples with a combinatory additive, CaO and Y_2O_3 were added in equal parts.

In samples with added CaO, large pores can be observed. This might stem from the decomposition of $CaCO_3$ during the sintering program. Fig. 26 shows a SE micrograph the fracture surface of a sample with 1.5 wt.% CaO and 1.5 wt.% Y_2O_3 at a lower magnification, revealing large pores.
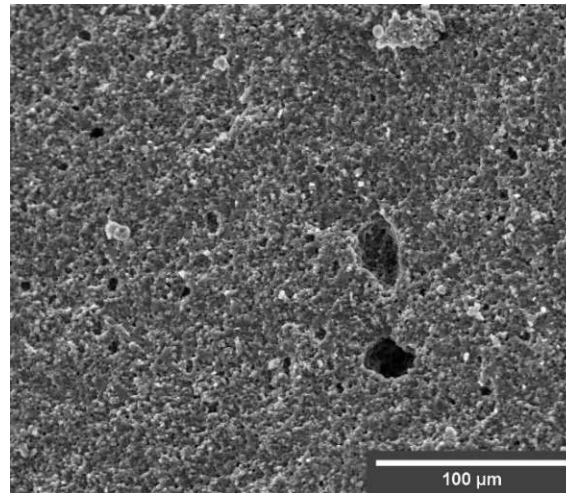
Fig. 26: SEM Micrograph (SE) of the fracture surface of a sample with 1.5 wt.% CaO and 1.5 wt.% Y_2O_3, revealing large pores.

4.3.3 CIP samples sintered in a graphite furnace

Taking the results from above, the combination of sintering additives was evaluated in more detail and sintered in a reducing environment, while other sintering parameters were not altered. As prior research showed, the decomposition of $CaCO_3$ during sintering might lead to increased porosity. To prevent the formation of pores, for some experiments the powder mixtures were thermally treated prior to shaping by CIP.

4.3.3.1 Heat treatment of powder mixtures to form oxides from sintering additive precursors

DTA and TG of the precursor compounds was performed to estimate decomposition temperatures of the carbonate – and later nitrate – additives. Fig. 27 shows the results of thermal analysis in N_2.
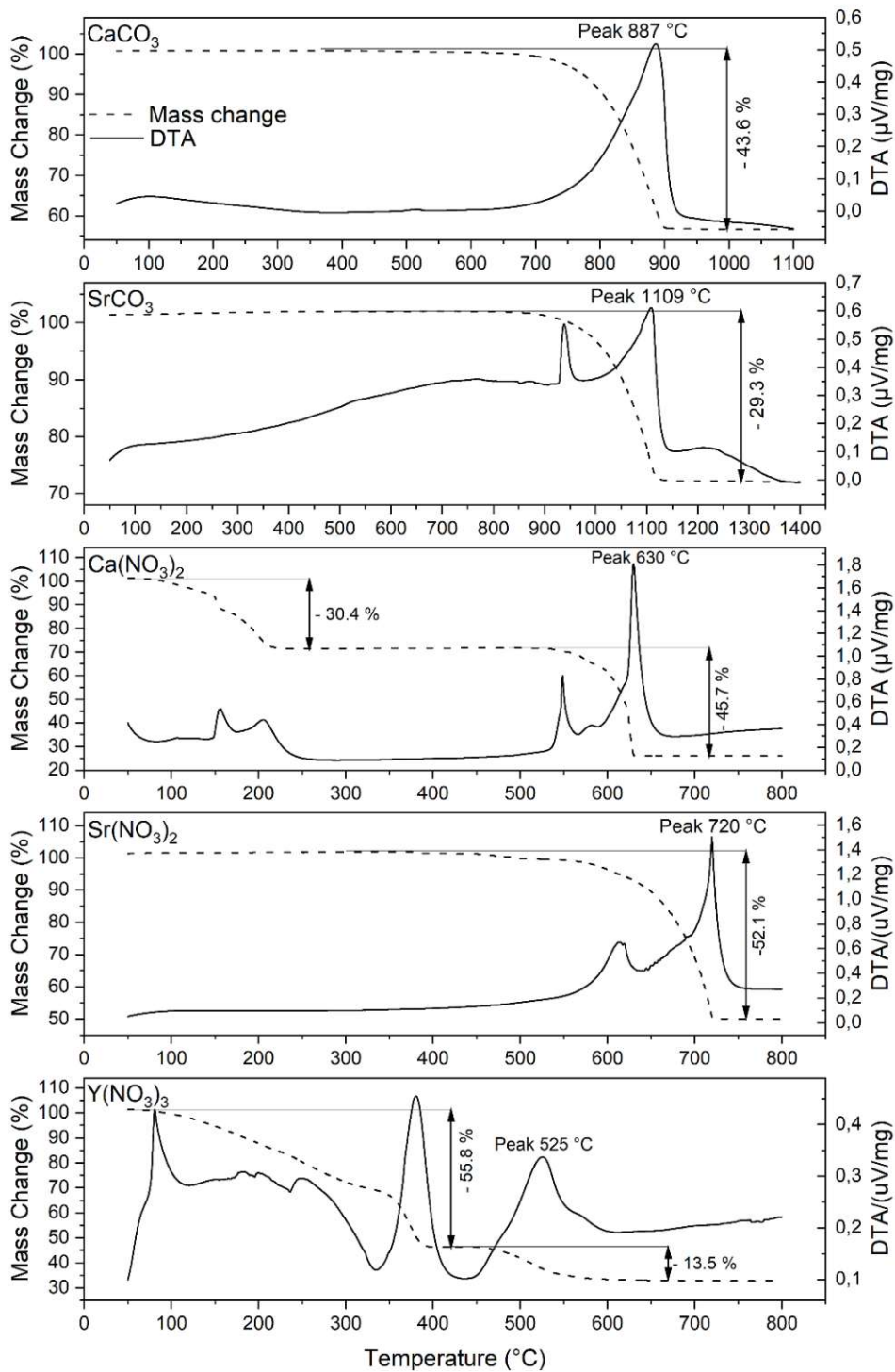
Fig. 27: Compilation of thermal analysis measurements of sintering additive precursor compounds to estimate their decomposition temperatures.

Based on the results from the thermal analysis, the temperatures in Table 17 were estimated.

For all thermal treatments the powders were held for two hours at the temperature indicated.

$SrCO_3$-containing mixtures were held at the indicated temperature for four hours, because the difference between the measured decomposition temperature and the actual temperature used in the heat treatment was below 50 °C.

Table 17: Results of thermal analysis, indicating the temperatures of decomposition of the sintering additive precursor compounds to the respective oxides and actual temperatures used in thermal treatment of powder mixtures. Holding times for thermal treatment were two hours (four hours in case of $SrCO_3$).

Sintering additive precursor	Full decomposition to oxide (°C)	Decomposition temperature chosen for powder mixtures (°C)
$CaCO_3$	900	950
$SrCO_3$	1118	1150 (4 h)
$Ca(NO_3)_2$	680	900
$Sr(NO_3)_2$	720	900
$Y(NO_3)_3$	620	900

Thermal treatment of powder mixtures was carried out in two different tube furnaces in N_2 atmosphere. Although the densification was higher for samples with powder mixtures treated in furnace A, it was also found that the atmosphere in furnace A proved to not be adequate, as the oxygen content of AlN (without sintering additives) increased significantly, as was shown by elemental analysis (see section 4.1.3).

4.3.3.2 Sintering of powder compacts

Samples sintered in the graphite furnace exhibited inhomogeneous appearances with parts of the samples being anthracite-colored and other parts appearing light gray.

Sintering additives in this set of experiments included CaO and SrO as single additives, derived from carbonates as well as in combination with Y_2O_3. Fig. 28 shows the densification and Vicker's hardness (10 kilopond force) of the samples. The nomenclature is best explained with an example; "1 Ca + 1 Y, TT A" stands for samples from a powder mixture including 1 wt.% CaO and 1 wt.% Y_2O_3 as sintering additives, while TT A indicates, that $CaCO_3$ as a precursor compound was thermally decomposed to the CaO prior to shaping in SA-precursor decomposition furnace A. Sintering additive combinations of CaO/SrO and Y_2O_3 in thermally treated powder mixtures led to the samples with the highest densities and hardness values. Single sintering additives and non-thermally treated powder mixtures resulted in lower values.
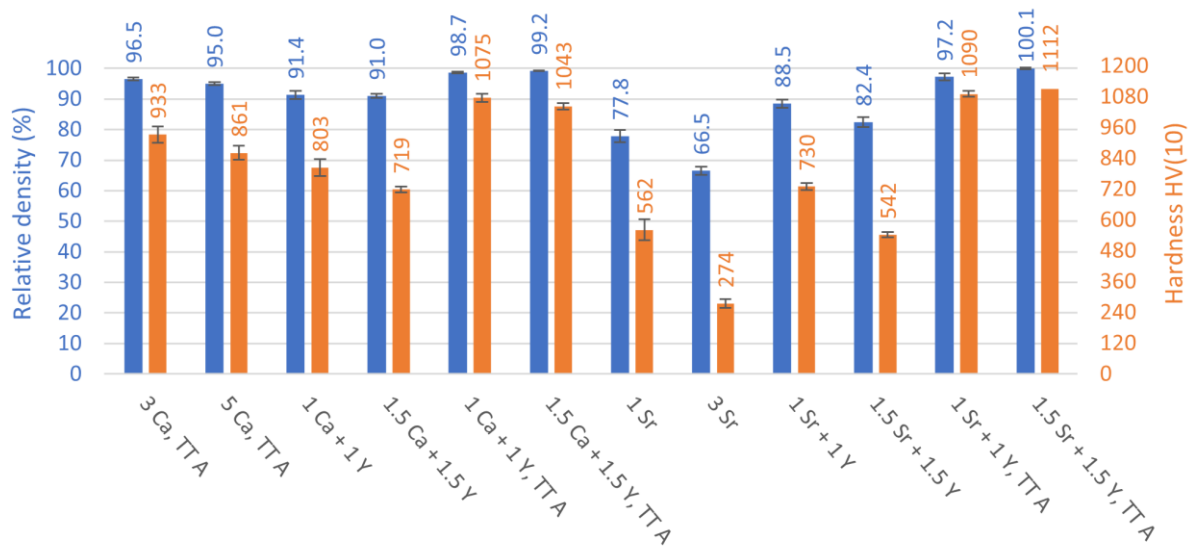
Fig. 28: Relative density and Vicker's hardness of samples from Grade C AlN powder with various types and amounts of sintering additives. Ca, Sr and Y are short for the respective oxides used as additives and TT denotes thermal treatment of powder mixtures to decompose sintering additive precursors - carbonates in this case - to the respective oxides prior to shaping. The samples were sintered in a graphite furnace at 1700 °C for two hours in N_2 atmosphere.

As mentioned in section 4.1.3, the decomposition of sintering additive precursors in the SA-precursor decomposition furnace A led to an increase of the oxygen content of the AlN powder. Some of the results shown in Fig. 28 are compared to the results of samples for which the powder mixtures were treated in SA-precursor decomposition furnace B, which did not lead to an increase in oxygen content. The treatment in furnace B led to a slight decrease in density and hardness in sintered samples, except for the powder mixture with 5 wt.% CaO, treated in furnace B, which produced samples with only slightly lower density and even higher hardness than corresponding samples from powder treated in furnace A.
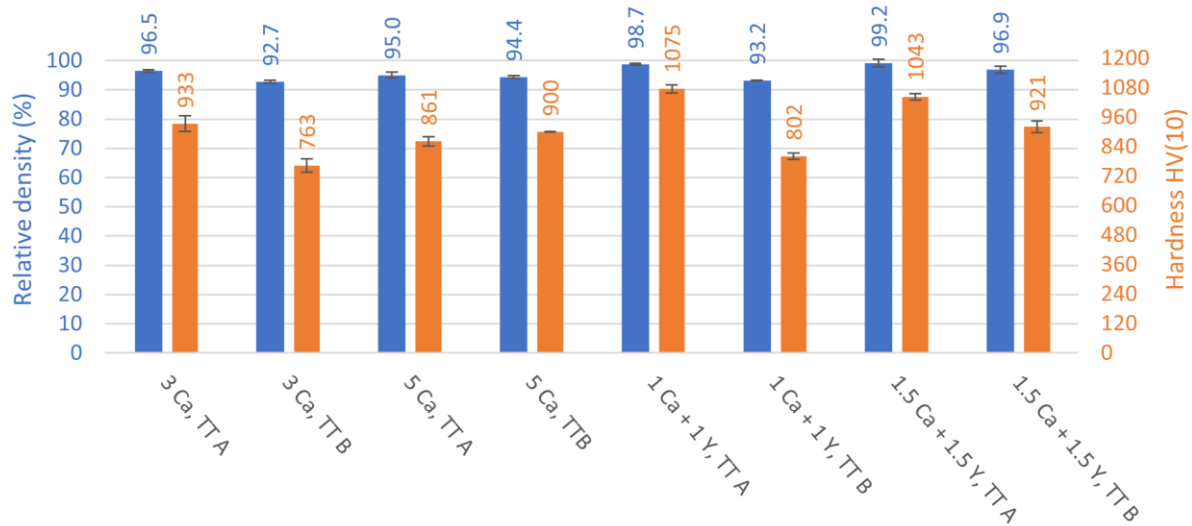
Fig. 29: Comparison of the relative density and Vicker's hardness of samples from Grade C AlN powder with various types and amounts of sintering additives. Ca and Y are short for the respective oxides used as additives. "TT A" and "TT B" denote the decomposition of the carbonate sintering additive precursors, prior to shaping, in SA-precursor decomposition furnaces A and B, respectively. Sintering of samples was conducted in a graphite furnace at 1700 °C for two hours in N_2 atmosphere.

The microstructures of the samples were systematically investigated by BSE-SEM (Fig. 30). Secondary phase distribution was different for all samples investigated. In samples with only CaO sintering additive very little secondary phase could be observed. The samples from powder mixtures containing a sintering additive combination, of which the precursor compounds were thermally decomposed in SA-precursor decomposition furnace A prior to shaping, showed secondary phase along the grain boundaries, which was observed to a lesser degree in samples from powder mixtures treated in SA-precursor decomposition furnace B.
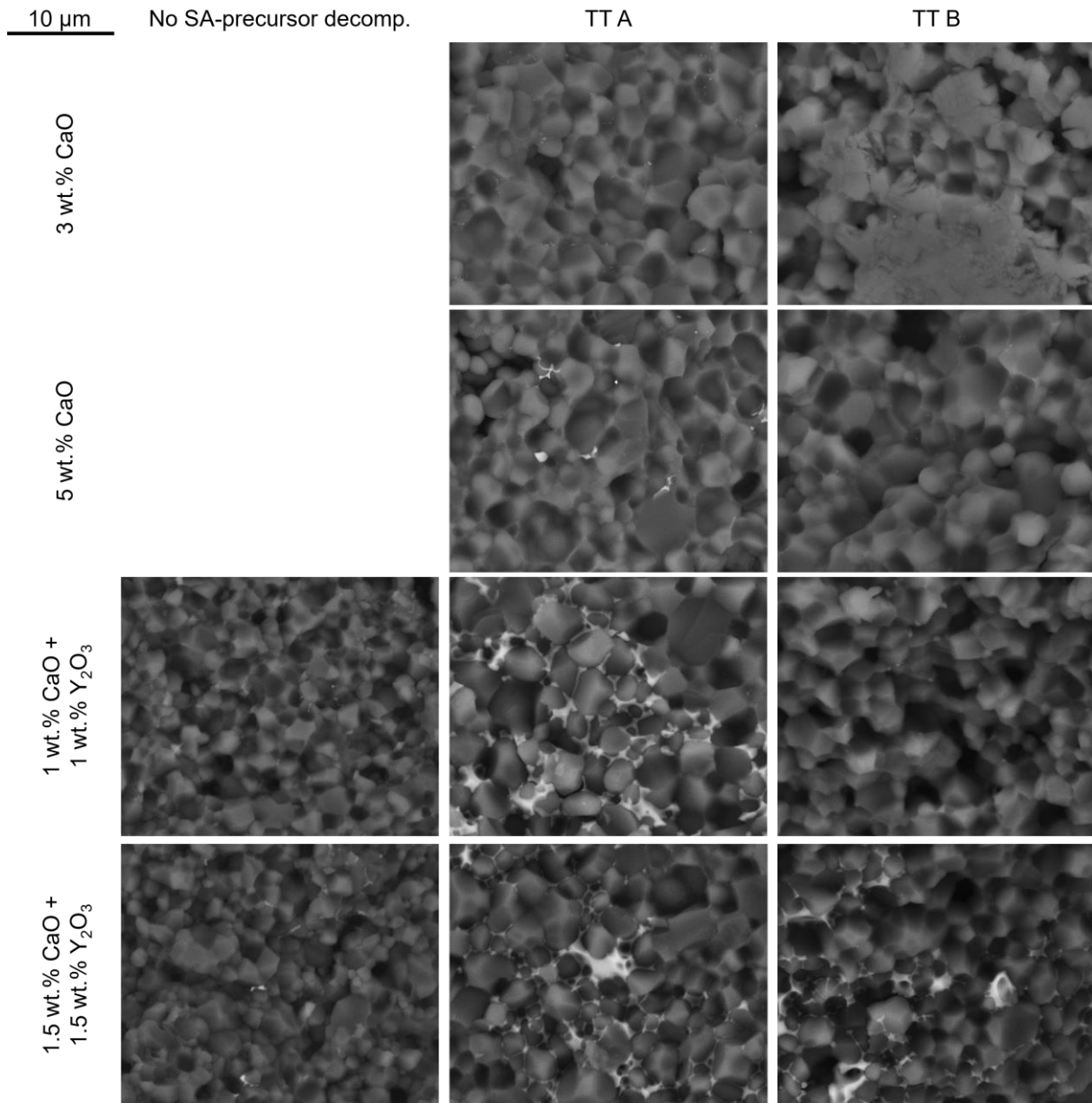
Fig. 30: Overview of BSE-SEM micrographs of the fracture surfaces of samples from Grade C AlN with CaO and Y_2O_3 sintering additives, sintered at 1700 °C for two hours in N_2 atmosphere. $CaCO_3$ was used as precursor compound for CaO, which was decomposed in the powder mixture prior to shaping in the samples showed in the second and third column. The brighter areas represent the secondary phase. The samples in which the $CaCO_3$ was decomposed in SA-decomposition furnace B show less secondary phase.

Fig. 31 shows additional micrographs of samples produced from powder mixtures treated in SA-presursor decomposition furnace B. Migrative behavior of the secondary phase, accumulating as a ribbon-like feature on a sample with 1 wt.% CaO and 1 wt.% Y_2O_3 sintering additives or leaving the sample to cover the surface in a sample made from a powder mixture containing 1.5 wt.% CaO and 1.5 wt.% Y_2O_3, can be observed.
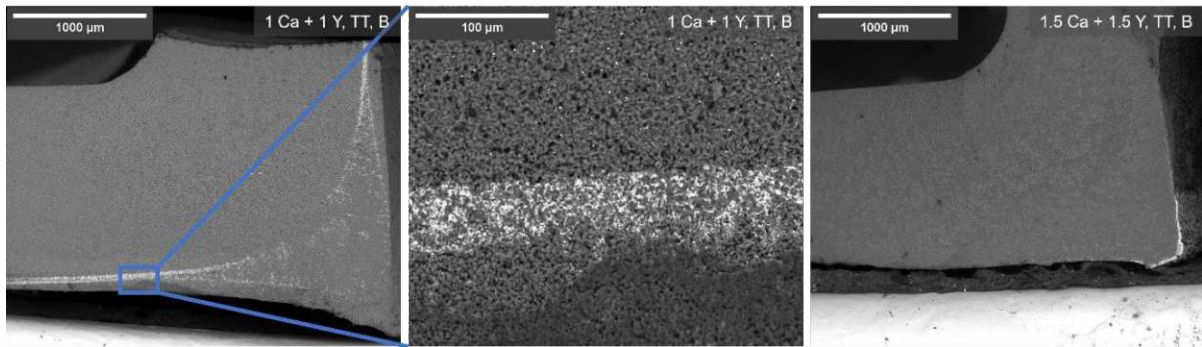
Fig. 31: BSE-SEM micrographs of fracture surfaces from samples created with powder mixtures including Grade C AlN, CaO and Y_2O_3. $CaCO_3$ was thermally decomposed in SA-decomposition furnace B prior to shaping. The samples were sintered at 1700 °C for two hours in a graphite furnace in N_2 atmosphere. They show a migration of secondary phase out of the center towards the sample surface. The first sample shows migration in a ribbon-like feature, which seemingly stopped before reaching the sample surface whereas migration seems to have been completed during sintering in the second sample shown.

The microstructure of Sr-containing samples, shown in Fig. 32, reflects the results of the density measurements clearly, showing that SrO as sole additive leads to a very porous microstructure, lacking the polyhedral grains that can be seen in typical dense microstructures of AlN. The combined additive system with SrO and Y_2O_3 leads to higher density, but only after thermal decomposition of sintering additive precursors in the powder mixture before shaping can a dense microstructure with secondary phase along grain boundaries be observed. The migrative behavior as seen in Fig. 31 was also observed when SrO was used instead of CaO (not shown).
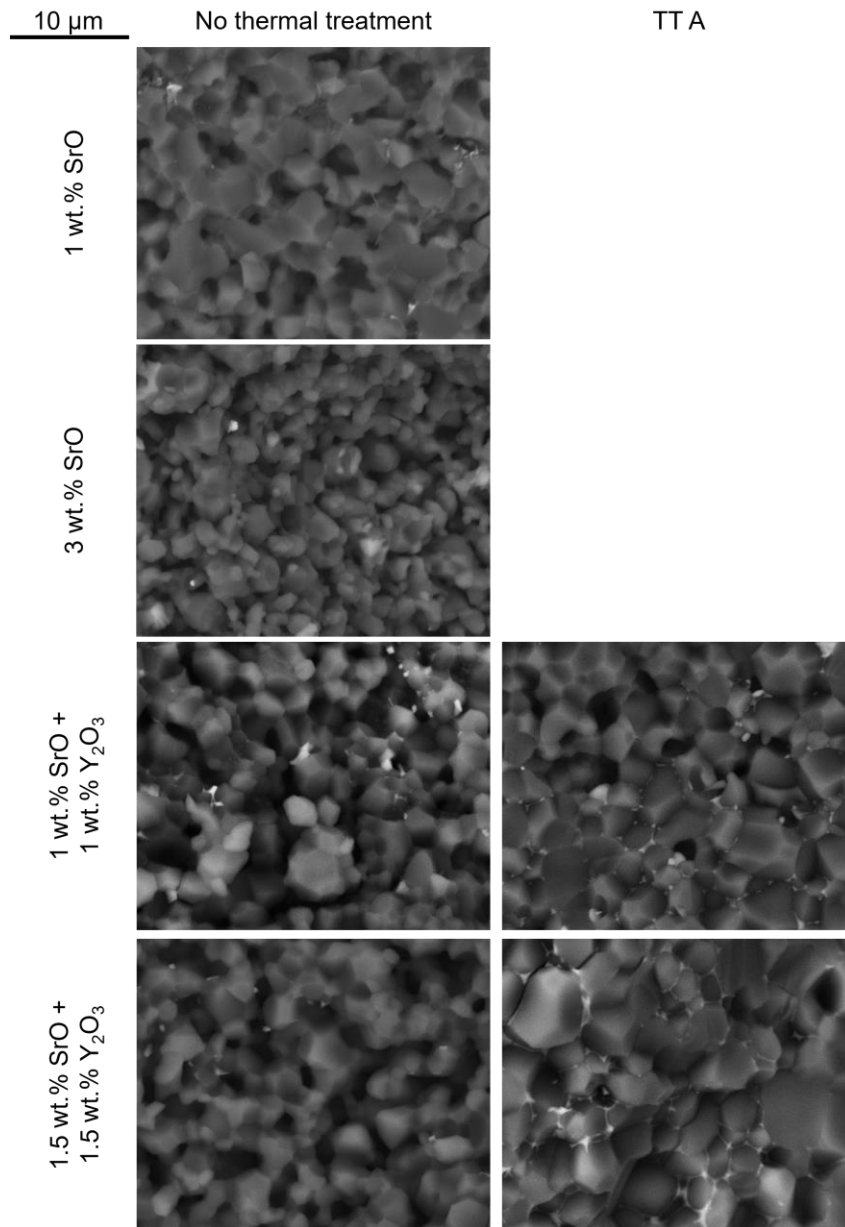
Fig. 32: BS-SEM micrographs of fracture surfaces of samples (sintered at 1700 °C for two hours in a graphite furnace in N_2 atmosphere) from Grade C AlN with SrO (added as $SrCO_3$) and Y_2O_3 as sintering additivea, which show that SrO does not lead to a high density sample, whereas the combination of SrO and Y_2O_3 leads to a dense microstructure, as long as the carbonate precursor was thermally treated prior to shaping.

In an attempt to increase the homogeneity of the powder mixtures, the additives were also added as nitrates, by first dissolving them in isopropyl alcohol or methanol (for strontium nitrate), which was then mixed with the AlN powder before the liquid phase was removed by rotary evaporation. The relative density and hardness of the samples can be seen in Fig. 33. While the combination of CaO and Y_2O_3 led to highly densified samples with correspondingly high hardness, the density and hardness of samples containing SrO and Y_2O_3 were lower.
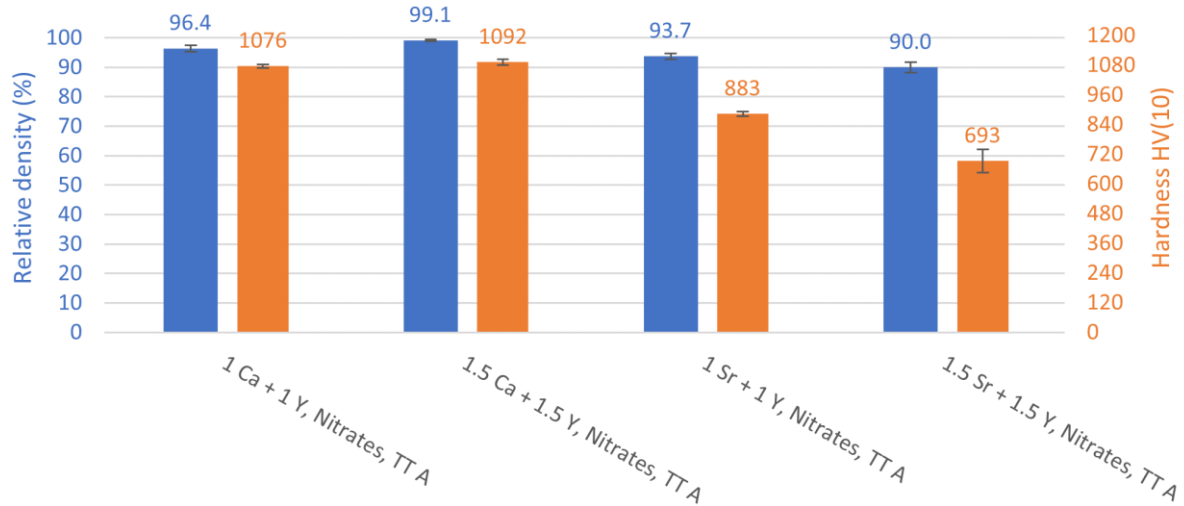
Fig. 33: Relative densities and hardness values of samples produced from powder mixtures in which CaO/SrO and Y_2O_3 were added to AlN as nitrates dissolved in the liquid medium used for mixing the powder mixtures. The powder mixtures were heated to 900 °C for two hours in SA-precursor decomposition furnace A, prior to shaping. Sintering was conducted at 1700 °C in the graphite furnace for two hours in a N_2 atmosphere.

The microstructures of fracture surfaces of samples prepared with nitrate sintering additives are shown in Fig. 34. Except for the sample with 1.5 wt.% SrO and 1.5 wt.% Y_2O_3, all samples exclusively show polyhedral grains. The secondary phases are more distinct in the samples with SrO sintering additive.
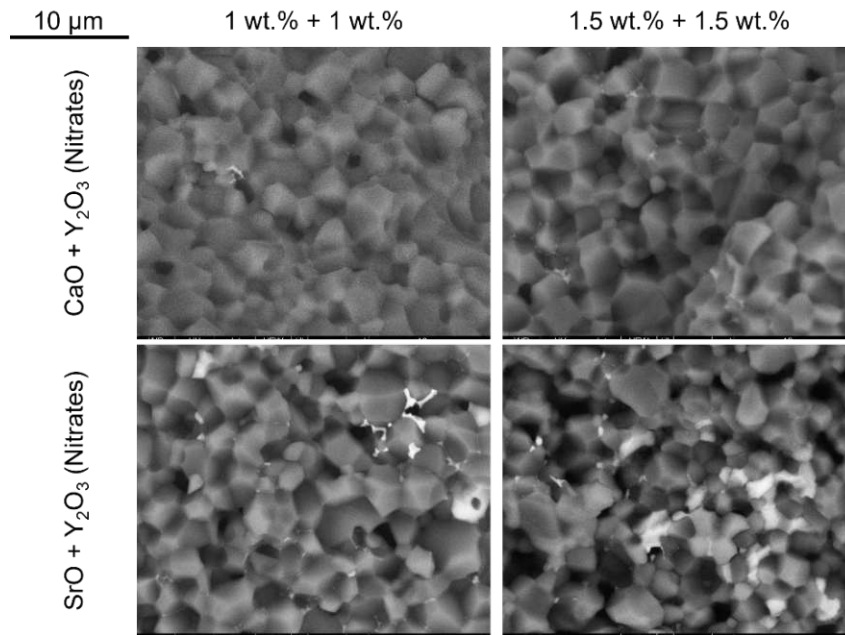
Fig. 34: BSE-SEM micrographs of fracture surfaces of samples produced from powder mixtures with nitrate sintering additives, which were thermally decomposed in SA-precursor decomposition furnace A at 900 °C for 2 hours before shaping and sintering (1700 °C, two hours, graphite furnace, N_2 atmosphere). The samples containing SrO as sintering additive have a microstructure indicating lower density, which confirms the data in Fig. 33.

4.3.4 Sintering of CIP AlN samples in powder beds

The experiments in the corundum tube and graphite furnaces produced samples inhomogeneous in appearance and properties. In an attempt to homogenize the sintering atmosphere for all samples inside the graphite furnace, powder beds were employed.

4.3.4.1 Sintering additives, sintering effects and their impact on densification, thermal conductivity and microstructure of sintered samples

Powder mixtures consisting of AlN and BN in equal parts by weight with or without 5 wt.% graphite were employed as bed material. Only CaO (as $CaCO_3$) and Y_2O_3 were used as sintering additives, with CaO set to 1 or 1.5 wt.%, while Y_2O_3 was varied from 1 to 5 wt.%. Sintering temperature was 1700 °C if not explicitly stated otherwise, and sintering times from two to six hours were utilized. The sintered samples were investigated by measuring density, thermal conductivity and analyzing the microstructures of the samples by SEM. Bending strength was determined for select samples.

Powder bed AB: Samples from thermally pre-treated powder mixtures

Powder mixtures from Grade C AlN with CaO and Y_2O_3 sintering additives were prepared. The same powder processing as described in section 4.3.3 was employed, including the thermal decomposition of $CaCO_3$ at 950 °C in N_2, although the pre-treatment time of powder mixtures was increased to 2 hours from 4 hours. Sintering was conducted in a graphite crucible in the graphite furnace. Fig. 35 shows the relative density evolution of samples with different compositions. The relative densities of samples sintered for 2 or 4 hours did not show a significant difference, whereas the samples sintered for 6 hours exhibited lower density, which increased with higher Y_2O_3 content. Since the density determined by the liquid displacement method showed high deviations in the density of samples sintered for six hours, the geometric demsity of said samples was included. The samples were taken from one sintering run per investigated sintering time.
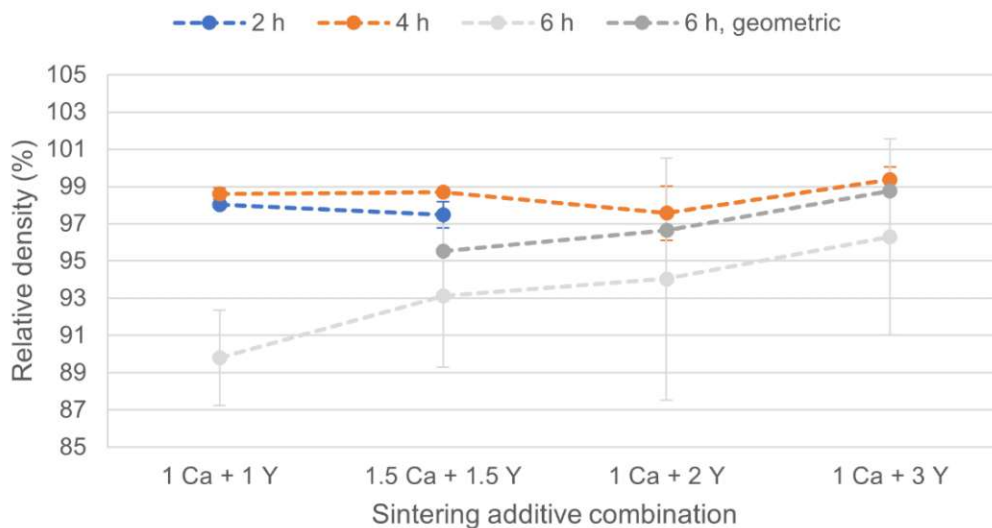

Fig. 35: Relative density AlN samples from powder mixtures of Grade C AlN including a combined sintering additive of CaO and Y_2O_3. The $CaCO_3$ SA precursor in the powder mixture was decomposed prior to shaping. Sintering was conducted at 1700 °C in a graphite furnace (N_2 atmosphere) in a powder bed of equal parts of AlN and BN by weight. All density values were determined by the liquid displacement method using water, except for the series "6h, geometric". The values for the "6 h" series (light gray) are low and exhibit high deviations, possibly indicating a systematic error (e.g. gas build-up on samples during immersion) of the density measurement, which is why geometric density values, listed as "6 h, geometric", are also shown. Geometric determination of density was conducted using bar-shaped samples for steady-state thermal conductivity measurements.

Fig. 36 shows the thermal conductivity evolution of the same series, which is proportional to the sintering time as well as the composition, even though the density of the samples sintered for 6 hours is lower than for the other sintering times.
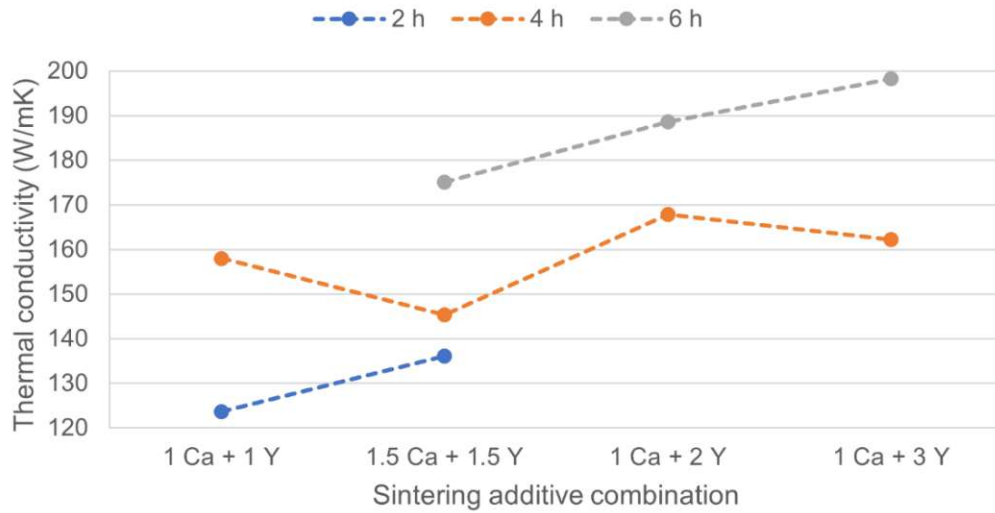
Fig. 36: Thermal conductivity (steady state method) of AlN samples from Grade C AlN powder mixtures including CaO and Y_2O_3. SA precursors in the powder mixtures were decomposed prior to shaping. Sintering was conducted in a graphite furnace at 1700 °C in a N_2 atmosphere and a powder bed of equal parts of AlN and BN by weight.

Powder bed AB: Samples from powder mixtures without thermal pre-treatment

In a preliminary experiment it was observed that the powder bed might alleviate the negative effect that $CaCO_3$ decomposition has on the densification during sintering of samples. Green bodies of powder mixtures of Grade C AlN with CaO and Y_2O_3 sintering additives, in which the $CaCO_3$ SA precursor was not decomposed prior to shaping, were prepared by CIP. Sintering was then conducted in the graphite furnace in a powder bed of equal parts (by weight) of AlN and BN. Fig. 37 shows the evolution of relative density for different compositions and sintering times. For all sintering times, the density increased with increased Y_2O_3 addition, with the exception of the samples containing 1.5 wt.% CaO after 2 and 6 h of sintering time. As in Fig. 35, the geometric density of samples sintered for six hours is shown, because values from the immersion method exhibited high deviations.
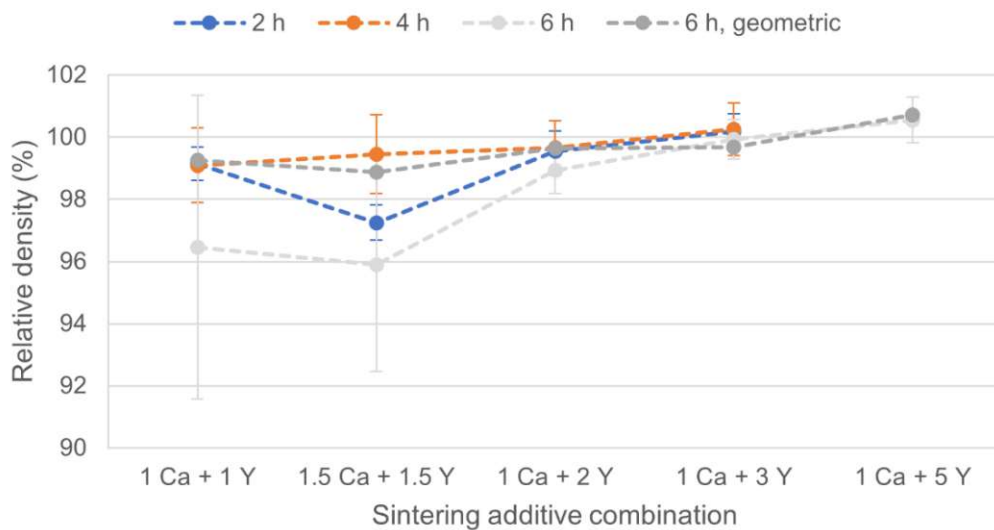

Fig. 37: Relative density versus sintering additive composition of AlN samples from Grade C AlN powder mixtures including CaO and Y_2O_3 as sintering additives, precursors of which were not decomposed prior to shaping. Samples were sintered in a graphite furnace (1700 °C, N_2) in a powder bed of equal parts of AlN and BN by weight for 2 to 6 hours. Akin to Fig. 35, the density values for the 6 h sample series showed high deviations, which is why geometric density values of this series are also displayed.

Similar to the earlier sample series (Fig. 36), thermal conductivity, as shown in Fig. 38, increases with higher sintering times and higher Y_2O_3 content up to 3 wt.% Y_2O_3, with a notable exception of the "1 Ca + 3 Y" sample, sintered for 2 h.
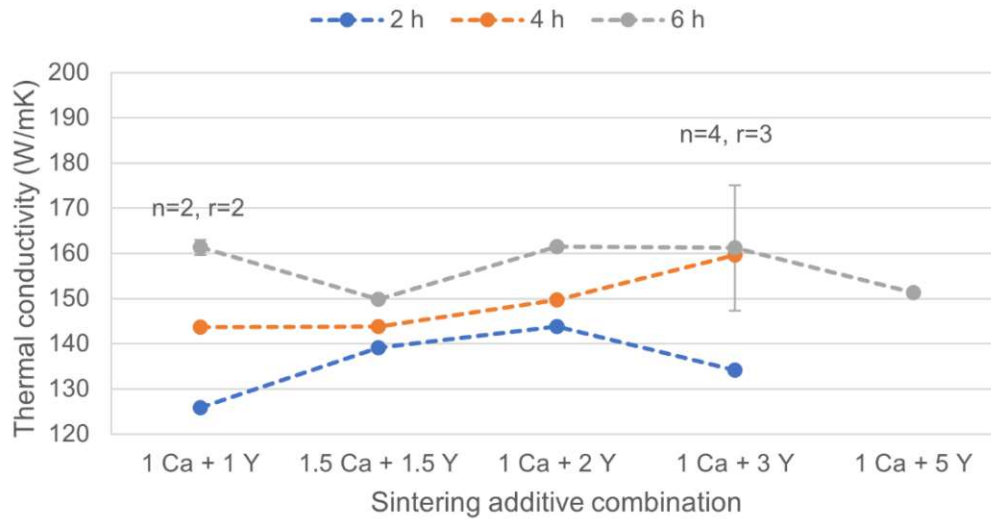
Fig. 38: Thermal conductivity (steady state) versus additive composition of AlN samples from Grade C AlN powder mixtures including a CaO and Y_2O_3 as sintering additives. $CaCO_3$ was not decomposed prior to shaping and sintering (1700 °C, graphite furnace, N_2 atmosphere, powder bed AB). If multiple samples were measured, *n* represents number of individual samples from *r* sintering runs.

Fig. 39 shows a compilation of BSE-SEM micrographs of fracture surfaces of samples produced from Grade C AlN powder mixtures with CaO and Y_2O_3 sintering additives. The $CaCO_3$ SA precursor was not thermally decomposed prior to shaping and sintering in a powder bed of AlN and BN. All micrographs show a dense microstructure with intercrystalline fracture, revealing polyhedral grains. While more clearly visible in samples with higher initial additive content, signs of secondary phases along grain boundaries can be observed in all micrographs.
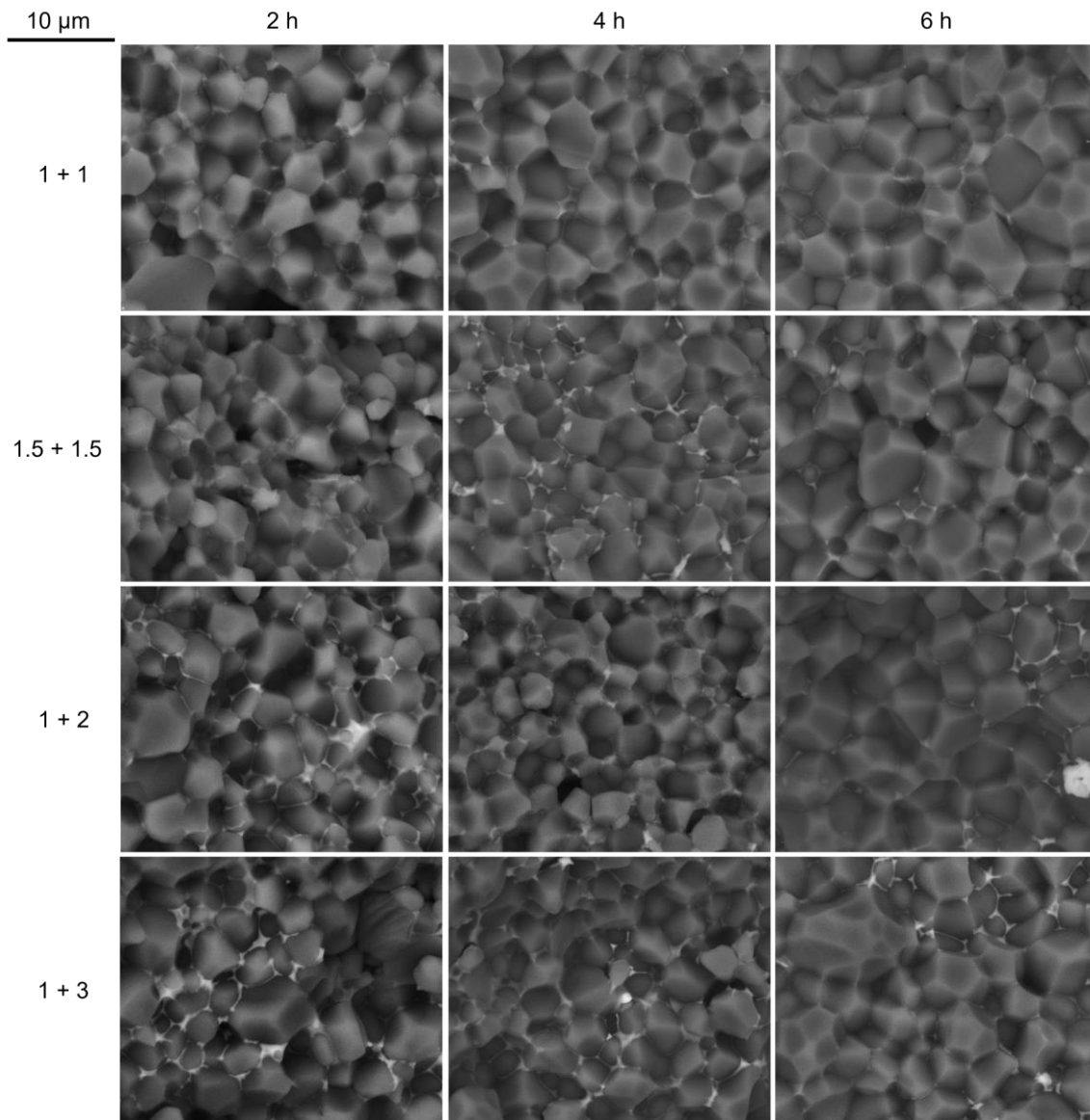
Fig. 39: BSE-SEM micrographs of fracture surfaces of samples made from Grade C AlN powder mixtures containing CaO and Y_2O_3 sintering additives. The SA precursor was not thermally decomposed before CIP and sintering, which was conducted in a graphite furnace (1700 °C, N_2 atmosphere) in a powder bed of AlN and BN for two to six hours. The microstructures of samples with different compositions and sintering times are shown. Brighter areas correspond to the secondary phase, which contains Y.

Fig. 40 shows SEM micrographs (SE) of polished surfaces of samples from Grade C AlN powder systems with CaO and Y_2O_3 sintering additives, sintered at 1700 °C in a graphite furnace and an AB powder bed for six hours. The average length of intersecting lines given in the inset. The secondary phase appears to decrease with increasing sintering additive content.
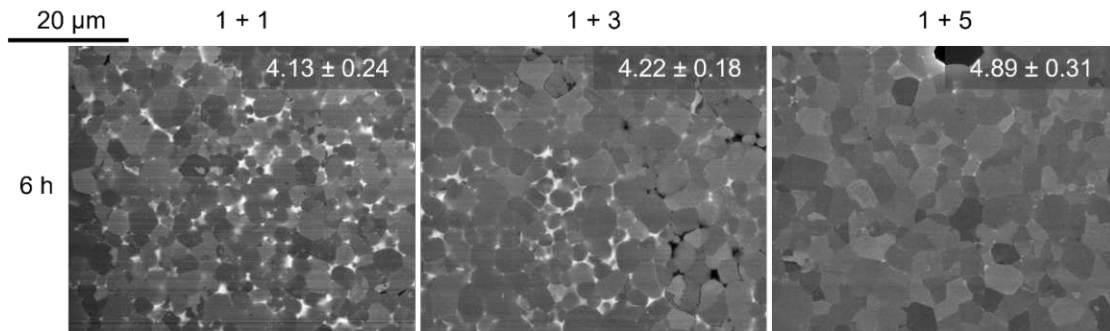
Fig. 40: SE-SEM micrographs of polished surfaces of samples from Grade C AlN powder mixtures with CaO and Y_2O_3 sintering additives, that were not thermally pre-treated. The samples were sintered in a graphite furnace in a powder bed of AlN and BN for six hours. The insets represent the average length of intersecting lines.

Powder bed ABC: Samples from powder mixtures without thermal pre-treatment

Multiple samples with 1 wt.% CaO and varying amounts of Y_2O_3 addition were sintered in a graphite furnace at 1700 °C for varying times in N_2 atmosphere and a powder bed consisting of 47.5 wt.% AlN, 47.5 wt.% BN and 5 wt.% C. Most sintering runs were conducted with samples with 3 wt.% Y_2O_3 addition, sintered for 6 h. Relative density of all samples exceeded 98 % for all investigated variations, as shown in Fig. 41.
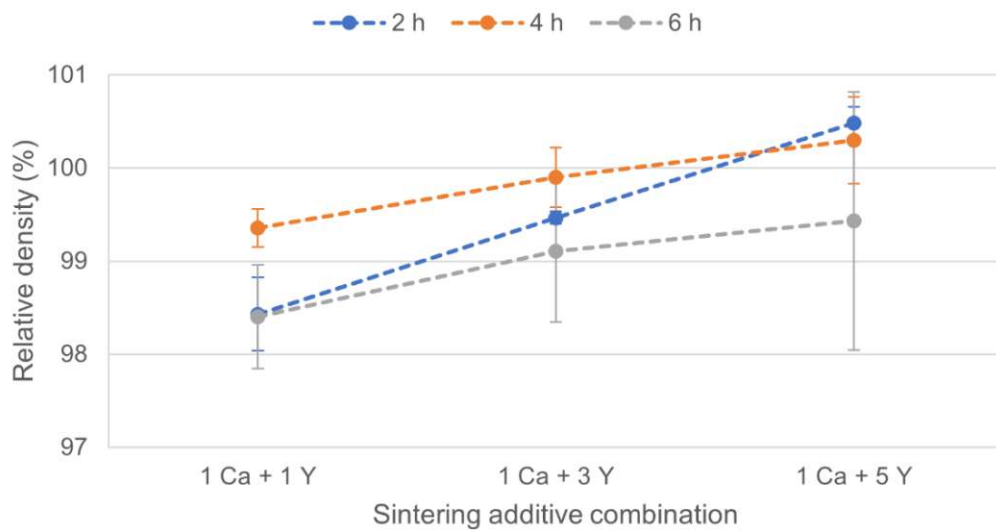
Fig. 41: Relative density (liquid displacement method) of sintered samples from Grade C AlN powder mixture containing 1 wt.% CaO (as $CaCO_3$) and Y_2O_3 sintered in a graphite furnace in a powder bed of AlN and BN with 5 wt.% graphite addition. The powder mixtures were not thermally pre-treated. The density of samples increases with higher sintering additive content and decreases with longer sintering times. The deviation for the "6 h" samples is lower than the deviation of density determined by immersion method for "6 h" samples in Fig. 35 and Fig. 37.

Thermal conductivity (steady state), as shown in Fig. 42, was only measured for one sample per data point, if not stated otherwise. The data shows that the highest thermal conductivity was achieved after 6 h of sintering. With the exception of a sample with 5 wt.% Y_2O_3 in the powder mixture, sintered for 6 h, which exhibited lower thermal conductivity than expected, thermal conductivity was found to be proportional to the Y_2O_3 added to the mixture.
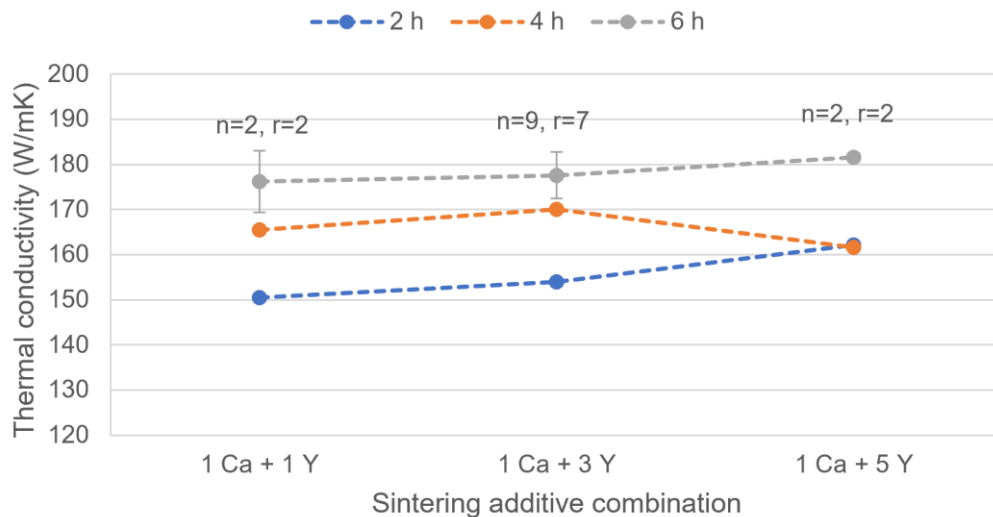
Fig. 42: Thermal conductivity (steady state) of samples sintered in a powder bed of AlN and BN with 5 wt.% graphite in a graphite furnace (1700 °C, N_2 atmosphere) with CaO and Y_2O_3 sintering additives. The $CaCO_3$ SA precursor was not decomposed prior to sintering. If more than one sample was measured, *n* denotes the number of individual samples and *r* the number of sintering runs from which samples were taken. Thermal conductivity increases with increased sintering time and a higher sintering additive content, except for "1 + 5"

Additional thermal conductivity measurements using the flash technique of samples sintered in these conditions will be shown in section 4.4, because the context and relation to other samples measured with this technique is more fitting.

Fig. 43 shows fracture surfaces of samples from Grade C AlN with CaO and Y_2O_3 sintering additives, sintered at 1700 °C in a graphite furnace in a powder bed (ABC). The amount of secondary phase, which appears brighter in the micrographs due to the use of a backscattered electron detector, seems to be directly proportional to the amount of sintering additives added and indirectly proportional to the sintering time.
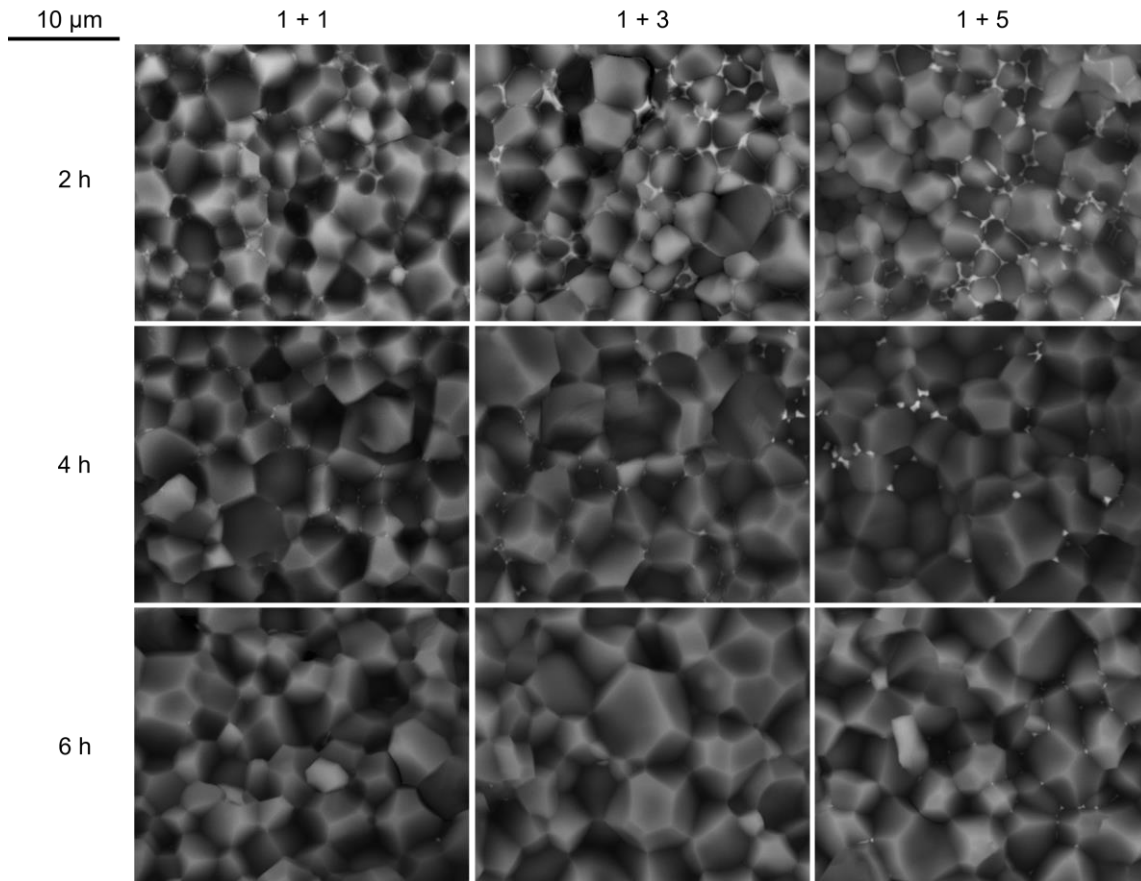
Fig. 43: BSE-SEM micrographs of fracture surfaces of samples from Grade C AlN with CaO and Y_2O_3 sintering additives, sintered in a graphite furnace (1700 °C, N_2 atmosphere) in a powder bed of AlN, BN and C. The effects of variations of composition and sintering time can be observed. Secondary phase (brighter areas in the micrographs) seems to be directly proportional to the amount of sintering additives added and indirectly proportional to the sintering times.

Fig. 44 shows micrographs (SE) of polished surfaces, with the average length of the intersecting lines displayed in the inset. The white dots visible in the 4 h sample set are presumably artifacts from polishing. The micrographs show the same trend as in Fig. 43, with the secondary phase being removed by longer sintering times. The grain size is lower in samples sintered for 2 hours, while the difference between samples sintered for 4 or 6 hours is not significant. The amount of sintering additives does not seem to affect grain sizes.
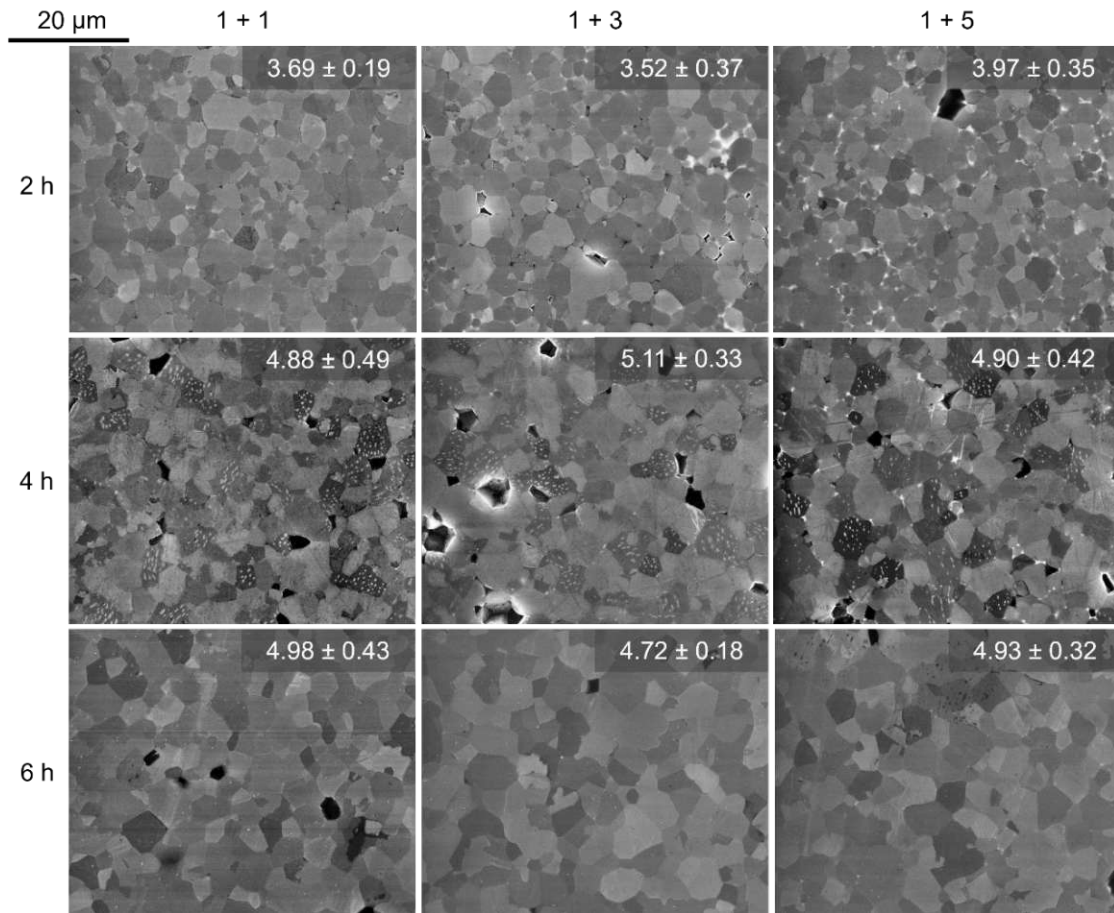
Fig. 44: SE-SEM micrographs of polished surfaces of samples from Grade C AlN powder mixtures with CaO and Y_2O_3 sintering additives, which were sintered at 1700 °C in a graphite furnace in N_2 atmosphere and a powder bed consisting of AlN, BN and C. Variations of the amount of sintering additives added and sintering times are shown. The values in the insets represent the length of intersecting lines in µm as an estimate of average grain size.

4.3.4.2 Effect of sintering environments, secondary phase migration and YN formation

This section summarizes results published in a research paper [7], focusing on the effects of different sintering environments on secondary phase migration and YN formation on samples surfaces.

Four variations of the sintering environment for samples sintered in a powder bed were investigated. The variations are detailed in Table 18. The composition of the powder mixture was not varied, and set to 1 wt.% CaO (as $CaCO_3$) and 3 wt.% Y_2O_3. $CaCO_3$ was not decomposed prior to shaping samples by CIP.

Table 18: Variations of sintering environments investigated to study their influence on the secondary phase and its migration behavior in AlN ceramic materials [7].

	Furnace	Sintering temperature (°C)	Holding time (h)	Powder bed (wt.%)	Crucible material
A	Furnace with graphite heating (HP W 150, FCT, Germany)	1700	6	50 % AlN, 50 % BN	Graphite
B	Furnace with graphite heating (HP W 150, FCT, Germany)	1700	6	47.5 % AlN, 47.5 % BN, 5 % C	Graphite
C	Corundum tube furnace (CTF 1800, Carbolite Gero)	1700	6	100 % AlN	Alumina
D	High Pressure Sintering Furnace (FP W 1, FCT, Germany)	1700	1 + 5 [†]	47.5 % AlN, 47.5 % BN, 5 % C	Graphite

[†] 1 hour of pre-sintering at 0.1 MPa and 5 h of sintering at 6 MPa.

Samples from approach A exhibited a non-homogenous surface after sintering, with some areas being light gray and other areas being blueish-black. The formation of the dark layer could be correlated with the proximity of graphite parts (e.g. graphite crucible) to the sample. The closer the samples were to graphite parts, the darker was the surface layer. XRD measurements (Fig. 46) of the different areas revealed that the dark areas were covered in a YN layer, which was not present at the lighter parts of the samples. Embedding samples in a powder bed with graphite homogenized their appearance After removal from the furnace,

samples were covered in a black layer, which would change colors through shades of blue to red and ultimately turning a very dark gray. This transformation usually lasted approximately half an hour. The dark gray layer reacted with the lab atmosphere over several days, resulting in the formation of a white powder on the surface of the samples. Samples from approach C were light gray with parts of the powder bed sintered onto the samples. Approach D led to complete coverage of the samples with the blueish-black layer, similar to approach B. Photographs of the samples are shown in Fig. 45.
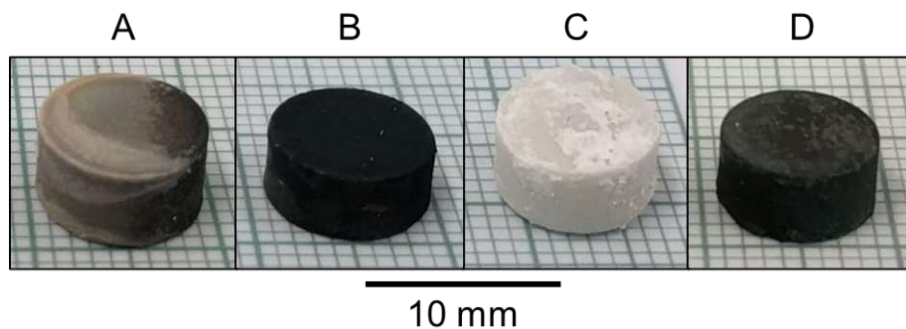
Fig. 45: Photographs of samples after recovery from the furnace for the four different sintering approaches.

Fig. 46 shows two X-ray diffractograms of a sample with 1 wt.% CaO and 2 wt.% Y_2O_3 addition after being sintered in a graphite furnace with powder bed "AB" (approach A). "1 + 3" samples showed the same behavior, but no XRD analysis of the light and dark areas was performed. As mentioned above and as can be seen in the inset of the figure, the sample showed lighter and darker surfaces, which were analyzed separately. The diffractograms revealed the existence of YN on the dark part of the samples, whereas the light area only showed Y_2O_3 signals in addition to AlN.
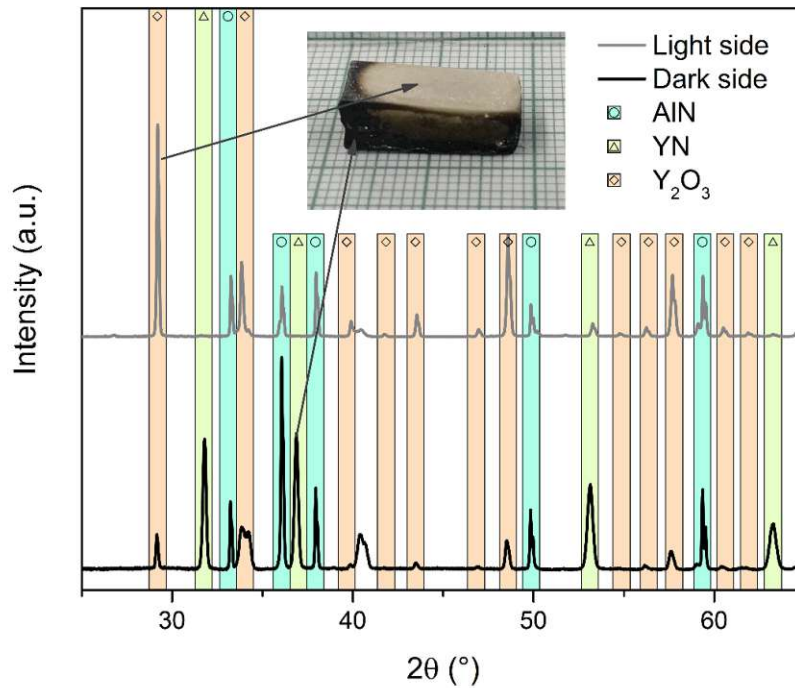
Fig. 46: XRD analysis of the light and dark areas of a sample sintered with approach A, showing YN signals on the dark areas, which are not present in the lighter areas. The sample contained 1 wt.% CaO and only 2 wt.% Y_2O_3 but similar behavior was observed in samples with 3 wt.% Y_2O_3. [7].

It could also be observed that the YN layer reacts with the lab atmosphere, producing a white powder in the process. To ensure stability of the samples during various analysis and characterization steps, this reaction was sped up for three of the four conditions by exposition of the samples to air at 500 °C for 4.5 h. Only samples from condition A were not thermally treated after sintering, because the instability of YN was only discovered at this point in the project, and the experiments were not repeated. Fig. 47 shows a comparison of samples sintered under condition B before and after thermal removal of the YN layer (the powder that formed during the thermal treatment was removed by ultrasonic cleaning).

Fig. 47: Effect of thermal treatment on samples (approach B), showing the removal of the YN layer.

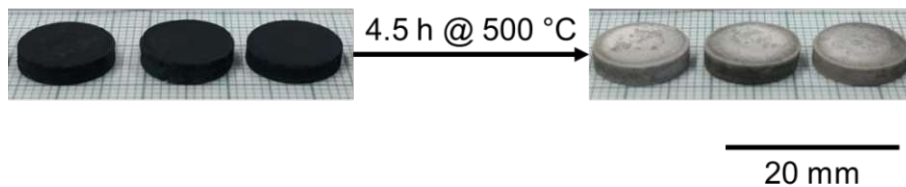The surface of samples from approach B was further investigated by X-ray diffractometry and SEM. Fig. 48 shows a comparison of the surface of a sample, which was stored in cyclohexane directly after removal from the furnace ("before oxidation") and after thermal treatment at 500 °C ("after oxidation"), confirming the oxidation of YN. In the SEM micrograph (taken before oxidation) it is also shown that an Y-containing phase accumulates at the surface.
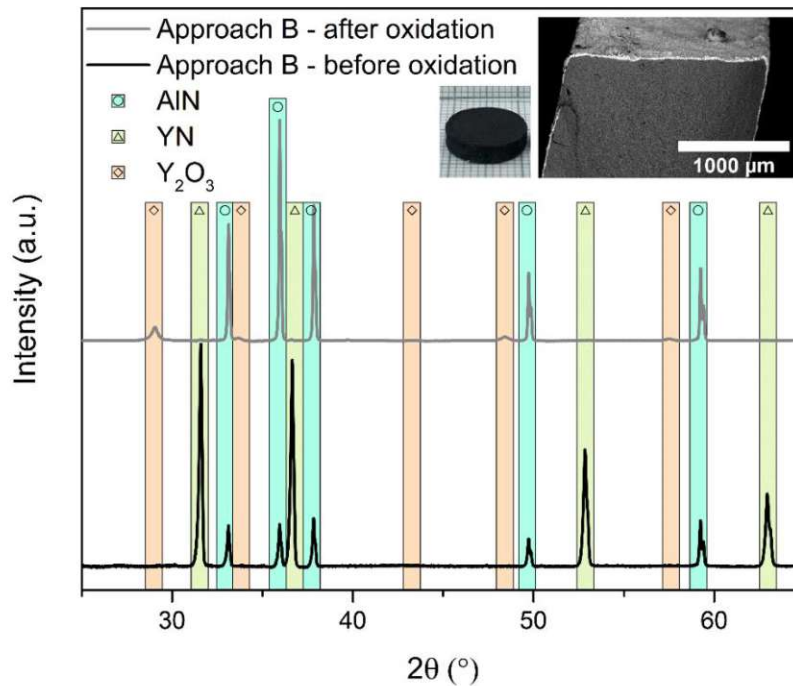
Fig. 48: Comparison of the surface X-ray diffractograms of a sample before and after oxidation of the YN layer at 500 °C in air for 4.5 h. The photograph and SEM micrograph (BS) in the insets were taken before oxidation. If the reflections of phases overlap, only the most dominant phase is represented by the shaded column [7].

In addition to the surface X-ray diffractograms, bulk XRDs of fracture surfaces of samples were conducted. The results are given in Fig. 49, which shows that most signals from the samples result from AlN, but for approaches other than B, secondary phase reflexes, which are highlighted by black frames, can still be detected. This indicates that the secondary phase is depleted in samples from approach B while the higher N_2 gas pressure - in an otherwise similarly reducing environment - might suppress this behavior in samples from approach D.
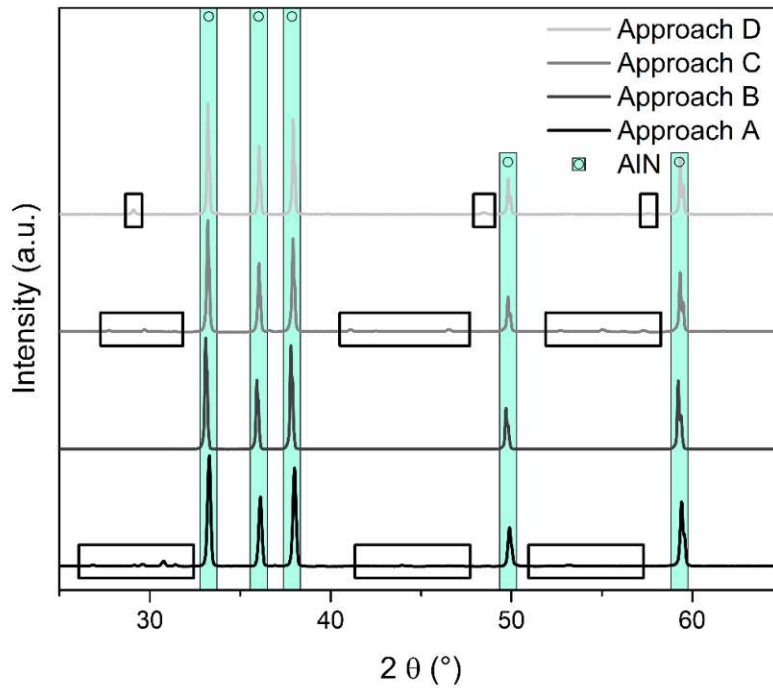
Fig. 49: X-ray diffractograms of the bulk of samples from all four approaches investigated. In the samples from approach A $Y_4Al_2O_9$, $YCaAl_2O_7$ and $CaYAlO_4$ were identified, whereas $Y_3Al_5O_{12}$ was the only secondary phase detected in the sample from approach C and Y_2O_3 was the only secondary phase detected in the sample from approach D [7].

SEM micrographs of polished samples showing cross-sections of the bulk of samples (Fig. 50) and the surface of samples (Fig. 51) confirm the behavior indicated above; graphite addition to the powder bed at 1 atm N_2 pressure during sintering (approach B) leads to samples that are mostly free of secondary phase (according to SEM and XRD), while samples from other approaches contain secondary phase along grain boundaries. In samples sintered in the corundum tube furnace (approach C), the secondary phases accumulated in larger areas of the cross-sections.
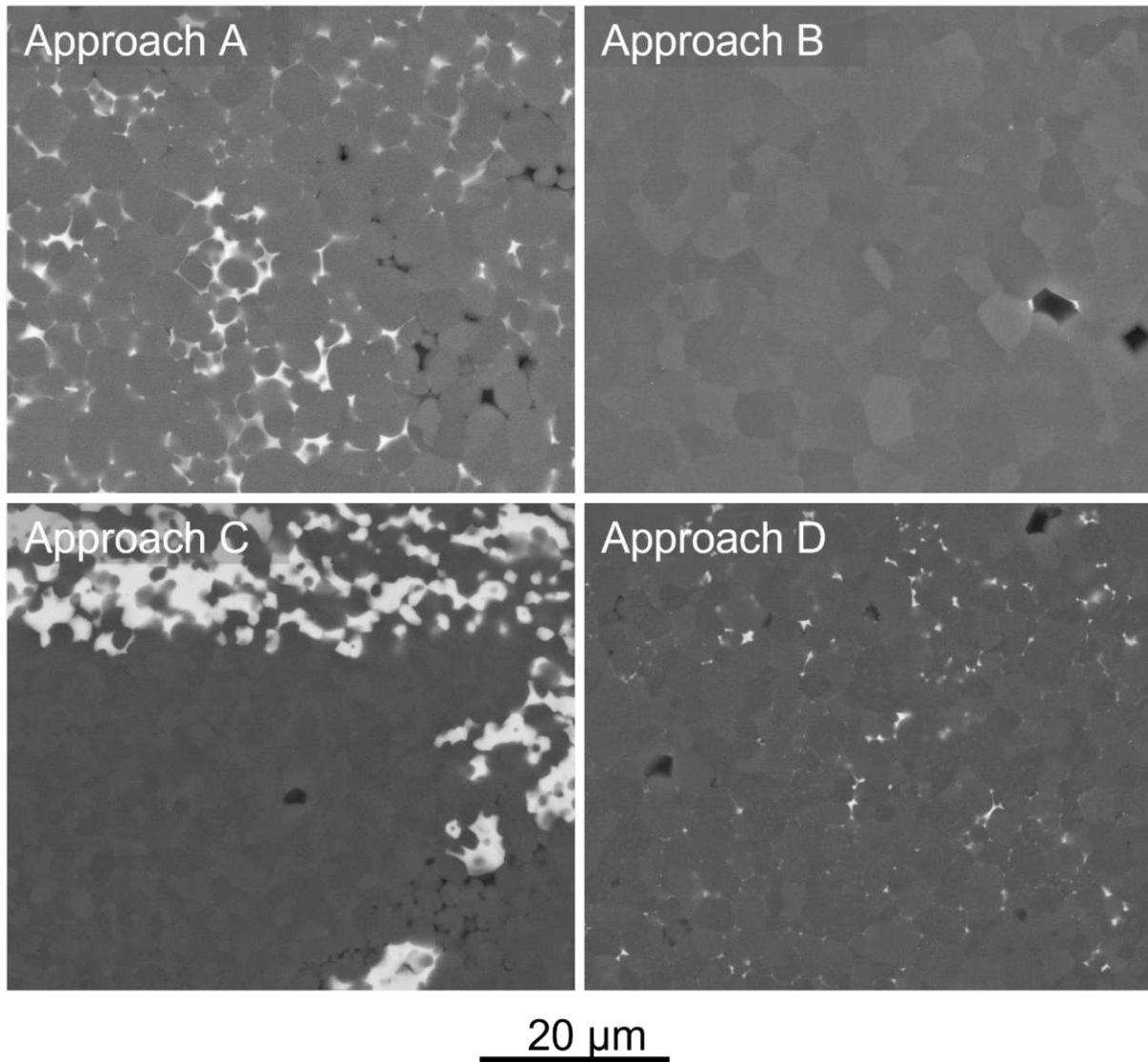
Fig. 50: Comparative BSE-SEM micrographs of polished cross-sections of the sample bulk prepared by the four sintering approaches investigated, show the different secondary phase distributions, dependent on the sintering environment. The addition of graphite to the powder bed while sintering at a N_2 pressure of 1 atm leads to an almost complete depletion of secondary phase in samples, whereas sintering in a carbon-free environment (approach C) leads to accumulation of secondary phase in large areas [7].

The micrographs recorded closer to the surface (Fig. 51) show a similar behavior. Graphite addition and sintering at ambient pressure (approach B) leads to a depletion of secondary phase, while samples sintered in a powder bed without added graphite (approach A) or sintered at increased N_2 pressure with graphite addition to the powder bed (approach D) show a homogeneous distribution of secondary phase in the microstructure. Sintering in a carbon-free environment (approach C) leads to an inhomogeneous distribution of secondary phase, with areas in which large amounts of the phase accumulate and areas where most of the secondary phase is eliminated. The micrographs were taken after oxidation of the YN surface layer.
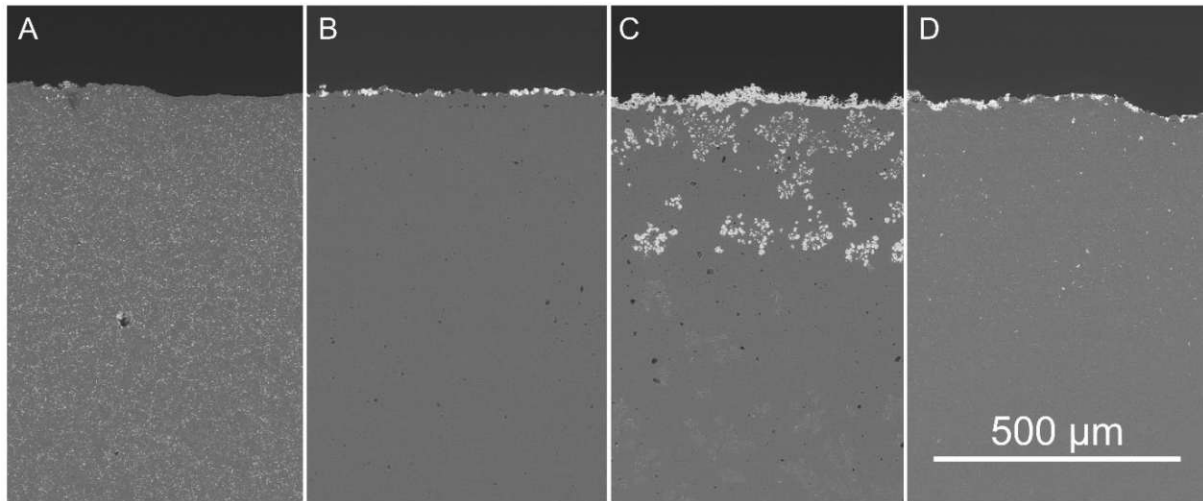
Fig. 51: BSE-SEM micrographs, recorded close to the surfaces of samples from all four sintering approaches, showing different migrative behavior of the secondary phase dependent on the sintering environment [7].

Even though SEM micrographs and XRD analysis indicate an absence of secondary phase in samples sintered at ambient N_2 pressure in a powder bed containing graphite (approach B), additional TEM investigations revealed small amounts of secondary phase at grain boundaries and triple grain junctions, as shown in Fig. 52. The upper insets show the results of EDX elemental mappings and the lower inset shows the results of electron scattering, confirming the crystallinity of the phase.
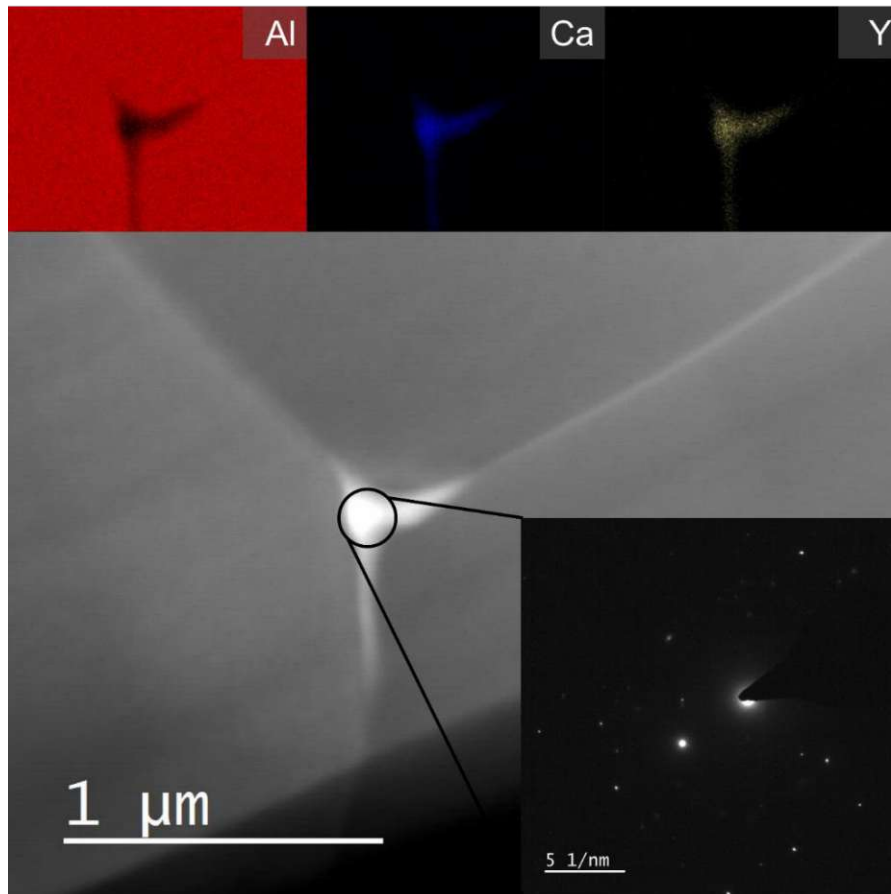
Fig. 52: TEM analysis, revealing the presence of secondary phase along a grain boundary and triple junction in an sample produced using sintering approach B. The insets at the top show elemental mappings of Al, Ca and Y, while the inset on the lower right shows the electron diffraction pattern of the area highlighted by the circle, which indicates a crystalline secondary phase. [7].

Mass loss of the samples during the thermal treatment in air of sintered samples was also studied for samples produced by approaches B through D, indicating more mass lost in samples sintered in environments with higher reducing power (Table 19)

Table 19: Mass loss analysis of samples from approaches B, C and D, confirming the difference in removal of secondary phase dependent on the sintering environment [7].

	Mass loss (%)	Number of sintering runs	Number of individual samples
Approach B	2.44 ± 0.40	6	46
Approach C	0.10 ± 0.10	1	7
Approach D	1.49 ± 0.14	1	7

Average densities of samples from all investigated sintering approaches exceeded 99 %. In Table 20, the average densities and average relative densities are listed. The number of individual samples contributing to the average values and the number of sintering runs in which

those samples were produced are also given. Samples from approach B exhibit the lowest density. The densities differ slightly from the results shown in section 4.3.4, because a different number of samples was used for evaluation.

Table 20: Density measurements of samples sintered with all four approaches [7].

Sintering approach	Density (g cm^{-3})	Relative density (%)	Number of sintering runs	Number of individual samples
A	3.26 ± 0.02	99.9 ± 0.6	4	16
B	3.23 ± 0.02	99.1 ± 0.7	8	52
C	3.25 ± 0.03	99.7 ± 0.8	1	7
D	3.27 ± 0.02	100.4[1] ± 0.5	1	7

[1] Values exceeding 100% are due to using the density of AlN as reference for relative density calculations.

Thermal conductivity was measured using the steady state method and average grain size was estimated according to EN ISO 13383-1 [109]. The results are shown in Fig. 53. Samples sintered in reductive environments exhibit higher thermal conductivity, especially when graphite is added to the powder mixtures, than in a non-reductive environment (approach C). Grain sizes do not follow this trend with samples from the graphite furnace (approaches A and B) exhibiting similar values and samples from the tube furnace and the hot-isostatic press (approaches C and D) also exhibiting similar values. The labels inside the columns indicate the number of individual samples n from sintering runs r used for thermal conductivity measurements.
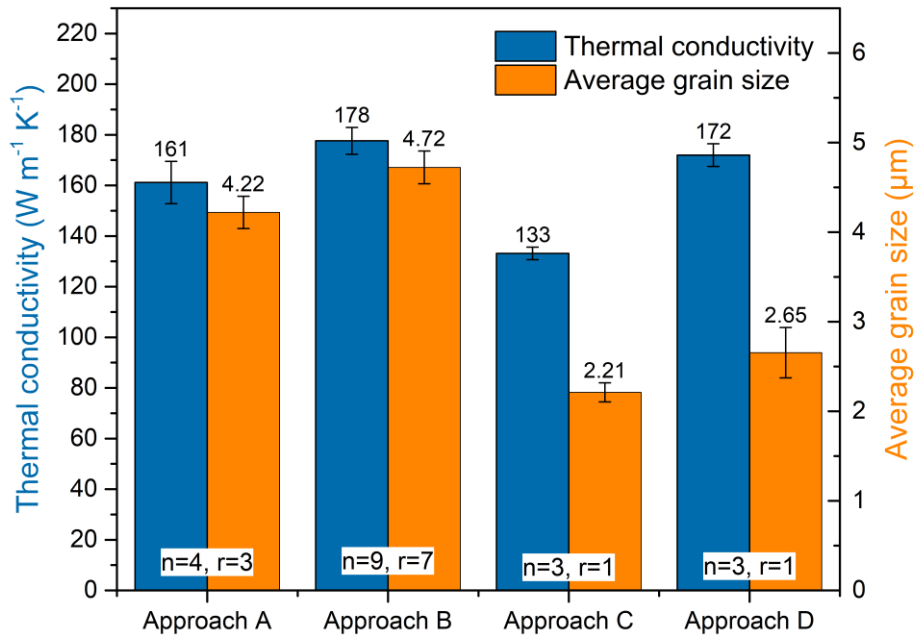
Fig. 53: Thermal conductivity and grain sizes of samples from all four sintering approaches investigated. The number of samples (n) from a number of sintering runs (r) used for thermal conductivity measurements are given. The average length of intersecting lines is denoted as "average grain size" in this graph. This graph was adapted from [7] by adding data labels.

For samples sintered in the graphite furnace, mechanical strength was measured by the B3B method and statistically evaluated according to EN 843-5 [108]. Samples from both approaches exhibited a characteristic Weibull strength of 390 MPa. By adding graphite to the powder bed the Weibull modulus increased from 8.1 for samples from approach A to 13.8 for samples from approach B.

4.3.4.3   Influence of the reduction of the sintering temperature to 1600 °C

One sintering run was performed to investigate the densification and thermal properties of CIP samples sintered for 6 hours at 1600 °C instead of 1700 °C, which was used for the rest of the samples (except for HP samples). The samples were all produced from powder mixtures using CaO (from $CaCO_3$) and Y_2O_3, without thermal treatment prior to shaping, and sintered in a graphite crucible with a powder bed consisting of AlN and BN. Table 21 gives an overview over the properties observed in the samples. The numbers in the brackets indicate the number of individual samples measured. Densities and thermal conductivities increased proportionally to sintering additives used.

Table 21: Densities, relative densities and thermal conductivities (steady state) of AlN samples from Grade C AlN powder mixtures containing CaO and Y_2O_3. $CaCO_3$ was not thermally decomposed prior to shaping and sintering in a graphite furnace at 1600 °C for six hours in N_2 atmosphere and a powder bed of equal parts AlN and BN (by weight). Density measurements were conducted on 4 samples for the "1 Ca + 1 Y" and "1 Ca + 5 Y" series and 5 samples for the "1 Ca + 3 Y" series.

	1 Ca + 1 Y	1 Ca + 3 Y	1 Ca + 5 Y
Density (g cm^{-3})	3.21 ± 0.05	3.25 ± 0.03	3.28 ± 0.03
Relative density (%)	98.4 ± 1.7	99.8 ± 0.9	100.6 ± 0.9
Thermal conductivity (W m^{-1} K^{-1})	120	126	132

Fig. 54 shows the microstructures of the samples sintered at 1600 °C. The top row shows fracture surfaces, whereas the bottom row shows polished surfaces. The secondary phase is more prevalent in samples with more additives added, which resulted in large areas of secondary phase in the "1 + 5" samples.
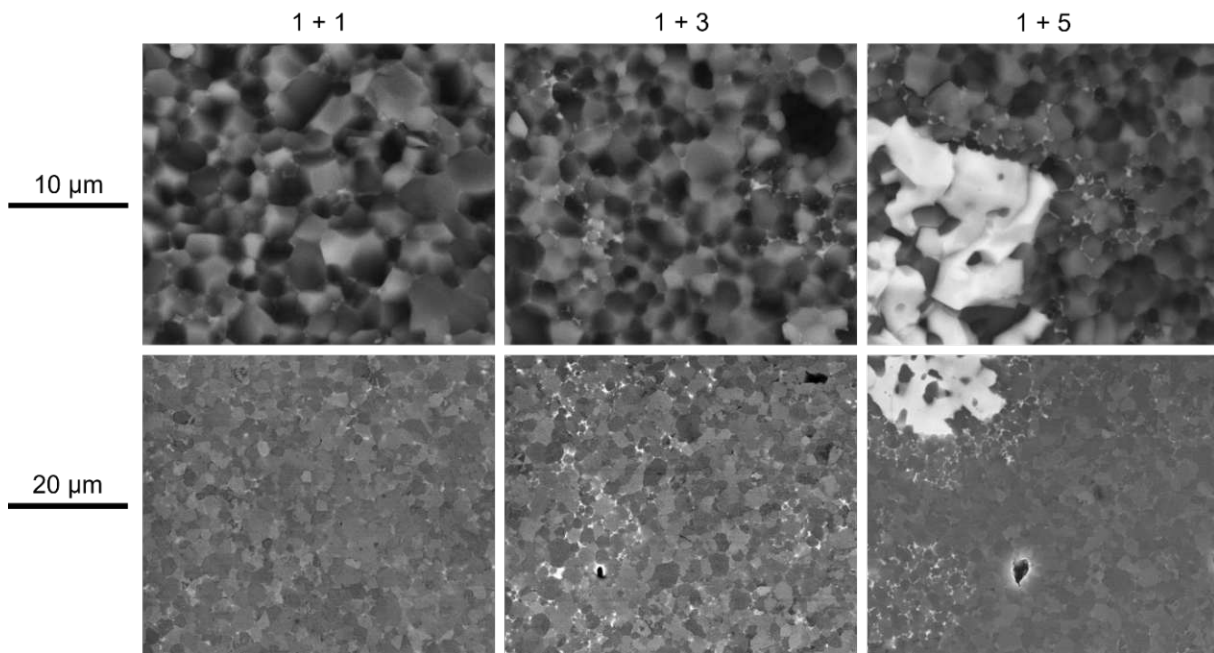
Fig. 54: SEM micrographs of fracture surfaces (BSE) and polished surfaces (SE) of samples from Grade C AlN powder mixture with CaO and Y_2O_3 sintering additives, which were sintered at 1600 °C in a graphite furnace in N_2 and a powder bed of AlN and BN.

In Fig. 55, the sample produced from a powder mixture with 1 wt.% CaO and 5 wt.% Y_2O_3 sintering additives is shown again. On the left, a cross-section over almost the entire sample (top to bottom) is shown, where the accumulation of secondary phase in large, almost cuboid particles can be observed in the center. Ribbons of secondary phase are migrating outwards.

The second micrograph shows the center in higher magnification, and the third micrograph shows an area near the surface of the sample.
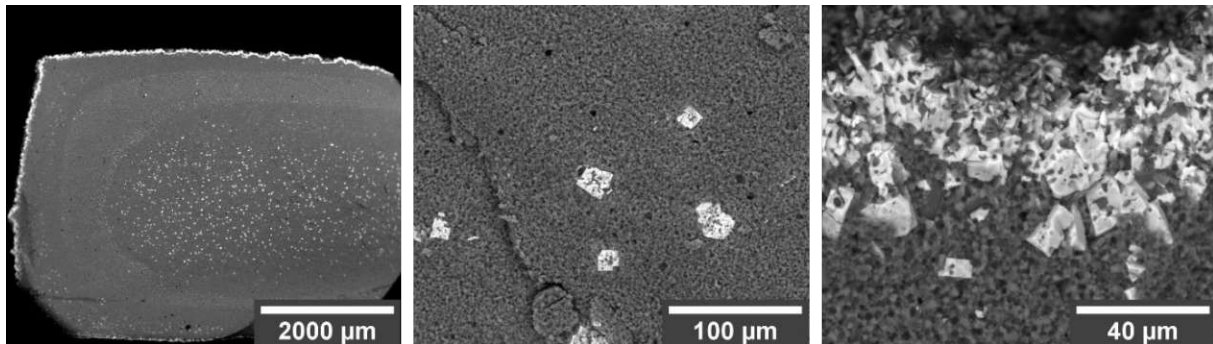

Fig. 55: BSE-SEM micrographs of fracture surfaces of a "1 Ca + 5 Y" sample (Grade C powder mixture with 1 wt.% CaO as $CaCO_3$ and 5 wt.% Y_2O_3), showing inhomogenous distribution of secondary phase, from large agglomerates in the center, ribbon-like features halfway to the edge and accumulation at the surface, in the lowest magnification. The middle micrograph shows the agglomerates in the center. The right micrograph shows the accumulation of secondary phase at the sample surface. The sample was sintered at 1600 °C for six hours in a graphite furnace (N_2 atmosphere, powder bed AB).

4.3.4.4   Influence of starting powder

Powder mixtures with 1 wt.% CaO (added as carbonate) and 3 wt.% Y_2O_3 were prepared with three different AlN starting powder grades from two manufacturers and compared. Sintering was conducted in a graphite crucible with a powder bed of AlN, BN and C at 1700 °C for 6 hours ("Approach B" in section 4.3.4.2). All samples for thermal conductivity and density measurements were produced in one sintering run to ensure comparability. The samples for mechanical tests were prepared in a separate sintering run due to spatial restrictions in the crucible. Samples of one of the variations exhibited high residual porosity after sintering and thermal removal of the YN layer, which is why density was measured by an immersion method with prior removal of air for all samples from that run, as described in EN 623-2 [99], calculating the raw density of the samples.

Thermal conductivity for samples from a Grade C AlN powder mixture was only determined for one sample, because the exact composition and sintering parameters had been used for many other samples up to that point, thus an outlier would have been easily spotted and, in consequence, more of the other samples could be placed in the crucible. Only two samples from powder mixtures containing Grade BT AlN were measured, because one of the prepared samples broke during sintering.

Table 22 shows the results of the experiments. The numbers in brackets next to the values correspond to the number of samples used for the respective measurements. Densification of samples from Grade C AlN and Grade JM AlN powder mixtures was similar, whereas samples from a powder mixture containing Grade BT AlN exhibited decreased densification, and overall decreased thermal and mechanical properties (with the exception of Weibull modulus) compared to samples from other AlN powder grades. The grain size for the sample from Grade C AlN powder mixture differs from the grain size stated in Fig. 44, because a sample from this comparative sintering run was used.

Table 22: Results of experiments varying the AlN starting powder. All samples were prepared from powder mixtures containing 1 wt.% CaO (as $CaCO_3$) and 3 wt.% Y_2O_3 but with different AlN powder grades. The samples were sintered in a graphite furnace at 1700 °C in N_2 atmosphere and a powder bed consisting of AlN, BN and C for six hours. Numbers in brackets next to values indicate the number of samples used for the respective measurements. The grain size for the samples made from a powder mixture containing Grade C AlN differs from the grain size reported in Fig. 44 and Fig. 53, because another sample (sintered in the same sintering run as the samples from Grade BT and Grade JM) was used for the determination.

	Grade C	Grade BT	Grade JM
Density (g cm^{-3})	3.18 ± 0.02 (3)	2.68 ± 0.03 (6)	3.21 ± 0.00 (5)
Relative density (%)	97.7 ± 0.5	82.2 ± 0.9	98.3 ± 0.1
Thermal conductivity (steady state) (W m^{-1} K^{-1})	180 (1)	129 ± 3 (2)	161 ± 1 (3)
Grain Size (µm)	5.38 ± 0.24	4.18 ± 0.20	4.57 ± 0.51
Characteristic Weibull Strength (MPa)	390 (36)	258 (34)	415 (32)
Weibull modulus	13.8	15.9	13.8

4.4   Processing, microstructure and properties of AM samples

This section summarizes results published in a research paper [8], focusing on the utilization of AlN in LCM, an AM technology in which three-dimensional parts are realized by layerwise photopolymerization of slurries which include ceramic particles and organic oligomers.

If not stated otherwise, the powder mixtures used for AM contained 1 wt.% CaO (introduced as CaC_2O_4) and 3 wt.% Y_2O_3. Powder mixtures used for CIP reference samples contained the same amount of sintering additives but CaO was introduced as $CaCO_3$. Sintering additive precursors were not thermally decomposed before shaping. Two different AlN powders were used for AM experiments. Grade C powder was off-white, whereas Grade JM powder was white. This already indicates higher light absorption of the Grade C powder, leading to lower curing depths for slurries including Grade C powder at the same energy. This behavior was confirmed by curing depth tests (conducted by Lithoz GmbH). The results, along with the viscosity of the slurries, are shown in Fig. 56.

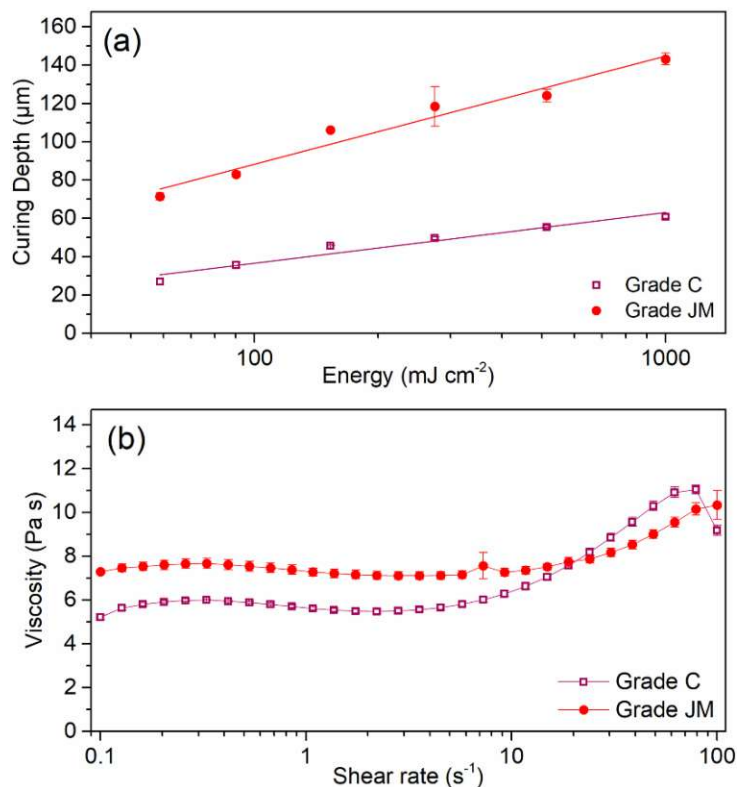

Fig. 56: Curing depth (measured at 80 mW cm^{-2}) and viscosity measurements at 25 °C on AM slurries from Grade C and Grade JM AlN powders. Curing depth was lower in slurries from Grade C AlN powder. Viscosity was comparable in both cases [8].

Stability of the AlN powders during processing steps and long-time storage in a model binding system, chemically similar to the actual binder used in the LCM process, was investigated. No significant increase in oxygen content of the AlN powders (Grade C, Grade BT and Grade JM) could be observed after 18 weeks of exposition, see section 4.1 for the respective results.

For thermal debinding of printed AlN samples, a debinding program up to 600 °C in air was defined. To ensure that AlN would not incorporate high amounts of oxygen, AlN powder without additives underwent the thermal debinding program in air and then its oxygen content was analyzed. In addition to loose powder, a CIPed green body was also investigated, since it was assumed that the surface area of the green body would be closer to that of AM green parts. The results are shown in Table 23.

Table 23: Oxygen contents of Grade C AlN powder and a CIPed Grade C AlN samples after exposing it to the thermal debinding program up to 600 °C in air, used for printed AlN samples.

	O-content (%)
Reference AlN powder	1.21 ± 0.04
AlN powder after "debinding"	1.48 ± 0.06
AlN pellet after "debinding"	1.38 ± 0.11

Fig. 57 shows the plot of a thermogravimetric analysis of polymerized slurry of the same composition (Grade C AlN, 1 wt.% CaO as CaC_2O_4 and 3 wt.% Y_2O_3) as used in the AM process. The results show that binder burnout occurs up to temperatures of approximately 600 °C. The weight increase after 650 °C presumably stems from the oxidation of AlN.
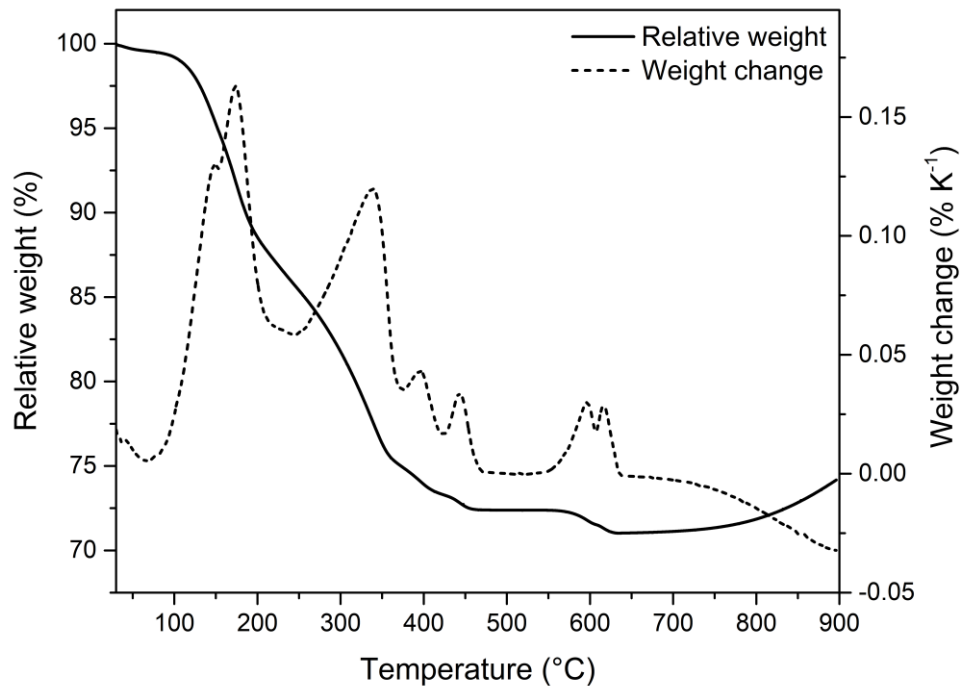
Fig. 57: TG measurements of a sample of polymerized LCM slurry containing Grade C AlN powder mixture with 1 wt.% CaO (as CaC_2O_4) and 3 wt.% Y_2O_3. Binder burnout occurs up to temperatures of about 600 °C. At 650 °C the weight begins to increase, suggesting oxidation of AlN [8].

Additionally, carbon content was investigated by combustion analysis before and after thermal debinding (600 °C, air) of two additively manufactured samples from a slurry containing Grade C AlN, 1 wt.% CaO (as CaC_2O_4) and 3 wt.% Y_2O_3, to confirm complete binder burnout and to confirm that calcium oxalate decomposes to calcium carbonate during the debinding process. The measured C values were compared to the theoretical C content of a powder mixture containing 96 wt.% AlN, 1 wt.% $CaCO_3$ and 3 wt.% Y_2O_3, which is the expected composition of the sample after thermal debinding. The results are shown in Table 24.

Table 24: Average carbon content of two debinded AM samples from a powder mixture containing Grade C AlN, 1 wt.% CaO and 3 wt.% Y_2O_3 and the theoretical carbon content of a powder mixture with 1 wt.% $CaCO_3$ and 3 wt.% Y_2O_3, which is the expected composition of the samples after thermal debinding.

	C-content (%)
Average of two debinded AM samples	0.217 ± 0.005
Theoretical C content of a sample containing 96 wt.% AlN, 1 wt.% CaO as $CaCO_3$ and 3 wt.% Y_2O_3	0.213

To further confirm the decomposition of CaC_2O_4 during debinding, a powder mixture containing Grade C AlN powder,1 wt.% CaC_2O_4 and 3 wt.% Y_2O_3 and a printed sample from the same powder mixture after debinding were analyzed by XRD. The results are shown in Fig. 58, with the signals from CaC_2O_4 highlighted by blue outlines. All other signals can be attributed to AlN, $CaCO_3$ and Y_2O_3. The absence of CaC_2O_4 signals in the diffractogram of the debinded sample confirms its decomposition.
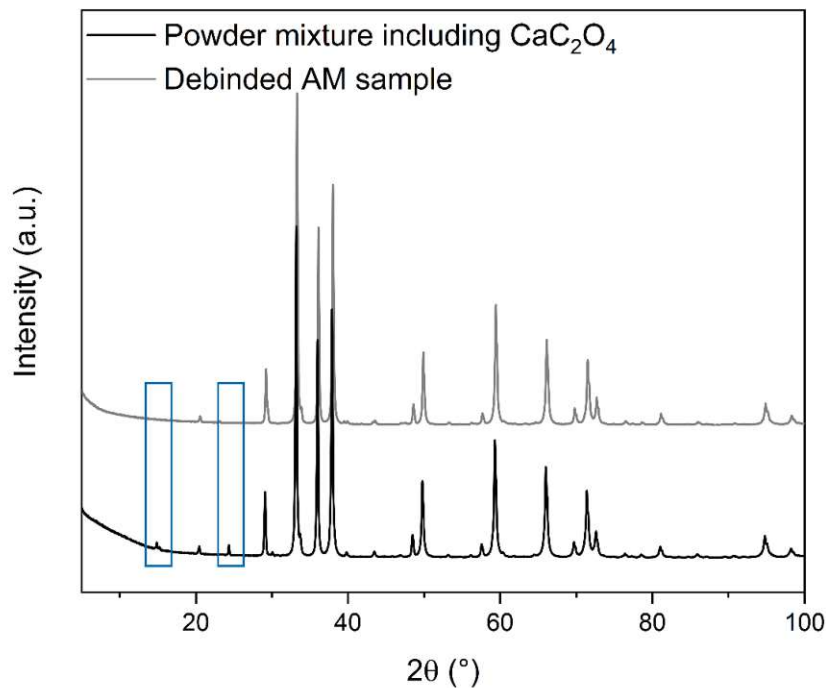
Fig. 58: XRD analysis of a Grade C AlN powder mixture containing 1 wt.% CaO (as CaC_2O_4) and 3 wt.% Y_2O_3, and an AM sample produced from the same powder mixture after the debinding process, confirming the decomposition of the CaC_2O_4 during debinding at 600 °C in air.

The green densities of CIP samples and AM samples (after debinding at 600 °C in air) made from powder mixtures containing 1 wt.% CaO and 3 wt.% Y_2O_3 were determined geometrically. Typical values for samples are listed in Table 25.

Table 25: Geometric green densities of AM and CIP samples produced from powder mixtures containing Grade C or Grade JM AlN, 1 wt.% CaO (as CaC_2O_4 for AM samples and as $CaCO_3$ for CIP samples) and 3 wt.% Y_2O_3. The AM samples were debinded at 600 °C in air before density was determined. The numbers of samples differ from the numbers listed in Table 26, because geometric measurement of green density was not possible for some samples.

	Grade C AM	Grade C CIP	Grade JM AM	Grade JM CIP
Green density (g cm^{-3})	1.69 ± 0.05	1.84 ± 0.33	1.67 ± 0.03	1.89 ± 0.05
Number of individual samples	59	27	13	12
Number of AM batches	7		3	

Table 26 shows the densities and relative densities of sintered AM samples compared to the values of sintered CIP samples. The powder mixtures for AM samples contained AlN (Grade C or Grade JM), 1 wt.% CaO (as CaC_2O_4) and 3 wt.% Y_2O_3, whereas the powder mixtures used for CIP samples contained CaO as $CaCO_3$. The AM samples were debinded at 600 °C. The sintering process was conducted at 1700 °C for six hours in the graphite furnace in N_2 atmosphere and a powder bed consisting of AlN, BN and C, and was the same for AM and CIP samples. The AM samples exhibit lower density values and higher deviations in density, especially between different AM batches. High variations in density values prevent a conclusive proposition about the densification of AM samples (Grade C) compared to CIP samples (Grade C). The densification in AM samples made from powder mixtures using Grade JM AlN powder is significantly lower than in CIP samples made from Grade JM AlN. CIP densities differ to earlier results, because here only samples from sintering runs also containing AM samples were considered.

Table 26: Densities and relative densities of AM samples and CIP samples produced from powder mixtures containing Grade C or Grade JM AlN, 1 wt.% CaO (as CaC_2O_4 for AM samples and as $CaCO_3$ for CIP samples) and 3 wt.% Y_2O_3. The AM samples were debinded at 600 °C in air. Sintering of AM and CIP samples was conducted in a graphite furnace in N_2 atmosphere and a powder bed (AlN, BN and C) at 1700 °C for six hours [8].

	Grade C AM	Grade C CIP	Grade JM AM	Grade JM CIP
Bulk density (g cm^{-3})	3.15 ± 0.08	3.23 ± 0.02	3.04 ± 0.07	3.24 ± 0.02
Relative density (%)	96.6 ± 2.4	99.1 ± 0.6	93.3 ± 2.2	99.5 ± 0.6
Number of individual samples	62	28	24	12
Number of AM batches	8		3	

Sintered AM samples (1700 °C, six hours, graphite furnace, N_2 atmosphere, powder bed ABC) made from powder mixtures containing 1 wt.% CaO (as CaC_2O_4) and 3 wt.% Y_2O_3 were fractured parallel to the building axis and investigated by SEM (Fig. 59). No visible accumulation of pores and defects can be observed between the building layers. However, as already observed in CIP samples, the secondary phase migrates towards the surface of samples during sintering. The bright spots in the bulks of the sample might stem from sample preparation (fracturing).
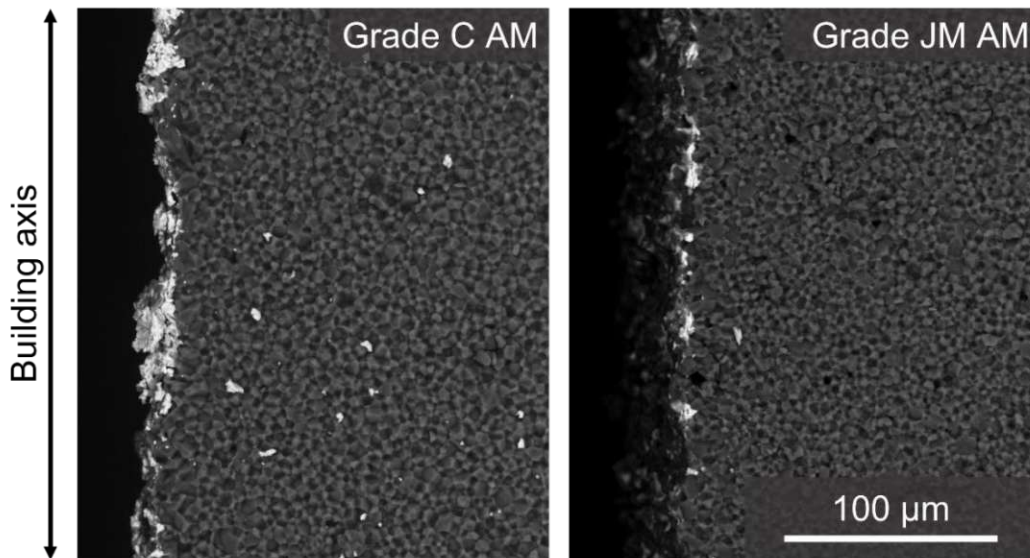

Fig. 59: BSE-SEM micrographs of fracture surfaces of sintered (1700 °C, six hours, graphite furnace, N_2 atmosphere, powder bed ABC) AM samples made from powder mixtures containing Grade C or Grade JM AlN powders, 1 wt.% CaO (as CaC_2O_4) and 3 wt.% Y_2O_3. The cross-sectional view parallel to the building axis shows no accumulation of microstructural defects along the separate building layers [8].

Fig. 60 and Fig. 61 show compilations of SEM micrographs of sintered AM and CIP samples (1700 °C, six hours, graphite furnace, N_2 atmosphere, powder bed ABC). All samples were made from a powder mixture consisting of Grade C or Grade JM AlN, 1 wt.% CaO and 3 wt.% Y_2O_3. The upper row shows fracture surfaces captured using a BS electron detector, whereas the lower row was captured using the SE detector, revealing the relief structure from the polishing process, also used for estimation of grain sizes. The nomenclature "xy" and "xz" with regard to AM samples corresponds to the orientation of the sample in relation to the building process, with "xy" noting a plane perpendicular to the building axis and "xz" noting a plane parallel to the building axis. No significant difference between AM and CIP samples can be observed. However, in samples made from powder mixtures containing Grade JM AlN (regardless of manufacturing technique), small pockets of secondary phase can be spotted, which are not visible in the samples made from powder mixtures containing Grade C AlN. The

white dots on the polished surfaces of Grade JM samples presumably are artifacts from polishing.

Fig. 60: Microstructures of AM and CIP samples made from powder mixtures of Grade C AlN, 1 wt.% CaO, and 3 wt.% Y_2O_3, sintered at 1700 °C for six hours in a graphite furnace in N_2 atmosphere and a powder bed of AlN, BN and C. "xy" notes a plane perpendicular to the building axis, whereas "xz" notes a plane parallel to the building axis [8].
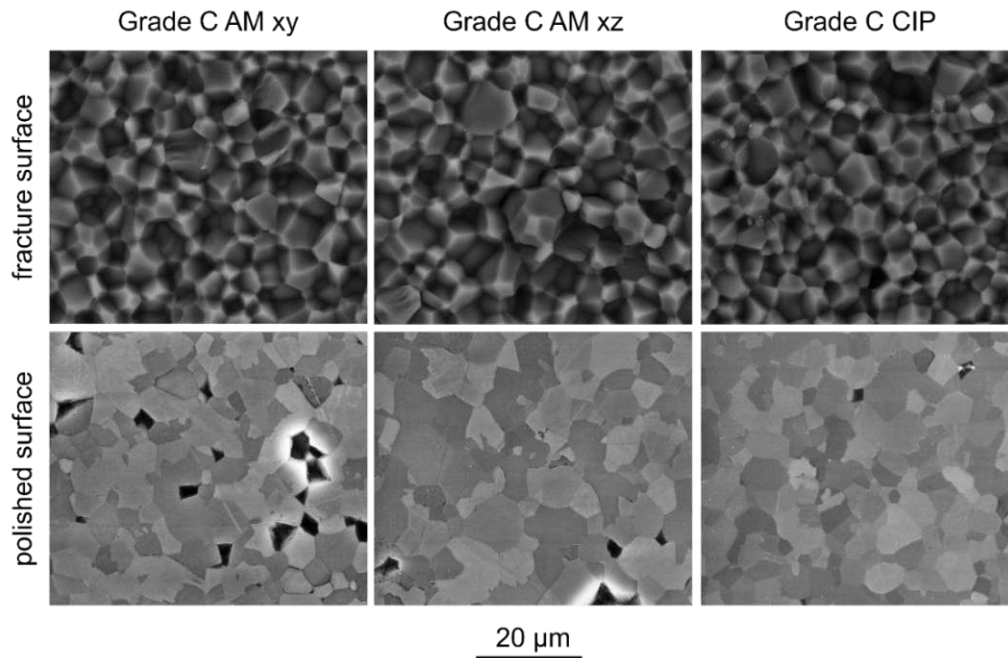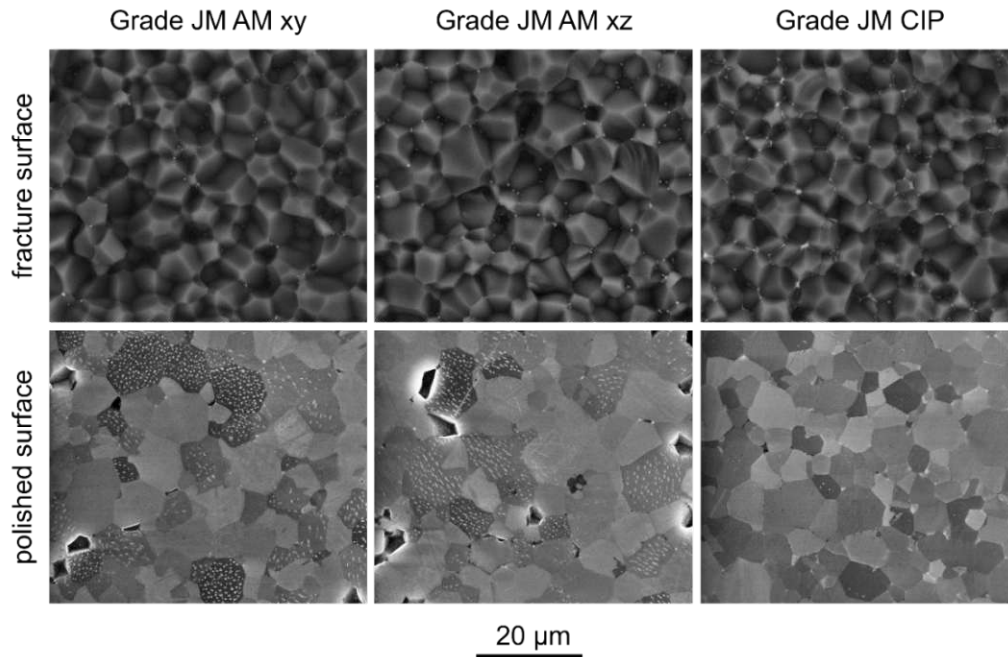
Fig. 61: Microstructures of AM and CIP samples made from powder mixtures of Grade JM AlN, 1 wt.% CaO, and 3 wt.% Y_2O_3, sintered at 1700 °C for six hours in a graphite furnace in N_2 atmosphere and a powder bed of AlN, BN and C. "xy" notes a plane perpendicular to the building axis, whereas "xz" notes a plane parallel to the building axis. The white spots in the micrographs from polished samples are presumably artifacts from the polishing process [8].

Table 27 lists the grain sizes (average length of intersecting lines) of the CIP and AM samples shown in Fig. 60 and Fig. 61.

Table 27: Grain size comparison of AM and CIP samples shown in Fig. 60 and Fig. 61.

	Grain sizes (µm)		
	AM (xy)	AM (xz)	CIP
Grade C	5.04 ± 0.50	4.76 ± 0.36	4.72 ± 0.18
Grade JM	5.66 ± 0.34	6.11 ± 0.33	4.69 ± 0.40

Using a B3B setup, flexural tests were performed with AM and CIP samples, for which the results are shown in Table 28. All samples were made from powder mixtures containing 1 wt.% CaO and 3 wt.% Y_2O_3. CaO was added as CaC_2O_4 to AM and as $CaCO_3$ to CIP powder mixtures. The samples were sintered for six hours at 1700 °C in a graphite furnace in N_2 atmosphere and a powder bed of AlN, BN and C. AM samples were tested with the force vector during the test being parallel (xy) or perpendicular (xz) to the building direction. The AM samples, regardless of starting powder, showed large discrepancies in strength between the

printing directions. Density variations between AM batches were expected to affect the strength of the materials, which is why average relative densities of batches are also shown in the table.

Table 28: Characteristic Weibull strength, Weibull modulus and the average relative densities of AM and CIP samples. The samples were produced using powder mixtures containing Grade C or Grade JM AlN powder, 1 wt.% CaO (as CaC_2O_4 in AM samples and $CaCO_3$ in CIP samples), and 3 wt.% Y_2O_3. The samples were sintered at 1700 °C for six hours using a graphite furnace, N_2 atmosphere and a powder bed of AlN, BN and C. The vector of applied force during testing is parallel (xy) or perpendicular (xz) to the building direction of AM samples [8].

	Characteristic Weibull strength (MPa)	Weibull modulus	Number of individual samples	Relative density of batch (%)
Grade C AM (xy)	498	14.0	9	96.7 ± 1.1
Grade C AM (xz)	320	10.0	17	94.2 ± 0.6
Grade C CIP	390	13.8	36	97.9 ± 0.2
Grade JM AM (xy)	468	9.1	8	95.1 ± 0.4
Grade JM AM (xz)	367	9.8	12	91.6 ± 0.4
Grade JM CIP	415	13.8	32	99.9 ± 0.3

Due to challenges during debinding of thick-walled samples, most bar-shaped samples prepared for steady-state thermal conductivity measurement could not be used due to the formation of defects (cracks, etc.) during debinding. As such, thermal conductivity was only measured by Xe-flash method (Fig. 62). Thermal conductivities of samples sintered at 1700 °C for six hours in a graphite furnace in N_2 atmosphere and a powder bed of AlN, BN and C were determined. 6 AM and 6 CIP samples made from powder mixtures (1 wt.% CaO + 3 wt.% Y_2O_3) containing Grade C AlN as well as 3 AM and 3 CIP samples made from powder mixtures (1 wt.% CaO + 3 wt.% Y_2O_3) using Grade JM AlN powder were determined. Heat flow during the measurement was parallel to the building axis in AM samples. Table 29 shows the exact values for each variation at room temperature, while Fig. 62 shows thermal conductivity evolution of the samples at increasing temperatures.

Table 29: Thermal conductivities of AM and CIP samples at RT as measured by Xe-flash technique. The direction of measurement was parallel to the building axis for AM samples. The samples were made from powder mixtures of Grade C or Grade JM AlN, including 1 wt.% CaO (as CaC_2O_4 for AM and $CaCO_3$ for CIP samples) and 3 wt.% Y_2O_3 as sintering additives. Sintering was conducted in a graphite furnace at 1700 °C for six hours in N_2 atmosphere and a powder bed of AlN, BN and C.

	Grade C AM	Grade C CIP	Grade JM AM	Grade JM CIP
Thermal conductivity at 25 °C (W m^{-1} K^{-1})	166.2 ± 9.1	162.0 ± 6.6	162.1 ± 0.8	174.0 ± 3.1
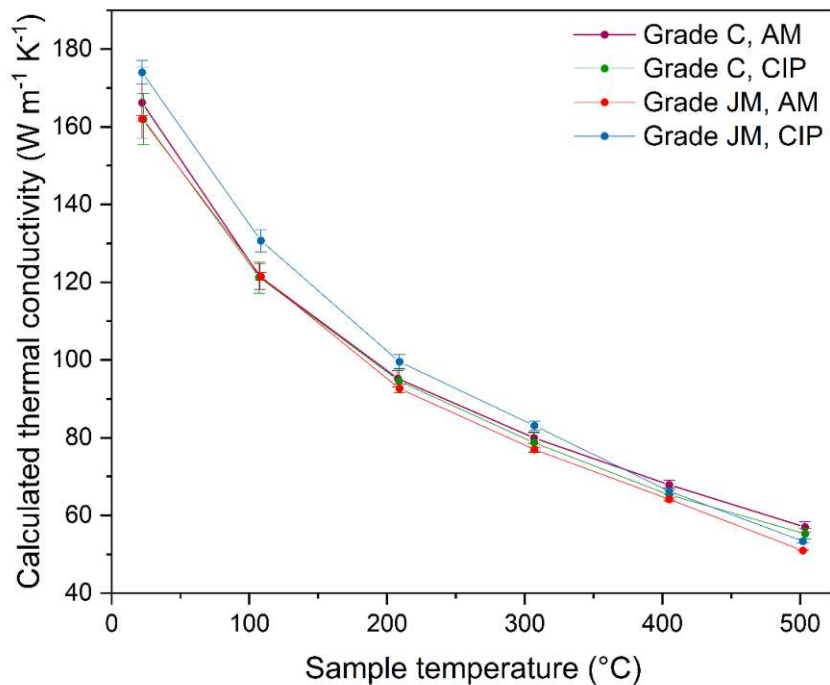
Fig. 62: Average thermal conductivities at increasing temperatures, as measured by Xe-flash method of AM and CIP samples made from powder mixtures consisting of Grade C or Grade JM AlN and 1 wt.% CaO and 3 wt.% Y_2O_3. The samples were sintered for six hours at 1700 °C in a graphite furnace using a N_2 atmosphere and a powder bed of AlN, BN and C [8].

To show the possibilities offered by the AM process, several complex shaped demonstrator parts were printed. Fig. 63 shows a green part of a heat exchanger design, not accessible by conventional shaping methods, made from a powder mixture containing Grade C AlN.
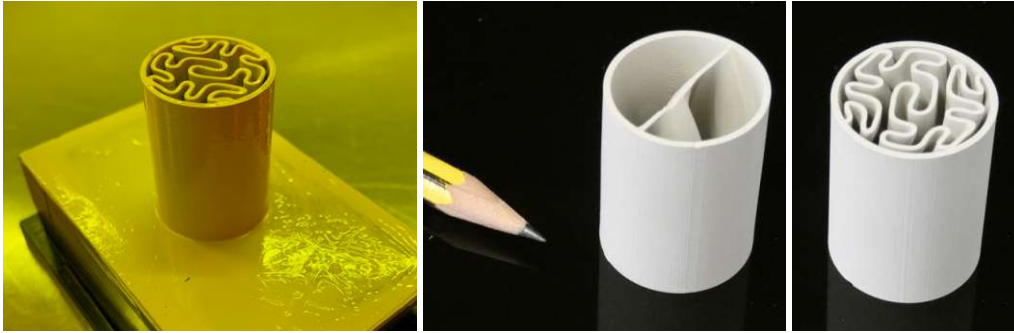
Fig. 63: Photographs of a green part from a powder mixture containing Grade C AlN after printing (left) and cleaning (middle and right) of a heat exchanger design [8].

In Fig. 64, a compilation of sintered AlN parts made powder mixtures consisting of Grade C AlN powder, 1 wt.% CaO and 3 wt.% Y_2O_3 is shown. The second row shows details of the hexagonal structure in the green state (left) and sintered state (right) in microscopic images (Keyence VHX-5000), indicating the shrinkage of the sample during heat treatments. Sintering was conducted utilizing the typical sintering programme in the graphite furnace at 1700 °C for six hours, in N_2 atmosphere and a powder bed of AlN, BN and C.
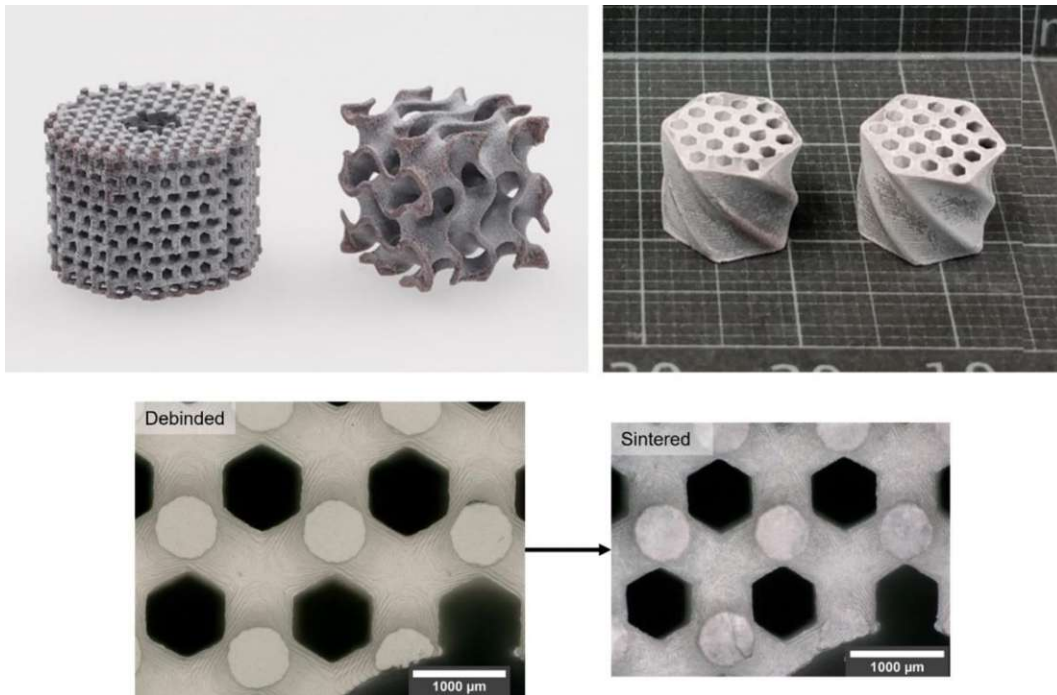
Fig. 64: Compilation of photographs of sintered (1700 °C, six hours, graphite furnace, N_2 atmosphere, powder bed ABC) complex shaped parts made from a powder mixture of Grade C AlN, 1 wt.% CaO and 3 wt.% Y_2O_3. The second row shows details of the hexagonal structure (top left) in a debinded state (left) and sintered state (right) [8].

A 3D scan of a sintered part was performed using a 3D inspection scanner (Autoscan-Inspec, Shining 3D Tec Co., Ltd.) with a resolution of 10 µm. The CAD design (corrected for shrinkage during debinding and sintering) of the part was then superimposed over the 3D scan, showing the deviations from the expected and the produced shape (Fig. 65).
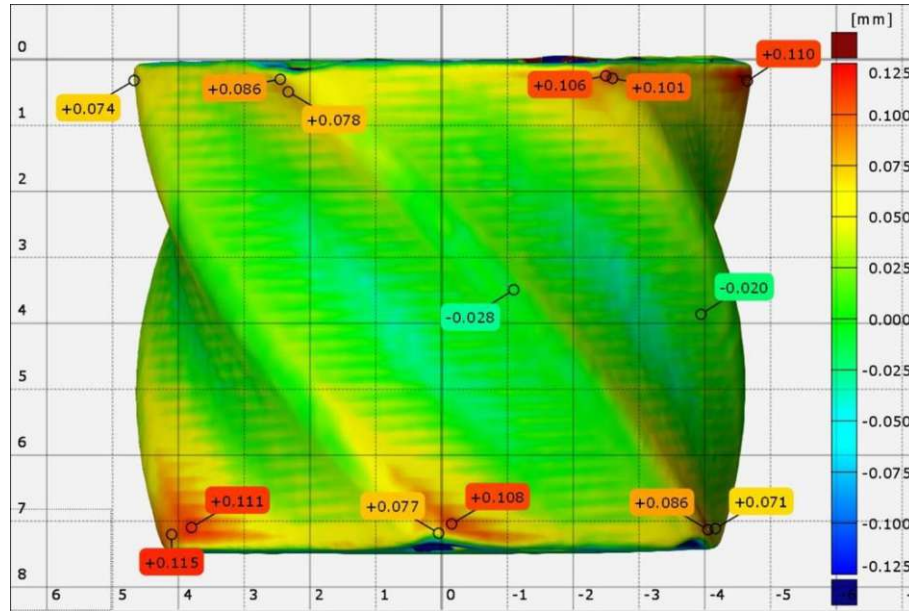
Fig. 65: 3D Scan of an AM part from Grade C AlN powder mixture containing 1 wt.% CaO and 3 wt.% Y_2O_3 sintered at 1700 °C for six hours in a graphite furnace in N_2 atmosphere in a powder bed of AlN, BN and C. The image was superimposed on the CAD design of the part (corrected for the expected shrinkages during debinding and sintering), showing the deviations of the design and the produced part [8].

131

5 Discussion

In this section the results presented in the previous parts of this work will be discussed, focusing on the following points:

- Stability of powders in different environments relevant for processing
- Characteristics of hot-pressed samples including layer formation and low thermal conductivities
- Influence of composition and processing parameters on CIP samples and how systematic evaluation of parameter variations led to the production of high thermal conductivity CIP samples
- Incorporation of the most promising powder systems from the experiments with CIP samples into the AM process and the challenges of this approach

5.1 Processing and powder properties

The grain morphology for all three AlN powders in this study was similar, as shown in SEM micrographs (Fig. 10), however, the color of the powders was off-white for Grade C and Grade BT AlN powders, whereas Grade JM AlN was white. The oxygen contents that were determined by the inert gas fusion method (Table 14) for all powders were higher than oxygen contents reported by the suppliers, although the trends were the same, with Grade C powder having the highest oxygen content, followed by Grade BT and the Grade JM powder. This is an indication that the method of measurement might not be perfectly suitable for AlN powder samples, especially with the reference materials at hand. The reference material for oxygen determinations contained 1.09 wt.% oxygen and the average of three measurements of this material was used to create a one-point calibration, which means that most of the measured values had to be extrapolated, leading to less consistent results. A different reference material was not available due to the appliance being used mostly for metallurgic samples with less oxygen content. In preliminary experiments, other reference substances such as Al_2O_3 were tested, but the oxygen contents of those exceeded the range of the device used, leading to inconsistent results. This also leads to the conclusion that the high oxygen contents of powders that were exposed to water should not be taken as true values, but rather only to show that the stability of AlN in water is not given.

The hydrolysis behavior of AlN in different environments (Fig. 11) was studied for practical reasons. Determination of oxygen content using the LECO TC400 led to high variations in the

measured values, due to the calibration mentioned in the paragraph above. However, it could be shown that AlN is stable in air, which allowed for storage in regular laboratory atmosphere, as opposed to storage (and manipulation of powders) in N_2 atmosphere using glove bags, which simplified the sample preparation process. The determination of the oxygen content of AlN powder exposed water was mostly conducted to gain better understanding of the hydrolysis process and to get a better perspective on the stability in other media. XRD (Fig. 12) showed that the first hydrolysis products were amorphous since higher oxygen contents in the powder were measured but additional signals from bayerite were only present in the diffractogram after 24 h of exposure. This confirms results from Bowen et al. [2], that were mentioned in section 2.1.3.1, detailing the course of the hydrolysis reactions of AlN to crystalline bayerite via an amorphous intermediate compound.

The stability of AlN in isopropyl alcohol for prolonged periods of time was a requirement for the selection as the liquid medium in which powder mixtures were to be processed in the planetary rotary mill. Technical grade isopropyl alcohol instead of a product with higher purity or even an absolute solvent was chosen to be used in the hydrolysis experiment because it would later be used for the processing of powders. Experiments investigating the whole powder processing chain (Fig. 13) further reinforced the claim that isopropyl alcohol is a suitable liquid medium for processing of AlN powder mixtures. A schematic summarizing the results of the investigation of the oxygen uptake of AlN during processing is shown in Fig. 66. The high oxygen content of the Grade C AlN powder after the first wet mixing step, which was higher than the oxygen content of the same powder batch after the dry mixing step, might stem from incomplete drying of the powder. The oxygen content of AlN after some of the processing steps is lower than the oxygen content of Grade C AlN powder taken directly from the storage container (in N_2 atmosphere). A possible explanation for this behavior is that powders were dried in a vacuum drying cabinet after the reaction to ensure all liquid media were evaporated before oxygen analysis.

The stability of the powders in a model binding agent even after 18 weeks of storage was another very important finding, because otherwise precautions preventing the reaction of AlN with the binding agent would have had to be taken.

Thermal decomposition of sintering additive precursor compounds in powder mixtures was necessary prior to the discovery that sintering in a powder bed alleviates the problem of gas porosity stemming from to the decomposition of sintering additive precursors. Heat treatment in SA-precursor decomposition furnace A led to a significant increase in oxygen content,

presumably due to leaks introducing oxygen into the atmosphere at elevated temperatures. Treatment in SA-precursor decomposition furnace B resulted in no oxygen uptake at 950 °C (as seen in Fig. 13 and Fig. 66).

Oxygen content of Grade C AlN powder after various processing steps:

Grade C AlN powder: 1.25 ± 0.11 wt.%	After wet milling in IPA and drying: 1.49 ± 0.12 wt.%	After dry milling: 1.35 ± 0.03 wt.%	After heating to 950°C in N_2(A): 2.50 ± 0.07 wt.%
		After wet milling in IPA, drying and dry milling: 1.27 ± 0.05 wt.%	After heating to 950°C in N_2(B): 1.19 ± 0.04 wt.%
Grade C AlN powder: 1.29 ± 0.02 wt.%	After exposure to a model binder system for 18 weeks: 1.09 ± 0.03 wt.%		

Fig. 66: Schematic of the oxygen content of Grade C AlN powder after several processing steps. Two sets of experiments with the same Grade C AlN powder batch were conducted, the first of which was heated to 950 °C in SA-precursor decomposition furnace A and the second in SA-precursor decomposition furnace B, listed in the schematic with (A) and (B). The long-term storage experiment in the model binder system was conducted with a different Grade C AlN powder batch with higher oxygen content.

5.2 Hot-pressing of AlN

Hot-pressing was used to produce AlN samples with high density, yielding benchmark values to which properties of AlN samples produced by other means could be compared to.

Hot-pressed samples produced during first trials at TU Wien exhibited a dark surface layer. SEM investigations (Fig. 15) showed differences in porosity between the different layers but no difference in BSE micrographs could be observed. An early working hypothesis was that the anthracite-colored layer might be aluminum carbide (Al_4C_3) due to the surface layer reacting with water resulting in gas evolution, but no definite proof for this claim was found, because XRD analysis was inconclusive. Assuming the incorporation of carbon into the dark surface layer of the samples, the compositional difference would have been hard to spot in the backscattered electron micrographs, due to a low Z difference in carbon and nitrogen. XRD investigations (Fig. 17) showed no significant difference between the white and gray materials. Externally produced samples did not exhibit this surface layer, even though the immediate surroundings of the lateral surface were the same. The upper and lower faces were different, due to externally produced samples being stacked during hot-pressing (up to 5 samples per hot-pressing run), whereas only one sample was sintered per sintering run at TU Wien, which entailed constant contact of the sample faces with graphite during the heat treatment. A conclusive hypothesis explaining the formation of the layers on HP samples has not been found yet.

The hot-pressing parameters employed in this study yielded samples with relative densities exceeding 96 % in all investigated samples, with only two samples below 99 %. These results show that hot-pressing leads to significant densification in AlN even without additives. The microstructures, observed in SEM micrographs (Fig. 20) are quite different for samples with and without sintering additives, revealing transcrystalline fracture mechanisms for samples without sintering additives and intercrystalline fracture mechanism in samples with sintering additives. This suggests a weakening of the grain boundaries by the presence of sintering additives, making fracture at said grain boundaries (at which the secondary phases are mostly located) more probable. The flexural strength of hot-pressed samples made from Grade C AlN with Y_2O_3 addition is significantly lower than in the Grade C AlN samples without sintering additives. However, the addition of CaO as sintering additive (regardless if in combination with Y_2O_3 or not) leads to samples exhibiting flexural strength values close to samples without sintering additives. The Weibull modulus increased for all samples with the addition of sintering

additives. A selection of micrographs of hot-pressed samples and the corresponding flexural strength parameters are summarized in Fig. 67.
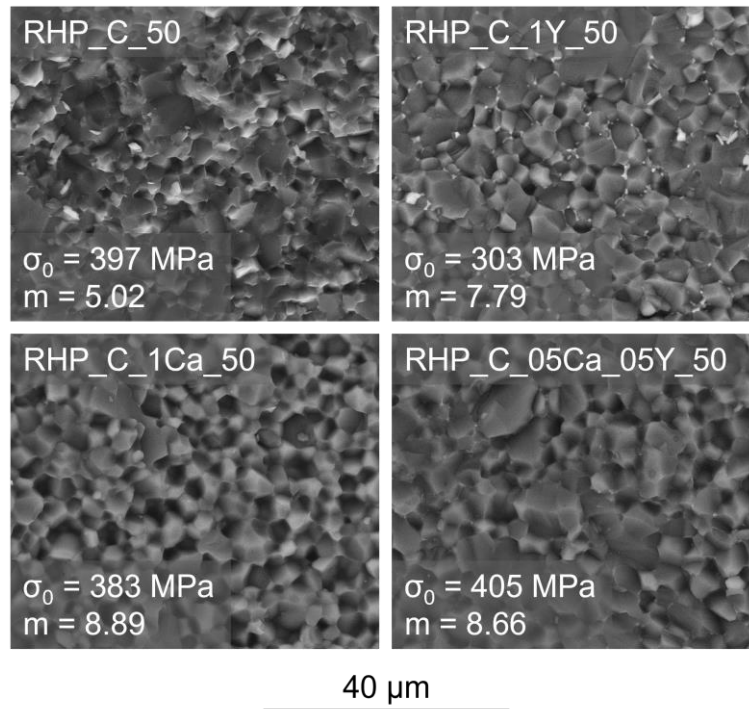
Fig. 67: SEM micrographs and corresponding strength parameters of select hot-pressed samples (Grade C AlN, 1800 °C, two hours, 35 MPa), showing the correlation between sample composition, the resulting microstructure after hot-pressing and the mechanical strength of HP AlN materials. The top left micrograph shows a sample without sintering additives, which exhibits transcrystalline fracture, whereas all other samples exhibit intercrystalline fracture.

Thermal conductivity (TC) of 6 HP samples was determined by laser flash technique resulting in values between 91 and 105 W m^{-1} K^{-1}, with the sample from Grade BT exhibiting the lowest value. This correlates with the finding that this sample also has the lowest density, which is known to be detrimental to thermal conductivity. The highest TC was determined for a sample made from Grade C AlN with 1 wt.% CaO addition, which might be explained by the purification of the AlN lattice from oxygen. The addition of sintering additives only led to very minor increases in thermal conductivity, with CaO having a seemingly larger effect than Y_2O_3. However, this does not correlate with findings discussed in the literature (see section 2.1.4.1).

Table 30: Thermal conductivity values of hot-pressed samples as determined by laser flash analysis at room temperature

Composition of hot-pressed samples (1800 °C, 35 MPa, 2 h in N_2)	Thermal conductivity at 25 °C (W m^{-1} K^{-1})
Grade C AlN, no additives	94 ± 1
Grade C AlN + 1 wt.% Y_2O_3	94 ± 1
Grade C AlN + 2 wt.% Y_2O_3	99 ± 1
Grade BT AlN + 1 wt.% Y_2O_3	91 ± 0
Grade C AlN + 0.5 wt.% CaO + 0.5 wt.% Y_2O_3	98 ± 0
Grade C AlN + 1 wt.% CaO	105 ± 1

Thermal conductivities of two additional HP samples were determined by the steady-state method to confirm the feasibility of this method for AlN materials. This method requires geometrically exact samples, which plane parallel and orthogonal faces. In spite of the brittle nature of AlN materials, suitable samples could be prepared and measured. Even though generated values were different from the results obtained by flash analysis, the method was considered feasible for subsequent optimization experiments with CIP and AM samples.

Initially, HP samples were planned to be used to generate benchmark values for density, mechanical and thermal properties to which the properties of CIP and AM samples could be compared to. Early experiments showed promising results for densification, however, the thermal conductivity of HP samples was rather low. No clear indication as to the reason behind the low thermal conductivity was found. The hot-pressing temperatures were higher than the sintering temperatures in all subsequent experiments, which was expected to yield higher diffusion and, in turn, purification of the AlN lattice. Two things to be considered are that the samples are rather large (70 g for a sample with 50 mm diameter), leading to longer migration pathways, and sintering additive contents (if added) were lower than in CIP or AM samples. Thus, the purification of the AlN lattice might be limited, leading to decreased thermal properties.

5.3 Sintering of CIPed AlN samples

The parameter variations of sintering additive contents, sintering times, environments, and temperatures will be discussed in the following sections. The first goal to be achieved was the generation of CIP samples with density values comparable to the density values achieved with HP samples. Later stages included the investigation of the influence of multiple processing parameters on the properties of sintered AlN materials, with a focus on increasing thermal conductivity of the materials.

5.3.1 Preliminary experiments on sintering without a powder bed

Preliminary experiments were focused on the identification of challenges during the sintering process and the production of samples with densities comparable to the density and hardness of HP samples. During dilatometry experiments conducted with a CIP sample from a powder mixture of Grade C AlN, 1 wt.% CaO and 3 wt.% Y_2O_3, the on-set of the shrinkage of the sample occurred at approximately 1450 °C. This information in conjunction with information from academic literature led to the conclusion that a sintering temperature of 1700 °C can yield samples with the high density, given the right sintering additives. Sintering CIP and AM samples at 1700 °C was also one of the goals outlined in section 1.

The results of first densification experiments in a corundum tube furnace showed that Y_2O_3 as sole sintering additive does not lead to adequate densification at a sintering temperature of 1700 °C, and while the secondary phase grains observed in SEM micrographs (Fig. 25) were larger than the initial particle size of Y_2O_3 powder added to the powder mixture, indicating solid-state sintering of the oxide, the heat treatment at 1700 °C did not lead to the liquid phase sintering mechanism of AlN and the densification associated with it. In contrast, the eutectic temperatures of secondary phases formed in the presence of CaO are lower, thus the sintering temperature of 1700 °C was sufficient to enable liquid phase sintering, which was also observed in samples made from powder mixtures containing a combination of CaO and Y_2O_3 as sintering additives. Decreased hardness values and large pores observed in SEM micrographs led to the hypothesis that decomposition of $CaCO_3$ during sintering might prevent complete densification of samples. Thermal decomposition of $CaCO_3$ in powder mixtures prior to shaping of samples by CIP was investigated in additional experiments to alleviate this behavior.

Further preliminary experiments were conducted using a graphite furnace, which was later shown to have a positive influence on material properties due to reducing sintering environments, which is also described in the literature (see section 2.1.4.2). Here, the focus was set on evaluating the influence of alternate sintering additives, including $SrCO_3$ or the use of nitrates as sintering additive precursor compounds, and the influence of thermal decomposition of sintering additive precursor compounds in powder mixtures prior to shaping on densification of the materials.

The relative density of samples in which the sintering additive precursors were not thermally decomposed prior to shaping did not exceed 95 %. SEM investigations did not lead to major insights into the lack of sintering activity, save the fact that only traces of secondary phase were observed on fracture surfaces. Thermal decomposition of SA precursors in powder mixtures prior to shaping in SA-precursor decomposition furnace A significantly increased densification, leading to relative densities exceeding 95 % for all investigated sintering additive combinations. Later experiments showed that the oxygen content of Grade C AlN powder heated to 950 °C in N_2 atmosphere in SA-precursor decomposition furnace A increased significantly. Increased oxygen content in the AlN lattice leads to increased secondary phase content during sintering. This in conjunction with the decomposition of the sintering additive precursors presumably facilitated densification of samples. This claim is reaffirmed by observations in SEM micrographs of fracture surfaces of samples made from powder mixtures that were heat-treated in SA-precursor decomposition furnace A, which showed higher contents of secondary phase than micrographs of samples made from powder mixtures in which the SA precursor was not thermally decomposed prior to shaping. Even though higher oxygen content in the AlN powder facilitates densification, it would ultimately be detrimental to thermal conductivity. In Fig. 68, a summary of microstructures observed in Grade C AlN samples with 1.5 wt.% CaO (as $CaCO_3$ with variations of thermal treatment) and 1.5 wt.% Y_2O_3 as sintering additives, sintered in the graphite furnace for 2 hours in N_2 atmosphere without a powder bed, is shown. The relative densities of the samples and the O content of the AlN powders, determined by the inert gas fusion technique (see 4.1.3) is given in the insets. The oxygen content of AlN which did not undergo thermal treatment at 950 °C (no TT) is the average of the oxygen contents of AlN powders after wet and dry milling. This comparison shows that relative density is closely related to the decomposition of the $CaCO_3$ sintering additive precursor, but also to the O-content of AlN powder.
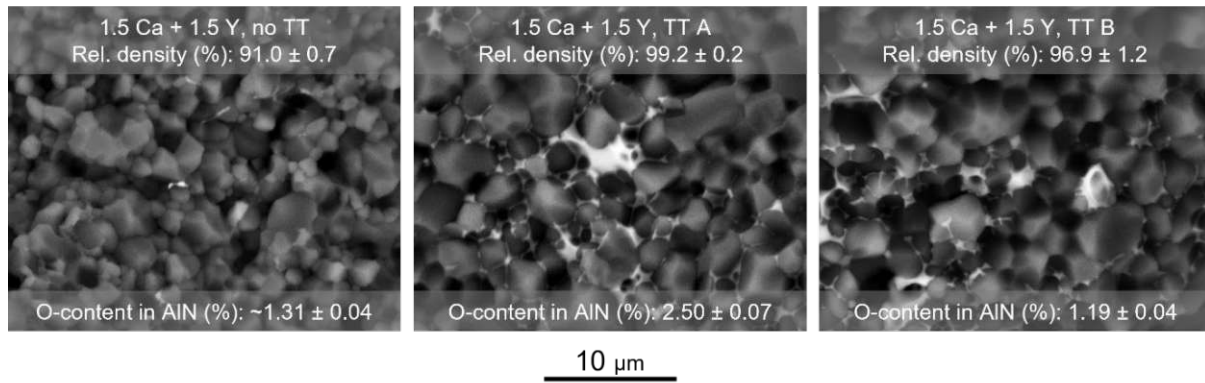
Fig. 68: BSE-SEM micrographs of fracture surfaces of samples made from powder mixtures of Grade C AlN, 1.5 wt.% CaO and 1.5 wt.% Y_2O_3. The $CaCO_3$ sintering additive precursor was either not thermally decomposed (left) or thermally decomposed in SA-precursor decomposition furnaces A (center) or B (right) prior to shaping and sintering at 1700 °C in a graphite furnace for two hours in N_2 atmosphere without a powder bed. The microstructures indicate that thermal treatment in SA-precursor decomposition furnace A leads to increased secondary phase content in sintered samples and correlates with the O content measured in Grade C AlN powder which was also exposed to the same heat treatment. Relative density is closely related to O content but also the decomposition of $CaCO_3$, since the "TT B" sample has a higher relative density than the "no TT" sample, even though it has a lower oxygen content.

The substitution of $CaCO_3$ by $SrCO_3$ led to samples with comparable density and hardness values when combined with Y_2O_3. However, this effect is suspected to stem mainly from the higher oxygen content in the AlN when treated at 1150 °C in SA-precursor decomposition furnace A (6.36 ± 0.88 %, as shown in Fig. 13). This becomes clearer when the relative densities of samples including nitrate sintering additive precursors are compared. The precursor compounds in the powder mixtures, were thermally decomposed at the same temperature (900 °C in SA-decomposition furnace A). After sintering, the relative densities of samples which included SrO as sintering additive are lower than densities of samples containing CaO as additive, which suggests a lower impact of SrO on the densification of AlN materials.

It was assumed that the dissolution of nitrate sintering additives in the liquid medium during the first mixing step would lead to better distribution of sintering additives by coating of AlN particles with the SA precursor compounds. However, the relative densities of sintered samples made from powder mixtures which originally contained nitrate precursors were lower than relative densities of the respective samples which contained carbonate precursor compounds (Fig. 69).
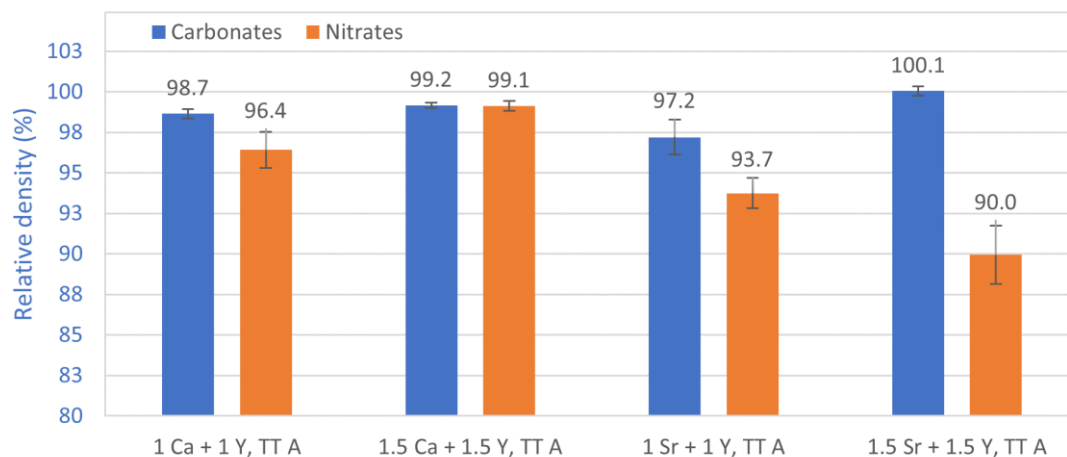
Fig. 69: Comparison of the relative density of samples produced from powder mixtures containing $CaCO_3$ or $SrCO_3$ and Y_2O_3 or the respective nitrates, sintered at 1700 °C for two hours in a graphite furnace in N_2 atmosphere without a powder bed.

An important discovery in this set of experiments was that the secondary phase migrates to sample surfaces (Fig. 31), resulting in samples with heterogeneous appearance. This phenomenon will be discussed in more detail in the next section.

5.3.2 Sintering of AlN materials in powder beds

For easier readability, the powder bed compositions and their abbreviations are listed again: A – aluminum nitride, AB – aluminum nitride and boron nitride, ABC – aluminum nitride, boron nitride, graphite. The exact powder bed compositions can be found in Table 9.

5.3.2.1 Additive compositions and sintering parameters

The preliminary experiments with CIP samples showed that a combination of CaO and Y_2O_3 yielded samples with high density, which is why only this system was systematically studied. However, it was apparent that the sintering environment also has a strong influence on samples. Close proximity to graphite (e.g. to the crucible) during sintering led to dark surface areas, whereas other parts of sintered samples were light. A powder bed was used to homogenize and control the sintering environment and provide similar sintering conditions for all samples within a sintering run. First experiments with a powder bed of AlN and BN showed increased densification of samples in which the $CaCO_3$ sintering additive precursor was not thermally decomposed prior to shaping. However, the surface of samples was still heterogeneous (exhibiting light and dark gray areas). As proximity to graphite was suspected

to be a major factor in this change in appearance, the reducing conditions during sintering were further adjusted by adding graphite to the powder bed, leading to a homogeneous sample appearance. Systematic investigations of sintering times, sintering additive compositions, and sintering environments were conducted to identify parameters leading to samples with optimized properties.

Some general observations were made when samples made from powder mixtures with various additive contents were sintered in powder beds at 1700 °C in the graphite furnace in N_2 atmosphere. The trends will be listed for each property investigated.

Relative density increased with higher sintering additive contents and increased up to sintering times of 4 hours. Samples sintered for 6 hours exhibited lower density values than samples sintered for shorter durations, which can be explained by increased migration and subsequent removal of the secondary phases, which generally have a higher density than AlN. Sintering in powder bed ABC led to samples with lower density than sintering in powder bed AB, which can also be explained by the increased removal of secondary phases from the samples. Samples sintered for six hours (powder bed AB with and without thermal decomposition of $CaCO_3$ in the powder mixture prior to shaping) exhibited very inconsistent density values when the liquid displacement method (in water) was used, which might be due to reactions of residual YN on the surface reacting with water, resulting in the formation of gases that eventually increase buoyancy over time.
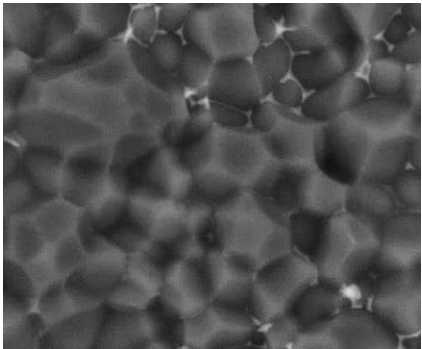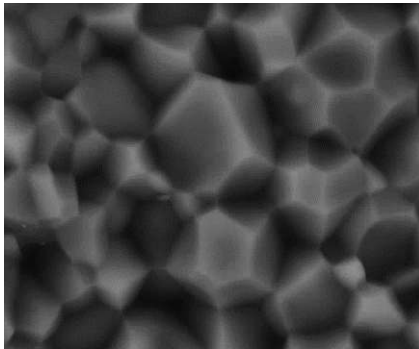
Thermal conductivity positively correlates to sintering times and sintering additive content with very few exceptions. Sintering in a reducing environment, as in powder bed ABC, had the highest impact on increasing this property. The reducing conditions lead to increased migration of the secondary phase, thus facilitating the purification, as will be described in detail in section 5.3.2.4. In the literature (see section 2.1.4.2), the thermal conductivity increase in AlN materials by purification of the AlN lattice through transfer of O from the lattice to the secondary phase and the influence of reducing conditions on the O content of the AlN lattice in general is also described.

Mechanical strength was only investigated for samples made from powder mixtures containing 1 wt.% CaO (as $CaCO_3$) and 3 wt.% Y_2O_3, without thermal decomposition of $CaCO_3$ prior to shaping, that were sintered at 1700 °C in a graphite furnace in N_2 atmosphere and either a powder bed consisting of AlN and BN, or AlN, BN and C. Characteristic strength values were 390 MPa for both approaches. However the Weibull modulus increased drastically

through the addition of graphite to the powder bed. A possible explanation for this lies in the homogenization of the reducing conditions in the sintering environment through graphite addition to the powder bed, since the specimens for B3B strength testing were cut from long cylinders, which would otherwise be exposed to different reducing conditions at different positions in the crucible during sintering due to their length. This could result in different sintering mechanisms along the length of the cylinder, resulting in a property gradient.

Table 31 summarizes micrographs of fracture surfaces and a selection of properties of samples made from powder mixtures containing Grade C AlN, 1 wt.% CaO (as $CaCO_3$, which was not thermally decomposed prior to shaping) and 3 wt.% Y_2O_3. The samples were sintered in a graphite furnace at 1700 °C for six hours in N_2 atmosphere in either a powder bed consisting of AlN and BN, or AlN, BN and C. In addition to the aforementioned increase in Weibull modulus due to the graphite addition to the powder bed, which is an indication for more homogeneous samples, the same trend can also be seen in the thermal conductivity of samples, showing not only higher thermal conductivity but also lower standard deviation of the thermal conductivity in samples sintered in a powder bed containing graphite.

Table 31: Comparison between thermal and mechanical properties and the microstructure (BS-SEM) of samples of the same composition (Grade C AlN, 1 wt.% CaO, 3 wt.% Y_2O_3), which were sintered in the graphite furnace at 1700 °C for six hours in a powder bed consisting of either AlN and BN or AlN, BN and C.

	1 Ca + 3 Y, 6 h, AB	1 Ca + 3 Y, 6 h, ABC
10 µm		
Relative density (%)	99.9 ± 0.6	99.1 ± 0.8
Thermal conductivity ($W\ m^{-1}\ K^{-1}$)	161 ± 14	178 ± 5
Char. Weibull strength (MPa)	390	390
Weibull modulus	8.1	13.8

5.3.2.2 Lowering the sintering temperature to 1600 °C

The typical sintering temperature used in this study was 1700 °C. Lowering sintering temperatures should be a high priority to realize a less energy intensive production process of materials. However, it was found that samples from powder mixtures of Grade C AlN with 1 wt.% CaO and up to 5 wt.% Y_2O_3, which were sintered in a graphite furnace 1600 °C for six hours in N_2 atmosphere in a powder bed AB, had significantly lower thermal conductivity at comparable degrees of densification than samples for which all production parameters were kept constant, except for an increased sintering temperature of 1700 °C. A graphical comparison is shown in Fig. 70. Density of the samples sintered at 1700 °C was measured using the geometric method due to high variations of the results of the liquid displacement method.
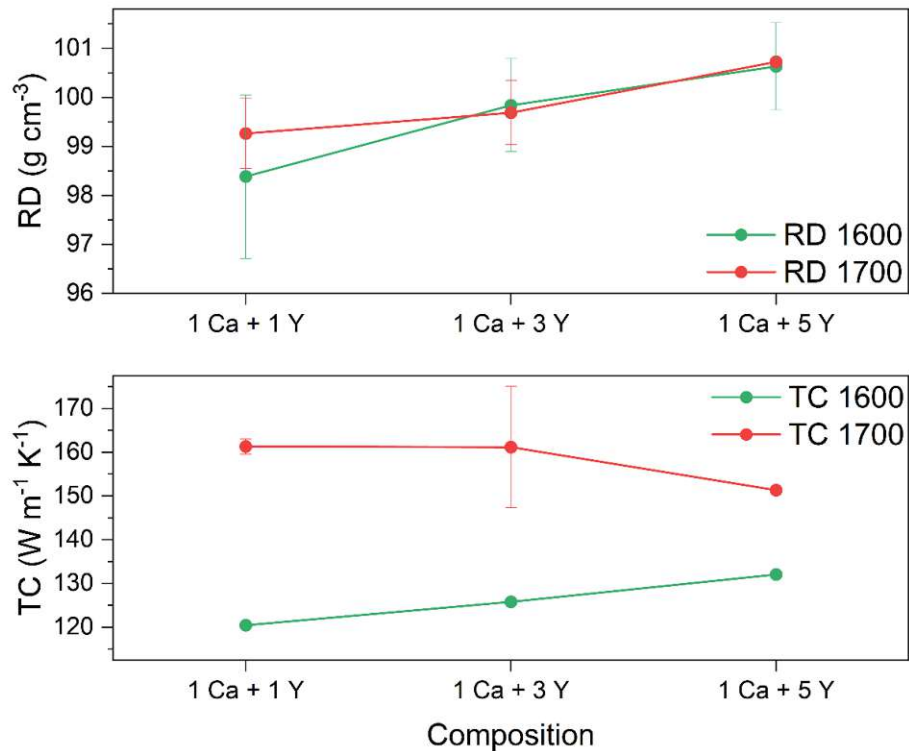
Fig. 70: Relative density (RD) and thermal conductivity (TD, steady-state) of samples made from Grade C AlN powder mixtures including 1 wt.% CaO (as $CaCO_3$, not decomposed prior to shaping) and various amounts of Y_2O_3, which were sintered at either 1600 °C or 1700 °C for six hours in a graphite furnace in N_2 atmosphere in powder beds from AlN and BN. This highlights the impact of lowering the sintering temperature by 100 °C, resulting in lower thermal conductivity at comparable degrees of densification of AlN samples.

The samples made from a powder mixture containing 1 wt.% CaO and 5 wt.% Y_2O_3 which were sintered at 1600 °C exhibited a vastly different microstructure when compared to SEM micrographs of other samples (e.g. a sample from a powder mixture containing 1 wt.% CaO and 5 wt.% Y_2O_3, sintered at 1700 °C). The secondary phase exhibited high levels of segregation into separate, large secondary phase areas. However, due to time constraints, no further investigations were conducted.

5.3.2.3 Variation of starting AlN powder grades

Powder mixtures from three different AlN powder grades (Grade C, Grade BT and Grade JM) with 1 wt.% CaO (as $CaCO_3$, no decomposition prior to shaping) and 3 wt.% Y_2O_3 were prepared and sintered in the graphite furnace at 1700 °C for six hours in N_2 atmosphere and powder bed ABC. Samples from Grade C and Grade JM AlN showed comparable levels of densification exceeding 97.5 % relative density, while the sample from Grade BT only exhibited a relative density of 82.2 %. The low densification presumably affects other properties as well,

such as mechanical strength (258 MPa) and thermal conductivity (129 W m^{-1} K^{-1}) being lower in the samples from Grade BT AlN powder mixture. Akin to the density, other material properties were also relatively similar in samples from Grade C and Grade JM AlN, with the most notable difference in thermal conductivity (180 W m^{-1} K^{-1} and 161 W m^{-1} K^{-1} for samples from Grade C and Grade JM AlN powder mixtures, respectively). The lower thermal conductivity for samples from Grade JM AlN powder mixture was especially surprising, since the O content in the Grade JM AlN powder was lower than the O content in Grade C powder, at 0.88 % and 1.29 %, respectively. These experiments were conducted to investigate the feasibility of substituting Grade C AlN with Grade JM or Grade BT, with the results that Grade JM AlN powders led to comparable sample properties (although thermal conductivity was slightly lower), whereas Grade BT cannot be used as a substitution for Grade C AlN due to inferior densification behavior.

5.3.2.4 Influence of the sintering environment on the migration of secondary phase and on the formation of YN

In addition to the systematic investigations discussed in the section above, additional experiments investigating the effects of different sintering environments on AlN materials and the migrative behavior of the secondary phase were conducted. These results were also published in a research paper [7].

In all experiments discussed in this section, CIP samples made from powder mixtures containing Grade C AlN, 1 wt.% CaO (as CaCO$_3$, which was not thermally decomposed prior to CIP) and 3 wt.% Y$_2$O$_3$ were used. Sintering was conducted at 1700 °C for six hours in N$_2$ atmosphere, but four different combinations of furnaces and powder beds were used, which are detailed again below:

Approach A: Graphite furnace + powder bed AB

Approach B: Graphite furnace + powder bed ABC

Approach C: Corundum tube furnace + powder bed A

Approach D: Hot isostatic press + powder bed ABC

After sintering, the surface of the samples sintered in a corundum tube furnace (approach C) did not exhibit a dark YN layer, because sintering was conducted in a non-reducing environment, preventing the formation of YN. Secondary phase migration was strongest in the samples sintered in the graphite furnace in a powder bed of AlN, BN and C (approach B), which was confirmed by a comparison of the microstructures (BSE-SEM) and XRD analyses

performed, in which no secondary phase was detected. A compilation of those results is shown in Fig. 71. The driving force for secondary phase removal is much higher in reducing conditions because the secondary phase, once it reaches the surface of the samples, is reduced according to the reactions mentioned in section 2.1.4.2. The reduction leads to the solidification of AlN and YN at the surface, which in turn increases capillary pressure, forcing more secondary phase out of the samples. Only TEM analysis shows remnants of secondary phase in triple junctions of samples from approach B.

An explanation for the reduced secondary phase migration observed in samples sintered at increased N_2 gas pressure (approach D), in spite of all other parameters being comparable to approach B, can be found in the Ellingham-diagram. Ishizaki and Watari [66] reported the conservation of O content in HIP-sintered samples when compared to regularly sintered samples. This behavior was explained using the Ellingham-diagram which predicts an increased stability of the oxides present in the material at higher gas pressures, which would also explain the behavior observed in samples from this study. Higher gas pressures result in decreased reduction of secondary phase at the surface of the samples, which in turn leads to less migration of the secondary phase.
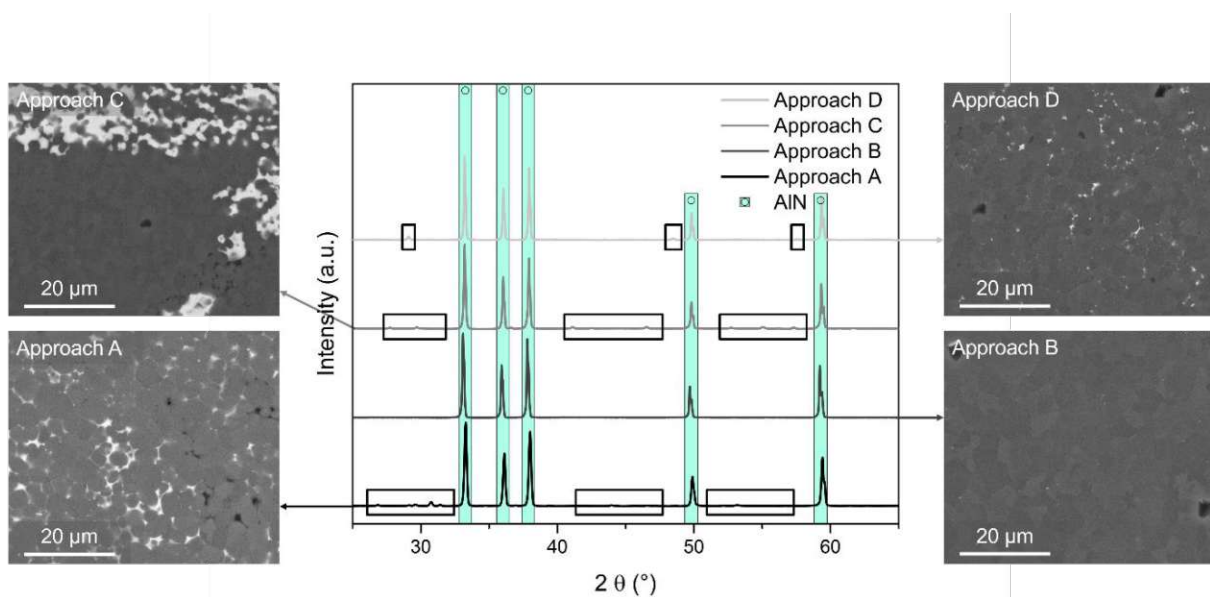
Fig. 71: Summary of the investigations of AlN samples of equal compositions (Grade C AlN, 1 wt.% CaO (as $CaCO_3$, without decomposition prior to shaping), 3 wt.% Y_2O_3), which were all sintered for six hours at 1700 °C in different furnaces and powder beds. The absence of secondary phases (which are highlighted by black borders) in X-ray diffractograms recorded for samples from approach B (graphite furnace, powder bed ABC) was confirmed by these investigations, although TEM measurements revealed remnants of secondary phase in triple-junctions.

The relative densities of the samples from the four approaches are within 1.5 % of each other, with all exceeding 99 %. However, thermal conductivities and grain sizes varied greatly between samples from the different approaches. Samples from the two approaches with the conditions with highest reduction potential due to graphite addition to the powder bed (approaches B and D) reached thermal conductivities exceeding 170 W m^{-1} K^{-1}, whereas the samples from approach A reached 162 W m^{-1} K^{-1}, and the samples sintered in the corundum tube furnace in non-reducing conditions (approach C) exhibited 133 W m^{-1} K^{-1}. The lower thermal conductivity in the samples sintered in non-reducing conditions, even though the density was similar to the samples from other sintering approaches, highlights the importance of a reducing sintering atmosphere.

5.4 Additive manufacturing of AlN ceramics

The basic premise of the LCM process is rather simple. A ceramic slurry containing a photopolymer and ceramic particles is cured layer by layer through selective exposition to light. The organic binder is then burned out of the samples, which can then be sintered. However, many requirements have to be met in order to obtain additively manufactured parts from AlN.

This section is split in three subsections discussing the incorporation of AlN powder systems into the LCM process chain, the systematic investigation of densification, microstructure, and mechanical as well as thermal properties, and lastly the creation of complex shaped AlN parts.

5.4.1 Implementation of the AM process chain with AlN powder systems

For AM slurries, powder mixtures developed and successfully implemented for CIP samples (see section 5.3) were used. In a first step, the stability of AlN in the organic binder was ensured by monitoring the O content of AlN after multiple weeks of exposure to the binder, which resulted in no increase in O content. However, it was discovered that $CaCO_3$ reacts with the organic binder, resulting in gaseous reaction products, which hinder the AM process. As such, $CaCO_3$ was substituted with CaC_2O_4 in powder mixtures to be used in the AM process. The comparability between already gathered data on CIP samples produced with powder mixtures containing $CaCO_3$ and AM samples produced with powder mixtures containing CaC_2O_4 had to be warranted. First, an AM sample made from a powder mixture containing 1 wt.% CaO (introduced as CaC_2O_4) and 3 wt.% Y_2O_3 was debinded and its C content assessed. The C content was compared to the theoretical value of powder mixture consisting of 96 wt.% AlN, 1 wt.% CaO (as $CaCO_3$) and 3 wt.% Y_2O_3, which was the expected composition of the AM sample after debinding. The measured and the calculated C contents matched, indicating decomposition of CaC_2O_4. An additional XRD analysis (Fig. 58) of the debinded AM sample showed no signals of CaC_2O_4, which was another confirmation of the decomposition of CaC_2O_4 during debinding. These results led to the conclusion that properties of CIP samples made from powder mixtures containing $CaCO_3$ can be compared to AM samples made from powder mixtures containing CaC_2O_4, since their compositions before the sintering step matched.

Thermal debinding of AM samples at 600 °C in air is necessary to remove organic compounds and enable the production of dense samples. Although a slight increase in oxygen content of AlN powders during the thermal debinding process was observed (Table 23), it was deemed acceptable to carry on with experiments. TG measurements of AM samples heated to 900 °C

in air, simulating the debinding process, showed that weight increase, presumably due to oxidation, only started at about 650 °C, which is 50 °C higher than the temperature at which thermal decomposition of the organic binder is completed. Since the thermal conductivity of AM samples was comparable to CIP samples, the oxygen content was either not detrimental to thermal conductivity or was reduced during sintering in reducing conditions.

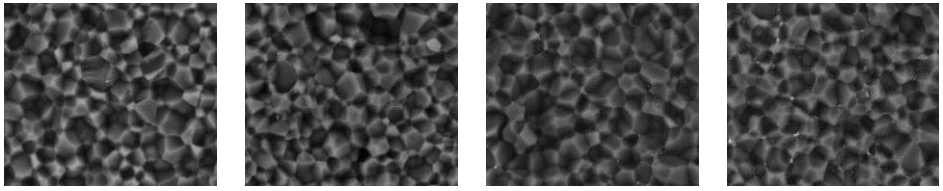## 5.4.2 Systematic investigation of properties of AM samples

Table 32, located at the end of this section, shows comparisons of select properties of AM and CIP samples. All samples discussed here were prepared from powder mixtures including 1 wt.% CaO (as CaC_2O_4 for AM and $CaCO_3$ for CIP samples) and 3 wt.% Y_2O_3 as sintering additives and were sintered at 1700 °C in the graphite furnace in N_2 atmosphere and a powder bed of AlN, BN and C.

The density of AM samples varied significantly between AM batches. For sintered AM samples from Grade C powder mixtures, the lowest relative density measured was 93.5 % and the highest 100.4 %. In AM samples made from Grade JM powder mixtures, the values were 91.6 % to 97.8 %, respectively.

A significant difference in the characteristic Weibull strength depending on the testing direction was observed in AM samples from Grade C and Grade JM powder mixtures. Flexural strength was higher for AM samples when the direction of force during testing was parallel rather than perpendicular to the building direction during the AM process (56 % and 28 % increase in Grade C and Grade JM AM samples, respectively). Two things have to be considered for this observation. First, the relative densities of the AM batches (94.2 % for Grade C and 91.6 % for Grade JM) from which samples were tested with the direction of force during flexural tests perpendicular to the building direction were lower than in the AM batches from which samples were tested parallel to the building direction. Second, the AM process might enable the development of stresses during sintering which might result in strengthening of the samples.

Thermal conductivity values between 160 and 175 W m^{-1} K^{-1} were determined for AM and CIP samples at room temperature, indicating high comparability between thermal properties of AM and CIP AlN materials. These results demonstrate that additively manufactured AlN materials with properties comparable to conventionally processed AlN materials could be obtained.

Table 32: Summary of the properties of AM and CIP samples made from equivalent powder mixtures (Grade C AlN or Grade JM AlN, 1 wt.% CaO (as CaC_2O_4 for AM and $CaCO_3$ for CIP samples) and 3 wt.% Y_2O_3) in which sintering additive precursor compounds were not thermally decomposed prior to shaping. Sintering was conducted at 1700 °C in the graphite furnace in N_2 atmosphere and powder beds consisting of AlN, BN and C. Density and thermal conductivity (flash method) values exhibit high variance. The difference between testing directions (parallel or perpendicular to the building axis) in flexural tests performed on AM samples presumably stems from density variations or from the AM process enabling the development of stresses during sintering.

	Grade C AM	Grade C CIP	Grade JM AM	Grade JM CIP
40 µm				
Relative density (%)	96.6 ± 2.4	99.1 ± 0.6	93.3 ± 2.2	99.5 ± 0.6
Thermal conductivity at 25 °C (W m-1 K-1)	166.2 ± 9.1	162.0 ± 6.6	162.1 ± 0.8	174.0 ± 3.1
Char. Weibull Strength (MPa); (Weibull modulus) (xy)	498; (14.0)	390; (13.8)	468; (9.1)	415; (13.8)
Char. Weibull Strength (MPa); (Weibull modulus) (xz)	320; (10.0)		367; (9.8)	
Grain size (xy)	5.04 ± 0.50	4.72 ± 0.18	5.66 ± 0.34	4.69 ± 0.40
Grain size (xz)	4.76 ± 0.36		6.11 ± 0.33	

5.4.3 Observations on AlN samples with complex geometries produced by LCM

Fig. 63, Fig. 64 and Fig. 65 show that the generation of complex AlN parts by LCM is indeed possible. The demonstrational parts printed feature low wall thicknesses and intricate geometries, which could also be found in practical parts, such as heat exchangers. The superposition of a 3D scan of a complex shaped part over its CAD design, taking into account shrinkage during thermal debinding and sintering, showed low dimensional deviations below 150 µm. Knowing this value is important because industrial applications often require low tolerances.

6 Summary and conclusions

The initial objectives of this work were to…

1) …investigate hydrolysis stability of AlN in environments relevant for processing
2) …produce samples by hot-pressing to generate benchmark values for mechanical and thermal properties
3) …find powder systems suitable for sintering without external pressure that yield samples with high mechanical and thermal properties
4) …sinter and characterize additively manufactured samples produced from the powder mixtures developed in the previous step

6.1 Evaluating hydrolysis and stability of AlN powders

AlN powders were exposed to water and various media utilized in the different processing steps for set amounts of time. Additionally, AlN powders were prepared in the same way that powder mixtures of AlN and sintering additives were prepared (e.g. mixing or thermal treatments). After exposure or the respective processing steps, O contents of the powders were measured by inert-gas fusion technique, and XRD analysis was used if significant hydrolysis was detected. Except for water, which was more or less a reference for a medium leading to strong hydrolysis, AlN was stable in all media used in processing and only heat-treatment steps in one furnace (SA-precursor decomposition furnace A) led to oxygen uptake of AlN. These results led to the conclusion that AlN powder may be stored in regular lab atmosphere (as opposed to N_2 inert atmosphere) and may be prepared without the need of hydrolysis protection by means of protective surface films.

6.2 Hot-pressing of AlN samples

Hot-pressing was used as a method to create fully densified AlN materials with or without sintering additives added to the AlN powder. The samples were characterized with respect to densification, microstructure, as well as mechanical and thermal properties. Densification and microstructures were promising in all samples investigated and mechanical properties were comparable to values found in the literature for AlN materials. However, thermal conductivity values were lower than expected. The reason behind this might be the low amount of sintering additives used in hot-pressed materials not facilitating sufficient purification of the AlN lattice.

6.3   Sintering of CIP samples without the application of external pressure

Consolidation of AlN materials without hot-pressing was necessary in order to be able to sinter additively manufactured parts. For this, powder systems containing AlN and sintering additives with high sinterability to produce materials with adequate properties had to be found. The first focus was set on the investigation of densification of powder mixtures containing various sintering additives with the result that combinations of CaO and Y_2O_3 lead to the highest densification of materials during sintering. Systematic investigations of the effect of various additive combinations and sintering parameters such as sintering time, temperature, and environments led to an optimization of AlN processing, yielding dense AlN materials with thermal conductivity of up to 180 W m^{-1} K^{-1} and characteristic Weibull strength of 390 MPa with high reproducibility.

During these investigations multiple phenomena occurring during sintering like the migration of secondary phase and nitridation thereof at sample surfaces were observed and systematically studied. The effects of reducing conditions on both migration and nitridation could be verified and correlated with positive developments of the resulting properties of AlN materials. The results of this research were also published in a scientific paper [7].

6.4   Incorporating AlN powder mixtures into the LCM process

The powder mixtures developed in the previous step were successfully incorporated into the LCM process and challenges with the process were identified and solved. An example would be the incompatibility of $CaCO_3$ in the organic binder system, which was solved by substituting $CaCO_3$ with CaC_2O_4. The substitution resulted in a powder mixture suitable for printing. The properties of AM samples were comparable to the properties of CIP samples generated throughout the preceding studies, since CaC_2O_4 decomposes to $CaCO_3$ during thermal debinding, which results in matching compositions of AM and CIP samples prior to sintering.

The utilization of an optimized powder system and processing routine resulted in AM samples with simple and complex geometric shapes with thermal and mechanical properties similar to CIP samples. However, repeatability of the process still needs to be improved, because the variations between AM batches were significant. The results of these studies were also published in a scientific research paper [8].

7 Outlook

The experiments and results discussed in this thesis provided a robust starting point for the development of additively manufactured AlN ceramics. With the generation of printed parts, the feasibility of the process was shown, and properties of AM samples were very promising when compared to properties of CIP samples. Complex geometries unobtainable by other means of ceramic manufacturing were printed and sintered. However, a number of questions have been left unanswered.

It was shown that reducing sintering environments have a positive effect on the final properties of AlN materials. In addition to increased densification and improved mechanical and thermal properties, the migration of secondary phase towards sample surfaces in conjunction with the formation of YN on the surfaces was observed. While longer sintering times led to enhanced thermal properties in the samples investigated, this might not be the case for all sample shapes. Especially when it comes to smaller or thin-walled samples, which are often produced by LCM, the effect of this migration has to be studied, because migration could lead to depletion of secondary phase before densification and purification of the AlN lattice is complete. Further investigations of the sintering behavior additive system used in this study and possibly alternative sintering additive systems might prove valuable for the optimization of the sintering process of AlN. The determination of migration coefficients for the secondary phase as function of sintering temperature and time could lead to the development of sintering simulations with which optimal parameters for sintering of AlN materials, depending on their geometry, could be calculated. This could possibly lead to energy savings during heat treatments if lower sintering temperatures and times could be realized and oversintering could be prevented.

It was shown that LCM-AlN materials have great potential in solving delicate thermal management challenges, but solutions for issues considering the repeatability of the process and the resulting consistency of material properties have to be found. A deeper understanding of the interactions of the organic binder and the ceramic powder during AM and thermal debinding can lead to a more consistent manufacturing process, which can be of industrial relevance for the generation in complex electronic substrates or chemically resistant heat-exchanger designs with high thermal conductivity.

References

[1] Y. Baik, R.A.L. Drew, Aluminum Nitride: Processing and Applications, Key Engineering Materials 122-124 (1996) 553-0.

[2] P. Bowen, J.G. Highfield, A. Mocellin, T.A. Ring, Degradation of Aluminum Nitride Powder in an Aqueous Environment, Journal of the American Ceramic Society 73(3) (1990) 724-728.

[3] G.A. Slack, Nonmetallic crystals with high thermal conductivity, Journal of Physics and Chemistry of Solids 34(2) (1973) 321-335.

[4] S.M. Olhero, S. Novak, M. Oliveira, K. Krnel, T. Kosmac, J.M.F. Ferreira, A thermo-chemical surface treatment of AlN powder for the aqueous processing of AlN ceramics, Journal of Materials Research 19(3) (2004) 746-751.

[5] A.V. Virkar, T.B. Jackson, R.A. Cutler, Thermodynamic and Kinetic Effects of Oxygen Removal on the Thermal Conductivity of Aluminum Nitride, Journal of the American Ceramic Society 72(11) (1989) 2031-2042.

[6] R.R. Lee, Development of High Thermal Conductivity Aluminum Nitride Ceramic, Journal of the American Ceramic Society 74(9) (1991) 2242-2249.

[7] J. Rauchenecker, S. Schwarz, W. Artner, T. Konegger, Atmosphere control and secondary phase migration during moderate-temperature sintering of aluminum nitride, Ceramics International 48(11) (2022) 16425-16431.

[8] J. Rauchenecker, J. Rabitsch, M. Schwentenwein, T. Konegger, Additive manufacturing of aluminum nitride ceramics with high thermal conductivity via digital light processing, Open Ceramics 9 (2022) 100215.

[9] G. Long, L.M. Foster, Aluminum Nitride, a Refractory for Aluminum to 2000°C, Journal of the American Ceramic Society 42(2) (1959) 53-59.

[10] R. Yu, G. Liu, G. Wang, C. Chen, M. Xu, H. Zhou, T. Wang, J. Yu, G. Zhao, L. Zhang, Ultrawide-bandgap semiconductor AlN crystals: growth and applications, Journal of Materials Chemistry C 9(6) (2021) 1852-1873.

[11] Toshiba, Fine Ceramics for Electronics. https://www.toshiba-tmat.co.jp/pdf/product/e_cmp_01.pdf. (Accessed 07/31/2022, 21:47).

[12] CeramTec, Advanced Ceramics for Electronic Applications. https://www.ceramtec-industrial.com/fileadmin/user_upload/Corporate/11_Downloads/06_Electronic_Heatsinks/CeramTec_Material_Properties_Electronic_Applications.pdf. (Accessed 07/31/2022, 21:40).

[13] W. Werdecker, F. Aldinger, Aluminum Nitride—An Alternative Ceramic Substrate for High Power Applications in Microcircuits, IEEE Transactions on Components, Hybrids, and Manufacturing Technology 7(4) (1984) 399-404.

[14] H. Nakano, K. Watari, H. Hayashi, K. Urabe, Microstructural Characterization of High-Thermal-Conductivity Aluminum Nitride Ceramic, Journal of the American Ceramic Society 85(12) (2002) 3093-3095.

[15] G.A. Slack, R.A. Tanzilli, R.O. Pohl, J.W. Vandersande, The intrinsic thermal conductivity of AlN, Journal of Physics and Chemistry of Solids 48(7) (1987) 641-647.

[16] N. Kuramoto, H. Taniguchi, Transparent AlN ceramics, Journal of Materials Science Letters 3(6) (1984) 471-474.

[17] R.B. Dinwiddie, A.J. Whittaker, D.G. Onn, Thermal conductivity, heat capacity, and thermal diffusivity of selected commercial AlN substrates, International Journal of Thermophysics 10(5) (1989) 1075-1084.

[18] Y. Kurokawa, K. Utsumi, H. Takamizawa, T. Kamata, S. Noguchi, A1N Substrates with High Thermal Conductivity, IEEE Transactions on Components, Hybrids, and Manufacturing Technology 8(2) (1985) 247-252.

[19] N. Yamada, J. Yoshikawa, Y. Katsuda, H. Sakai, Electrical Resistivity Control of Hot-Pressed Aluminum Nitride Ceramics, Key Engineering Materials 403 (2008) 49-52.

[20] Y. Xiong, H. Wang, Z. Fu, Transient liquid-phase sintering of AlN ceramics with CaF_2 additive, Journal of the European Ceramic Society 33(11) (2013) 2199-2205.

[21] M. Hirano, K. Kato, T. Isobe, T. Hirano, Sintering and characterization of fully dense aluminium nitride ceramics, Journal of Materials Science 28(17) (1993) 4725-4730.

[22] F. Miyashiro, N. Iwase, A. Tsuge, F. Ueno, M. Nakahashi, T. Takahashi, High thermal conductivity aluminum nitride ceramic substrates and packages, IEEE Transactions on Components, Hybrids, and Manufacturing Technology 13(2) (1990) 313-319.

[23] A. Bouaiss, A. Largeteau, C. Collado, G. Demazeau, Solvothermal synthesis of AlN, High Pressure Research 18(1-6) (2000) 227-232.

[24] F.J.-M. Haussonne, Review of the Synthesis Methods for AlN, Materials and Manufacturing Processes 10(4) (1995) 717-755.

[25] L.M. Sheppard, Aluminum nitride. A versatile but challenging material, American Ceramic Society Bulletin 69(11) (1990).

[26] H. Scholz, P. Greil, Synthesis of high purity AlN by nitridation of Li-doped Al-melt, Journal of the European Ceramic Society 6(4) (1990) 237-242.

[27] M. Mashhadi, F. Mearaji, M. Tamizifar, The effects of NH_4Cl addition and particle size of Al powder in AlN whiskers synthesis by direct nitridation, International Journal of Refractory Metals and Hard Materials 46 (2014) 181-187.

[28] K. Baba, N. Shohata, M. Yonezawa, Synthesis and properties of ultrafine AlN powder by rf plasma, Applied Physics Letters 54(23) (1989) 2309-2311.

[29] X. Zeng, D. Qian, W. Li, H. Peng, C. Lei, X. Liu, Effects of Additive on the Microwave Synthesis of AlN Powder, Journal of the American Ceramic Society 90(10) (2007) 3289-3292.

[30] A. Tsuge, H. Inoue, M. Kasori, K. Shinozaki, Raw material effect on AlN powder synthesis from Al_2O_3 carbothermal reduction, Journal of Materials Science 25(5) (1990) 2359-2361.

[31] Y. Baik, K. Shanker, J.R. McDermid, R.A.L. Drew, Carbothermal Synthesis of Aluminum Nitride Using Sucrose, Journal of the American Ceramic Society 77(8) (1994) 2165-2172.

[32] P. Ravenel, R. Bachelard, J.-P. Disson, P. Joubert, Continuous Process for the Preparation of Aluminum Nitride by the Carbonitriding of Alumina, Arkema France SA, 1997.

[33] L.V. Interrante, L.E. Carpenter, C. Whitmarsh, W. Lee, M. Garbauskas, G.A. Slack, Studies of Organometallic Precursors to Aluminum Nitride, MRS Online Proceedings Library 73(1) (1986) 359-366.

[34] D. Chen, J. Wang, D. Xu, Y. Zhang, The influence of defects and impurities in polycrystalline AlN films on the violet and blue photoluminescence, Vacuum 83(5) (2009) 865-868.

[35] J. Shin, D.-H. Ahn, M.-S. Shin, Y.-S. Kim, Self-Propagating High-Temperature Synthesis of Aluminum Nitride under Lower Nitrogen Pressures, Journal of the American Ceramic Society 83(5) (2000) 1021-1028.

[36] K. Sardar, C.N.R. Rao, AlN nanocrystals by new chemical routes, Solid State Sciences 7(2) (2005) 217-220.

[37] P. Colombo, G. Mera, R. Riedel, G.D. Sorarù, Polymer-Derived Ceramics: 40 Years of Research and Innovation in Advanced Ceramics, Journal of the American Ceramic Society 93(7) (2010) 1805-1837.

[38] M.M. Seibold, C. Rüssel, Thermal Conversion of Preceramic Polyiminoalane Precursors to Aluminum Nitride: Characterization of Pyrolysis Products, Journal of the American Ceramic Society 72(8) (1989) 1503-1505.

[39] I. Teusel, C. Rüssel, Aluminium nitride coatings on silicon carbide fibres, prepared by pyrolysis of a polymeric precursor, Journal of Materials Science 25(8) (1990) 3531-3534.

[40] S. Koyama, H. Takeda, T. Tsugoshi, K. Watari, Y. Sugahara, Organic-to-inorganic conversion process of a cage-type AlN precursor poly (ethyliminoalane), Nippon Seramikkusu Kyokai Gakujutsu Ronbunshi/Journal of the Ceramic Society of Japan 114(1330) (2006) 563-566.

[41] Y. Saito, S. Koyama, Y. Sugahara, K. Kuroda, Characterization of aluminum nitride from a precursor poly (isopropyliminoalane), Nippon Seramikkusu Kyokai Gakujutsu Ronbunshi/Journal of the Ceramic Society of Japan 104(2) (1996) 143-145.

[42] S. Fukumoto, T. Hookabe, H. Tsubakino, Hydrolysis behavior of aluminum nitride in various solutions, Journal of Materials Science 35(11) (2000) 2743-2748.

[43] A. Kocjan, The hydrolysis of ALN powder – a powerful tool in advanced materials engineering, Chemical Record 18(7-8) (2018) 1232-1246.

[44] D. Hotza, O. Sahling, P. Greil, Hydrophobing of aluminium nitride powders, Journal of Materials Science 30(1) (1995) 127-132.

[45] K. Krnel, T. Kosmač, Protection of AlN powder against hydrolysis using aluminum dihydrogen phosphate, Journal of the European Ceramic Society 21(10) (2001) 2075-2079.

[46] M. Oliveira, S. Olhero, J. Rocha, J.M.F. Ferreira, Controlling hydrolysis and dispersion of AlN powders in aqueous media, Journal of Colloid and Interface Science 261(2) (2003) 456-463.

[47] S.M. Olhero, M.S. Jensen, M.-A. Einarsud, T. Grande, J.M.F. Ferreira, Thermodynamic Studies on the AlN Sintering Powders Treated With Phosphate Species, Journal of the American Ceramic Society 90(11) (2007) 3589-3595.

[48] T. Sato, K. Haryu, T. Endo, M. Shimada, High temperature oxidation of hot-pressed aluminium nitride by water vapour, Journal of Materials Science 22(6) (1987) 2277-2280.

[49] H.-E. Kim, A. J. Moorhead, Oxidation Behavior and Flexural Strength of Aluminum Nitride Exposed to Air at Elevated Temperatures, Journal of the American Ceramic Society 77(4) (1994) 1037-1041.

[50] W.D. Kingery, Densification during Sintering in the Presence of a Liquid Phase. I. Theory, Journal of Applied Physics 30(3) (1959) 301-306.

[51] K. Watari, M. Kawamoto, K. Ishizaki, Sintering chemical reactions to increase thermal conductivity of aluminium nitride, Journal of materials science 26(17) (1991) 4727-4732.

[52] K. Watari, High Thermal Conductivity Non-Oxide Ceramics, Journal of the Ceramic Society of Japan 109(1265) (2001) S7-S16.

[53] T.B. Jackson, A.V. Virkar, K.L. More, R.B. Dinwiddie Jr, R.A. Cutler, High-Thermal-Conductivity Aluminum Nitride Ceramics: The Effect of Thermodynamic, Kinetic, and Microstructural Factors, Journal of the American Ceramic Society 80(6) (1997) 1421-1435.

[54] A. Horiguchi, F. Ueno, M. Kasori, Y. Sato, M. Hayashi, H. Endo, K. Shinozaki, A. Tsuge, AlN sintered body having high thermal conductivity and a method of fabricating the same, Toshiba Corp, 1988.

[55] K. Watari, H.J. Hwang, M. Toriyama, S. Kanzaki, Effective Sintering Aids for Low-temperature Sintering of AlN Ceramics, Journal of Materials Research 14(4) (1999) 1409-1417.

[56] A.L. Molisani, H. Goldenstein, H.N. Yoshimura, The role of CaO additive on sintering of aluminum nitride ceramics, Ceramics International 43(18) (2017) 16972-16979.

[57] L. Qiao, H. Zhou, H. Xue, S. Wang, Effect of Y2O3 on low temperature sintering and thermal conductivity of AlN ceramics, Journal of the European Ceramic Society 23(1) (2003) 61-67.

[58] L. Qiao, H. Zhou, K. Chen, R. Fu, Effects of Li2O on the low temperature sintering and thermal conductivity of A1N ceramics, Journal of the European Ceramic Society 23(9) (2003) 1517-1524.

[59] T.B. Troczynski, P.S. Nicholson, Effect of Additives on the Pressureless Sintering of Aluminum Nitride between 1500° and 1800°C, Journal of the American Ceramic Society 72(8) (1989) 1488-1491.

[60] H.-J. Lee, W.-S. Cho, H.J. Kim, H.-T. Kim, S.-S. Ryu, Effect of Additive Size on the Densification and Thermal Conductivity of AlN Ceramics with MgO–CaO–Al2O3–SiO2 Additives, Journal of the Korean Ceramic Society 54(1) (2017) 43-48.

[61] P.S. Baranda, A.K. Knudsen, E. Ruh, Effect of Silica on the Thermal Conductivity of Aluminum Nitride, Journal of the American Ceramic Society 76(7) (1993) 1761-1771.

[62] T. Yoshioka, Y. Makino, S. Miyake, H. Mori, Intergranular Microstructure of Yb2O3-added AlN Sintered by Millimeter-Wave Heating, in: S. Miyake (Ed.), Novel Materials Processing by Advanced Electromagnetic Energy Sources, Elsevier Science Ltd, Oxford, 2005, pp. 173-176.

[63] H.M. Lee, D.K. Kim, High-strength AlN ceramics by low-temperature sintering with CaZrO3–Y2O3 co-additives, Journal of the European Ceramic Society 34(15) (2014) 3627-3633.

[64] J. Yoshikawa, Y. Katsuda, N. Yamada, C. Ihara, M. Masuda, H. Sakai, Effects of Samarium Oxide Addition on the Phase Composition, Microstructure, and Electrical Resistivity of Aluminum Nitride Ceramics, Journal of the American Ceramic Society 88(12) (2005) 3501-3506.

[65] S.Y. Kim, D.-H. Yeo, H.-S. Shin, H.G. Yoon, Effects of Samarium Oxide on Thermal and Mechanical Properties of Y2O3-CaCO3 Added Aluminum Nitride, Journal of Nanoscience and Nanotechnology 17(5) (2017) 3528-3532.

[66] K. Ishizaki, K. Watari, Oxygen behavior of normal and HIP sintered AlN, Journal of Physics and Chemistry of Solids 50(10) (1989) 1009-1012.

[67] A.M. Hundere, M.-A. Einarsrud, Effects of reduction of the Al・Y・O containing secondary phases during sintering of AlN with YF3 additions, Journal of the European Ceramic Society 16(8) (1996) 899-906.

[68] T. Nakamatsu, F. Pomar, K. Ishizaki, The effect of carbon coating of AlN powder on sintering behavior and thermal conductivity, Journal of Materials Science 34(7) (1999) 1553-1556.

[69] Y. Kurokawa, K. Utsumi, H. Takamizawa, Development and Microstructural Characterization of High-Thermal-Conductivity Aluminum Nitride Ceramics, Journal of the American Ceramic Society 71(7) (1988) 588-594.

[70] F. Ueno, H. A., Grain Boundary Phase Elimination and Microstructure of Aluminum Nitride, The 1st European Ceramic Society Conference (1989) 383-387.

[71] R. Fu, K. Chen, S. Agathopoulos, M.C. Ferro, D.U. Tulyaganov, J.M.F. Ferreira, Migration of liquid phase in low temperature sintering of AlN, Journal of Materials Science 40(9) (2005) 2425-2429.

[72] H. Buhr, G. Müller, Microstructure and thermal conductivity of AlN(Y2O3) ceramics sintered in different atmospheres, Journal of the European Ceramic Society 12(4) (1993) 271-277.

[73] X. Xu, H. Zhuang, W. Li, S. Xu, B. Zhang, X. Fu, Improving thermal conductivity of Sm2O3-doped AlN ceramics by changing sintering conditions, Materials Science and Engineering: A 342(1) (2003) 104-108.

[74] J. Yang, Theory of Thermal Conductivity, in: T.M. Tritt (Ed.), Thermal Conductivity: Theory, Properties, and Applications, Springer US, Boston, MA, 2004, pp. 1-20.

[75] K. Watari, K. Ishizaki, T. Fujikawa, Thermal conduction mechanism of aluminium nitride ceramics, Journal of Materials Science 27(10) (1992) 2627-2630.

[76] C.F. Chen, M.E. Perisse, A.F. Ramirez, N.P. Padture, H.M. Chan, Effect of grain boundary phase on the thermal conductivity of aluminium nitride ceramics, Journal of Materials Science 29(6) (1994) 1595-1600.

[77] J.H. Harris, R.A. Youngman, R.G. Teller, On the nature of the oxygen-related defect in aluminum nitride, Journal of Materials Research 5(8) (1990) 1763-1773.

[78] G.E. Potter, A.K. Knudsen, J.C. Tou, A. Choudhury, Measurement of the Oxygen and Impurity Distribution in Polycrystalline Aluminum Nitride with Secondary Ion Mass Spectrometry, Journal of the American Ceramic Society 75(12) (1992) 3215-3224.

[79] R.L. Xu, M. Muñoz Rojo, S.M. Islam, A. Sood, B. Vareskic, A. Katre, N. Mingo, K.E. Goodson, H.G. Xing, D. Jena, E. Pop, Thermal conductivity of crystalline AlN and the influence of atomic-scale defects, Journal of Applied Physics 126(18) (2019) 185105.

[80] CEN/TC 438 Additive Manufacturing, Additive manufacturing - General principles - Fundamentals and vocabulary (ISO/ASTM 52900:2021), CEN European Committee for Standardization, 2021.

[81] S. Weingarten, U. Scheithauer, L. Gollmer, P. Horn, J. Ziener, L. Rebenklau, H. Barth, Additive Fertigung von keramikbasierten Multimaterialbauteilen mittels CerAM MMJ, Keramische Zeitschrift 73(6) (2021) 38-43.

[82] J. Schlacher, A.-K. Hofer, S. Geier, I. Kraleva, R. Papšík, M. Schwentenwein, R. Bermejo, Additive manufacturing of high-strength alumina through a multi-material approach, Open Ceramics 5 (2021) 100082.

[83] A. Zocca, P. Colombo, C.M. Gomes, J. Günster, Additive Manufacturing of Ceramics: Issues, Potentialities, and Opportunities, Journal of the American Ceramic Society 98(7) (2015) 1983-2001.

[84] C.W. Hull, Apparatus for production of three-dimensional objects by stereolithography, 3D Systems Inc, 1984.

[85] M.L. Griffith, J.W. Halloran, Freeform fabrication of ceramics via stereolithography, Journal of the American Ceramic Society 79(10) (1996) 2601-2608.

[86] M. Schwentenwein, J. Homa, Additive Manufacturing of Dense Alumina Ceramics, International Journal of Applied Ceramic Technology 12(1) (2015) 1-7.

[87] J. Schlacher, T. Lube, W. Harrer, G. Mitteramskogler, M. Schwentenwein, R. Danzer, R. Bermejo, Strength of additive manufactured alumina, Journal of the European Ceramic Society 40(14) (2020) 4737-4745.

[88] H. Wu, W. Liu, R. He, Z. Wu, Q. Jiang, X. Song, Y. Chen, L. Cheng, S. Wu, Fabrication of dense zirconia-toughened alumina ceramics through a stereolithography-based additive manufacturing, Ceramics International 43(1) (2017) 968-972.

[89] M. Revilla-León, N. Al-Haj Husain, L. Ceballos, M. Özcan, Flexural strength and Weibull characteristics of stereolithography additive manufactured versus milled zirconia, Journal of Prosthetic Dentistry 125(4) (2021) 685-690.

[90] A.A. Altun, T. Prochaska, T. Konegger, M. Schwentenwein, Dense, Strong, and Precise Silicon Nitride-Based Ceramic Parts by Lithography-Based Ceramic Manufacturing, Applied Sciences 10(3) (2020).

[91] Z. Liu, H. Liang, T. Shi, D. Xie, R. Chen, X. Han, L. Shen, C. Wang, Z. Tian, Additive manufacturing of hydroxyapatite bone scaffolds via digital light processing and in vitro compatibility, Ceramics International 45(8) (2019) 11079-11086.

[92] X. Huang, H. Dai, Y. Hu, P. Zhuang, Z. Shi, Y. Ma, Development of a high solid loading β-TCP suspension with a low refractive index contrast for DLP -based ceramic stereolithography, Journal of the European Ceramic Society 41(6) (2021) 3743-3754.

[93] N.R. Jankowski, L. Everhart, B.R. Geil, C.W. Tipton, J. Chaney, T. Heil, W. Zimbeck, Stereolithographically fabricated aluminum nitride microchannel substrates for integrated power electronics cooling, 2008 11th Intersociety Conference on Thermal and Thermomechanical Phenomena in Electronic Systems, 2008, pp. 180-188.

[94] A.C. Aguilar, C.A. Diaz-Moreno, A.D. Price, R.K. Goutam, C.E. Botez, Y. Lin, R.B. Wicker, C. Li, Non-destructive optical second harmonic generation imaging of 3D printed aluminum nitride ceramics, Ceramics International 45(15) (2019) 18871-18875.

[95] W. Duan, S. Li, G. Wang, R. Dou, L. Wang, Y. Zhang, H. Li, H. Tan, Thermal conductivities and mechanical properties of AlN ceramics fabricated by three dimensional printing, Journal of the European Ceramic Society 40(10) (2020) 3535-3540.

[96] L. Lin, H. Wu, Y. Xu, K. Lin, W. Zou, S. Wu, Fabrication of dense aluminum nitride ceramics via digital light processing-based stereolithography, Materials Chemistry and Physics 249 (2020).

[97] P. Ożóg, P. Rutkowski, D. Kata, T. Graule, Ultraviolet Lithography-Based Ceramic Manufacturing (UV-LCM) of the Aluminum Nitride (AlN)-Based Photocurable Dispersions, Materials 13(19) (2020).

[98] M. Belmonte, G. Lopez-Navarrete, M.I. Osendi, P. Miranzo, Heat dissipation in 3D printed cellular aluminum nitride structures, Journal of the European Ceramic Society 41(4) (2021) 2407-2414.

[99] CEN/TC 184 Advanced technical ceramics, Advanced technical ceramics - Monolithic ceramics - General and textural properties - Part 2: Determination of density and porosity, CEN European Committee for Standardization, 1993.

[100] C. Edtmaier, T. Steck, R.C. Hula, L. Pambaguian, F. Hepp, Thermo-physical properties and TEM analysis of silver based MMCs utilizing metallized multiwall-carbon nanotubes, Composites Science and Technology 70(5) (2010) 783-788.

[101] V.I. Koshchenko, Y.K. Grinberg, A.F. Demidenko, Thermodynamic properties of AlN (5-2700 K), GaP (5-1500 K) and BP (5-800 K), Inorganic Materials 20(11) (1984) 1550 - 1553.

[102] W.M. Haynes, CRC Handbook of Chemistry and Physics : a ready-reference book of chemical and physical data, 93rd edition 2012-2013. ed., CRC Press, London, 2016.

[103] W.J. Parker, R.J. Jenkins, C.P. Butler, G.L. Abbott, Flash Method of Determining Thermal Diffusivity, Heat Capacity, and Thermal Conductivity, Journal of Applied Physics 32(9) (1961) 1679-1684.

[104] CEN/TC 184 Advanced technical ceramics, Advanced technical ceramics - Mechanical properties of monolithic ceramics at room temperature - Part 1: Determination of flexural strength, CEN European Committee for Standardization, 2006.

[105] A. Börger, P. Supancic, R. Danzer, The ball on three balls test for strength testing of brittle discs: stress distribution in the disc, Journal of the European Ceramic Society 22(9) (2002) 1425-1436.

[106] P. Boch, J.C. Glandus, J. Jarrige, J.P. Lecompte, J. Mexmain, Sintering, oxidation and mechanical properties of hot pressed aluminium nitride, Ceramics International 8(1) (1982) 34-40.

[107] D. Munz, Mechanisches Verhalten keramischer Werkstoffe : Versagensablauf, Werkstoffauswahl, Dimensionierung, Berlin [u.a.] : Springer, Berlin [u.a.], 1989.

[108] CEN/TC 184 Advanced technical ceramics, Advanced technical ceramics - Mechanical properties of monolithic ceramics at room temperature - Part 5: Statistical analysis, CEN European Committee for Standardization, 2006.

[109] CEN/TC 184 Advanced technical ceramics, Fine ceramics (advanced ceramics, advanced technical ceramics) - Microstructural characterization - Part 1: Determination of grain size and size distribution (ISO 13383-1:2012), CEN European Committee for Standardization, 2016.

[110] CEN/TC 184 Advanced technical ceramics, Advanced technical ceramics - Mechanical properties of monolithic ceramics at room temperature - Part 4: Vickers, Knoop and Rockwell superficial hardness, CEN European Committee for Standardization, 2005.

CV - Johannes Rauchenecker

Personal Information

Acad. Degree:	Dipl.-Ing. BSc.
Date of Birth:	January 2, 1994
Citizenship:	Austria

Education

Since 06/2018:	**Doctoral programme in Technical Sciences**, TU Wien, Institute of Chemical Technologies and Analytics, Austria
	Specialization: Processing and sintering of aluminum nitride ceramics
	Thesis title: *Development of aluminum nitride material systems suitable for additive manufacturing*
02/2017 - 06/2018:	**Master's programme Technical Chemistry**, TU Wien, passed with distinction
	Specialization: High performance materials
	Thesis title: *Deposition of polymer-derived ceramic layers with asymmetric porosity*
10/2013 - 02/2017:	**Bachelor's programme Technical Chemistry**, TU Wien
	Thesis title: *Porosity control in SiCN Ceramics*
09/2004 - 06/2012:	**BRG Enns** (grammar school), 4470 Enns, Austria
	Specialization: Science

Work Experience:

10/2017 - 06/2022:	Project Assistant, TU Wien, Institute of Chemical Technologies and Analytics
	Projects:

- *Micropore development in polymer-derived ceramics (FWF)*
- *Addhance – Additive Manufacturing of high-performance aluminum nitride ceramics (FFG)*

Since 08/2022:	Development engineer, Electrovac Metall-Glaseinschmelzungs GmbH

Vienna, August 2022